INSTITUT DE MICROTECHNIQUE

Université de Neuchâtel

ELECTRONIC OVULATION DETECTION

Clinical experiments, mathematical modeling and computer-assisted image analysis of breast thermograms

K.H.S. RAO

Imprimerie Centrale Neuchâtel

IMPRIMATUR POUR LA THÈSE

Electronic Ovulation Detection

de Monsieur *Sathyanarayana K.H. Rao*

UNIVERSITÉ DE NEUCHATEL

FACULTÉ DES SCIENCES

La Faculté des sciences de l'Université de Neuchâtel,
sur le rapport des membres du jury,

MM. A. Shah, N.F. de Rooij, B. Rüedi,

M. Walther (Berne), E.F.S. Ring (Bath),

W. Frei (Los Angeles) et J.M. Spieler (Washington)

autorise l'impression de la présente thèse.

Neuchâtel, le *5 novembre 1985*

Le doyen:

François Sigrist

François Sigrist

PREFACE

'Ovulation detection' plays an important role in solving fertility/infertility problems. The work presented in this thesis is towards a simple, non-invasive method of ovulation detection that can be used at home even by a illiterate person.

The work is based on our hypothesis that the preovulatory phase of the menstrual cycle is associated with pronounced vascularity in breasts and hence leads to a dynamic temperature distribution over the breast's skin surface. Measurement of differential temperature between a dynamic temperature spot and a static temperature spot can indicate the approaching ovulation.

The thesis is organized in 7 chapters. Each chapter can be read independently with a little prior knowledge of the cyclic phenomena involved during the menstrual cycle.

Chapter 1 provides an overview of biological phenomena involved in human reproduction and a brief summary of the available methods of birth control followed by a few possible eletronic solutions for ovulation detection.

Chapter 2 is an introduction to the basic physics of thermokinetics and its application in the calculation of human body temperature.

Chapter 3 presents our hypothesis of 'differential skin temperature (DST)' measurement for ovulation detection.

Chapter 4 describes the clinical tests conducted with the help of infrared thermography (IRT) and the results obtained with these experiments.

Chapter 5 presents a simple mathematical modeling of breast thermograms to describe the temperature variation over the menstrual cycle.

Chapter 6 details the computer-assisted thermography system developed for the analysis of breast thermograms recorded during the clinical tests. The results based on computer-assisted image analysis of breast thermograms are presented.

Chapter 7 describes the design and development of 'FERTITHERM', an absolute/differential temperature measuring digital thermometer.

Contents Page

4. Clinical experiments and results

5. Mathematical modeling and computer simulation

6. Computer-assisted image analysis

CHAPTER 1

Most of the matter presented in this chapter is published as a journal paper in 'Sadhana', Proc. of Indian Academy of Sciences, Vol. 7, Part I, Jun 1984, pp. 73-89. The title of this paper is:

"Natural birth control: A brief review and some bioelectronic solutions."

1. HUMAN REPRODUCTION AND BIRTH CONTROL

1.1 Human reproduction

1.1a Introduction

Ovulation is a key function in the process of mammal reproduction. What is 'ovulation' ? and What is the role of 'ovulation' in the reproductive process ? are common questions that one come across in understanding the reproduction phenomena. Towards this understanding, biological phenomena involved in the reproductive process are briefly explained in the following section.

1.1b Basic biological phenomena

Mammal reproduction is the result of male-female union, at the proper time of peak fertility interval in the female's menstrual cycle. Female being the carrier of reproduction, she is also associated with cyclic physiological and hormonal changes (called menstrual cycle) involving fertility and infertility intervals throughout her productive life period. These being true in all mammals, our discussion throughout the text is limited to human reproduction only.

Birth control meaning to have children when desired and to limit further child birth when not desired , termed as conception and contraception respectively, is of great socio-economic importance for all the countries in the world. For controlling consciously either conception or contraception, one has to identify the fertility interval, which primarily depends on the time of ovulation. So, to explain 'ovulation', its timing and the fertility interval in the menstrual cycle, the details of cyclic biological functions are looked into.

1.1c Menstrual cycle

The menstrual cycle is a repetitive operation of the hypothalmic-pituitary-ovarian (HPO) system, with associated structural and functional changes in the reproductive tract of a woman, consisting of uterus, endometrium and vagina /1/. Fig. 1.1 shows the various parts of the genetic section of a woman /2/.

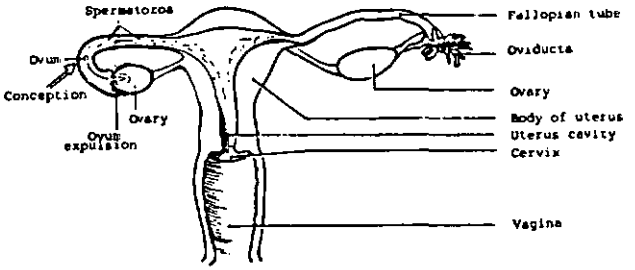

Fig. 1.1 Schematic representation of the female genetic parts and the steps involved in causing pregnancy (conception of a baby).

The ovaries consist of millions of follicles which develop further with the hormonally dependent menstrual cycle, throughout the productive life of a woman, confined between puberty and menopause. Fig. 1.2a shows the various hormonal, and follicle changes involved and Fig. 1.2b shows the cycle of stages associated with the menstrual cycle /2/.

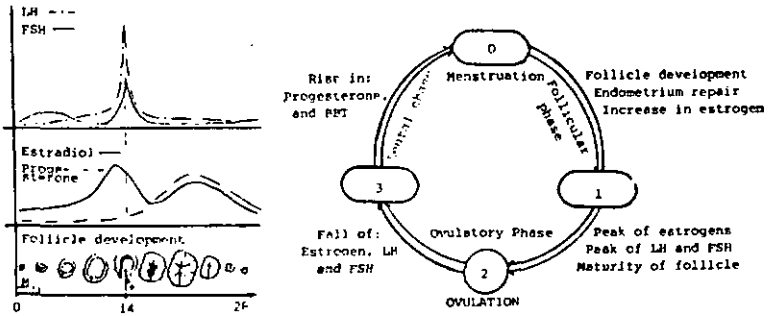

Fig. 1.2 The menstrual cycle:
a) Relationship between hormonal cycle and follicle development
b) Various stages of the menstrual cycle.

The reproduction process can be explained in three phases of the menstrual cycle:

Follicular phase

The follicular phase is characterized by the ovarian secretion of estradiol (E_2), estrone (E_1) and other estrogen compounds, and is related to the development and maturation of the follicle to an ovum as a result of pituitary follicle stimulating hormone (FSH) stimulation /3/. This phase is an infertile phase of the menstrual cycle; it corresponds to the interval between post-menstruation and the rise in plasma estrogen concentration and covers approximately the first 10 days of the cycle.

Ovulatory phase

The ovulatory phase is the most fertile period of the menstrual cycle. This phase begins with the rise in plasma estrogen compounds and ends with the rise in plasma progesterone concentration. Rise in estradiol increases the vascularity in the genetic targets and initiates the peak secretion of the follicle stimulating hormone (FSH) and leutinizing hormone (LH) by the pituitary glands /4/. The peak LH surge in the plasma is supposed to lead to the final maturation of ovum and to a follicular rapture which expels the ovum into the oviducts /5/. The expulsion of an ovum from the ovaries is known as 'Ovulation'.

Leutal phase

The post-ovulatory phase is known as leutal phase. After a day of ovulation, the second infertile phase of the menstrual cycle begins. This phase is characterized by a rise in progesterone to reach a peak around 8 days after ovulation. Estradiol hormone concentration keeps a low level during early post-ovulatory phase and rises again in the middle part of leutal phase. Both estradiol and progesterone fall back to low levels before the following menstruation.

The whole cycle covering follicular, ovulatory and leutal phases repeats over approximately 28 days.

The ovulatory phase is the most fertile phase for reproduction. Once the ovulation occurs the waiting oviducts trap the expelled ovum and direct it to flow through the fallopian tubes into the uterus. During the ovum's travel, if it comes in contact with spermatozoa already deposited by a man from prior intercourse, the ovum unites with the spermatozoa to cause pregnancy (called at this level as conception). The life span of

spermatozoa is expected to be 72 hours and that of an ovum (after ovulation) is expected to be of the order of 24 hours /5/. So, the total fertile phase corresponds to (3+1=) 4 days out of 28 days of menstrual cycle. If the ovulation timing can be predicted reliably and in advance, reproduction can be controlled. Conception can be achieved with higher probability by proper timing of intercourse, or by artificial insemination. Contraception, by simple periodic abstinence, acccptable to all religions of the world can also be achieved with high reliability. From this, the importance of 'ovulation time' detection can be judged.

1.2 Conventional methods of birth control

High birth rate and thus explosion of population is a major problem in developing nations. Various types of contraception methods have been known and are being developed for high reliability, and minimum side-effects to the anatomical functions of the human body. In a broad way, all contraceptive methods could be classified into 4 principal groups. These are:

1. Pharmaceutical method of contraception
2. Mechanical contraceptives
3. Surgical intervention
4. Natural birth control (NBC)

Each of these methods is discussed in brief, with respect to their functioning, reliability, ease in application, acceptability and the associated side-effects on the anatomical functions, in tables 1 and 2. A detailed discussion concerning NBC willbe presented in the next section.

1.3 Measurable Physiological parameters for ovulation detection

To improve the reliability of NBC to minimize the period of abstinence, the fertile interval of the menstrual cycle has to be dettermined in advance. The three major factors interfering with the exact estimation of the fertile interval /5/ are:

1. the length of menstrual cycle (varying between 22 and 45 days),
2. the life span of spermatozoa in the vagina (normally 2 to 3 days) and
3. the life span of the ovum (known to be around 24 hours).

Table 1. Brief summary of conventional contraceptive methods.

Pharmaceutical contraceptives

Contraception is achieved by controlling the estrogen and progesterone levels in the woman's body through oral pills, implant capsules, long-durable injections, etc.: all these suppress the LH surge and thus avoid the ovulation, making the whole menstrual cycle infertile. General problems: by disturbing the natural hormonal functions of the body, pharmaceutical contraceptives increase body's weakness to thromboembolism, stroke, myocardial infection, hepatic adenoma, gallbladder disease, hypertension, etc. Not very economical for the Third World.

Oral pills

Problems: Besides the regular need of intake and rather high economical load on an individual user, supply and proper choice of oral pills to suit an individual are not guaranteed in third world countries.

Implant capsules

Release slow and steady level of progesterone, providing the protection against conception over a year. Could perhaps be good in third world countries, among the illiterate section of the population.
Problem: Involves a doctor for implantation. Long-term results on side-effects are not yet known.

Estrogen-Progesterone injection

An injection once a month provides a complete protection over one cycle. Higher dosage of hormones injected in the body may have serious side-effects in the long run, which are not yet fully known.
Problem: Involves medical personnel.

Monthly pills for men

Recent reports claim a successful development of pills for men, to limit the production of spermatozoa without affecting the natural sex drive. Side-effects and problems associated with this new development remain to be seen.
General advantage of the above methods remain to be seen.

Vaginal spermicides

Often used as a contraceptive. They block the cervix and kill the spermatozoa deposited in the vagina.
Problem: They should be applied at least 10 minutes before the act of intercourse for good protection.
Problem : Reliability is poor. Failure rate is around 4%.

Mechanical Contraceptives

Contraception is achieved by blocking the cervical path for the spermatozoa in the case of diaphragm, cervical cap, vaginal ring and condom, or by changing the enzyme function in the uterus with the presence of intra-uterine device, avoiding thus the implantation of fertilized ovum. General problems: Psychologically not acceptable among many sections of the population.
General advantages: Easily available, economical and sufficiently reliable. Relatively simple to use.

Intra-Uterine Device (IUD)

Problems: many women experience increased bleeding during the menstruation. Therefore not recommended for anaemic or malnourished women. Pelvic inflammations are observed with women having venereal disease. Expulsion rate is high with young women. Because of bleeding, expulsion risk, etc. a follow-up phase by a doctor is necessary which is unfortunately not guaranteed in rural areas of third world countries.
Progistin-coated IUDs have shown improved performance compared to ordinary CU-7 or Lippies-loop type of IUD. Failure rate varies between 3% to 10% depending on type of IUD and individual attention.

Diaphragm

Made of rubber/plastic material. When properly placed in the vagina, it protects the cervix from spermatozoa.
Problems: It has to be inserted properly in the vagina before each act of intercourse. Requires prior training. Failure rate is as high as 15% among untrained users.

Vaginal ring

Similar to diaphragm but contains progesterone coating. Has an advantage that it can remain in the vagina for one complete cycle.

Cervical cap

Made of lucine/rubber material. It is held in position by suction and has an adjustable property to adopt itself for little changes of cervix. Failure rate is around 3%. It can remain in position for longer period; to be cleaned at convenience and reintroduced.

Condom

Made of thin strong latex rubber to fit the erect penis to block the path of spermatozoa.
Problems: Aesthetically not attractive. Some men complain of loss in natural sensation due to lack of direct contact between penis and vagina. Not too economical for the poorer class of third world countries. Failure rate is around 2.5%.

Table 2. Brief summary of conventional contraceptive methods.

Surgical methods	Abortion	Natural birth control
Permanent barrier to conceive is achieved by a simple operation either on man or on woman. Surgical method of contraception is well suited for those couples who are sure of their present family size and could decide once for all against having further children. General problems: Permanent contraceptive method. The couple opting for this method cannot easily have children later on, though some doctors claim for this possibility by a second operation. Some people have general aversion to surgery. Advantages: High reliability. Failure rate is below 0.01%. No economical problems are involved. After the operation free sexual activity is possible. Vasectomy A simple operation on man wherein the "vas-deferns" canal carrying the spermatozoa is surgically interrupted. Problems: Some men cumplain about change in coital performance after the operation due to psychological factors. Tubectomy This is a simple operation, in which the fallopian tubes are raised to a knuckle and the tube included within is cut-off, blocking the ovum path. This operation is recommended just after a vaginal delivery. Problems: More of psychological nature and basically same as for vasectomy.	Interruption of pregnancy before the foetus is matured sufficiently. Aortion's surgical implications extend from that of a simple operation at an early stage of pregnancy to a complicated surgery like hysterectomy at the later stage of pregnancy. Abortion certainly does not constitute a rational method for birth control. Problems: Basically immoral as it involves killing of foetus and is therefore banned by almost all relisgions of the world. Needs hospitalization and safety depends on the stage of pregnancy. In many third world countries illegal abortions in unhygenic conditions are common due to the fear of society. Mortality is as high as 4.2% in case of hysterectomy. Further it is not at all economical. Advantages: When mother's health is in danger due to pregnancy, abortion may be recommended rather than risking her life.	Contraception is achieved by periodic abstinence from sexual intercouse. Advantages: Safest method of contraception. As theris no interference with the biologicalaspects of anotomy, there is no pussibility of any side-effects. Natural birth control (NBC) has been accepted by all religions as a method of contraception. Natural sexual activity may bring more harmuny and understanding to the couple. Also wuamn can have a personal knowledge of her cycle status with proper motivation. Problems: Precise and reliable estimation of fertile interval for abstinence remain a fundamental problem. Reliability of the method suffers when this fertility interval is minimised or wrongly estimated. NBC demands good motivation from buth partners. Failure rates between 4% and 20% are quoted for methods presently used. The measurable parameters to estimate the fertile interval of woman's menstrual cycle and the actually known methods are briefly discussed in chapter 3.0

Assuming a maximum of 3 days' life span for spermatozoa in the vagina, the minimum fertile interval can be reduced to 4 days, if the ovulation time is detected in advance. Determination of the fertile interval is of interest, not only to achieve contraception by abstinence, but also to achieve conception with higher probability among couples desiring children by proper timing of natural intercourse or through artificial insemination. It has been reported that the relation between ovulation time and the time of natural intercourse also plays a certain part in determining the child's sex on conception /6/.

Various physiological factors changing during the menstrual cycle are shown in fig. 1.3 /5/. Different methods have been developed to estimate the fertile/infertile interval of the woman's menstrual cycle, and are briefly discussed here:

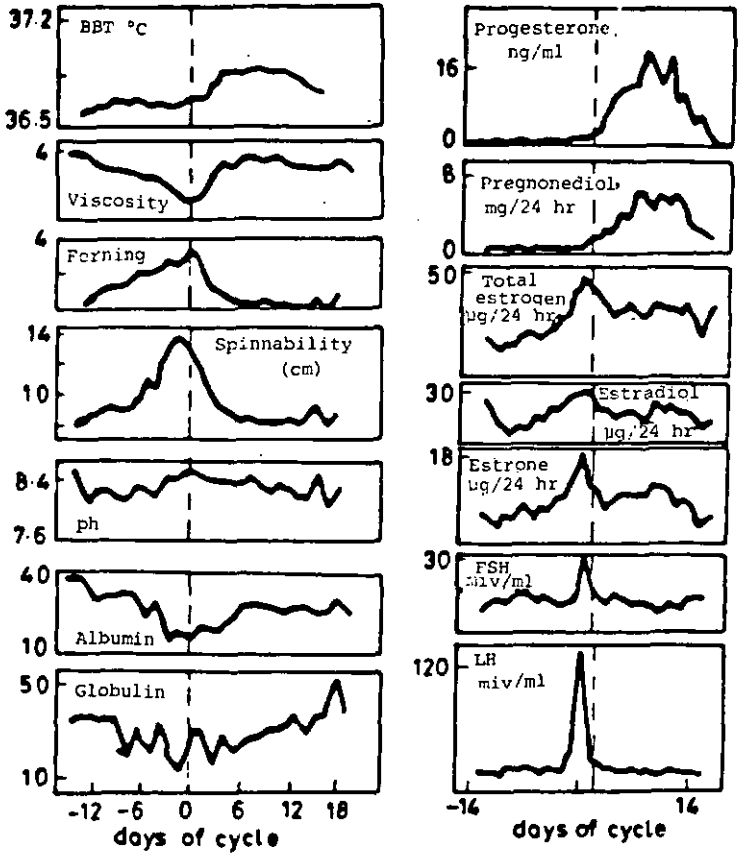

Fig. 1.3 Variation of various measurable parameters over the menstrual cycle /5/.

1.3.1 Ogino-Knaus method

This method, also known as 'calender method', is the simplest form of NBC /5/: Here the woman calculates her fertility interval depending on the minimum and maximum length of her menstrual cycles during the past 12 months.

First day of fertile interval = [length of shortest cycle - 18];

Last day of fertile interval = [length of longest cycle - 11]

Based on this principle , M/S Kowa limited of Japan have brought out an electronic gadget to indicate the abstinence period.

1.3.2 Basal body temperature (BBT) method

A woman's menstrual cycle has a cyclic hormonal activity. It has three phases as explained in 1.1c. Progesterone hormone being thermogenic in nature, body temperature rises in the leutal phase by 0.2 C to 0.4 C over the normal temperature. Hence body temperature can confirm the occurence of ovulation and the beginning of post-ovulatory infertile interval. Steady morning temperature called basal body temperature (BBT) has thus come to be used among NBC practitioners. However, the reliability of this method suffers due to disturbing physiological factors, mental stress and any long journey involved, which tend to change the body temperature and mislead the NBC practitioners. Development of electronic thermometers incorporating statistical algorithms to improve the reliability of BBT method has been reported /7,8,9/.

1.3.3 Billing's method

Cervical mucus viscosity has been observed to be a function of menstrual cycle status /10/. Dr. Billings has divided the menstrual cycle into 5 phases with respect to cervical mucus viscosity and the fertility interval:

Phase 1: period of menstruation flow - infertility interval,

Phase 2: feeling of dryness in the vagina - infertility interval,

Phase 3: flow of mucus with whitish cloudy colour, pasty and sticky in nature, providing a favourable condition for the spermatozoa in the vagina - fertility interval,

Phase 4: increase of cervical discharge, very clear and less viscous mucus, lubricative and stretchy in nature - peak fertility interval,

Phase 5: mucus loses its stretchy nature and becomes more watery - infertility interval.

The use of Billing's method needs prior training to decide the nature of mucus and therefore this method suffers from unreliability among

untrained and non-motivated people /11/. Dr. Kosasky of U.S.A has reported the design of a simple ovumeter to measure precisely the mucus viscosity condition /12/.

1.3.4 Sympto-thermic method

This is a combination of BBT and Billing's method and is practiced by well-trained NBC practitioners /5/. Failure rate as low as 4% has been reported /11/.

1.3.5 Mucus spinnability

The measurement of spinnability or "Spinnbarkeit" of mucus is an extension of Billing's method. The day on which mucus can be drawn into the largest thread is estimated to be the day of ovulation /13/.

1.3.6 Fern Test

Chloride content in the mucus has been observed to be maximum during the ovulation time /14/. There are reports of chloride test papers which change colour depending on the degree of chloride content to determine the ovulation time /5/.

1.3.7 Vaginal blood flow

Increased vaginal blood flow has been correlated with ovulation time /15/. Vaginal blood flow is measured indirectly by measuring thermal conductance in the vagina /16/.

1.3.8 Follicle explosion

Some women feel and experience within themselves the follicle explosion and a kind of tickling sensation associated with it /17/.

1.3.9 Bio-potential measurement

Some scientists have claimed skin surface potential to have significant changes prior to ovulation /18,19/. Ovutron Company has brought out a finger potential measuring gadget to correlate with ovulation time /20/. However, Utah University studies have shown no such correlation /21/. Further, any external or internal injury is expected to cause significant skin surface potential change outdoing those due to ovulation /22/.

1.3.10 Vaginal wall optical back scattering

Optical back scattering of infrared radiation from the vaginal walls are claimed to indicate the ovulation time in advance /16/.

1.3.11 Hormonal measurement

So far, only hormonal measurements are accepted for precise determination of ovulation time. Measuring LH, FSH and estradiol hormones by standard radioimmunoassay in the laboratory is well known in clinical analysis, but is very expensive, time-consuming and laborious. Therefore, hormonal analysis is not useful as a contraception method unless a simple electronic measuring device can be realized.

1.3.12 Protein/enzyme analysis:

Analysis of proteins like albumin, globulin and enzymes like N-acetyl-B-D Glucosaminadase concentration in mucus/saliva can provide advance information of ovulation timing /5,23-28/. However, so far these analysis are meant only for clinical purposes in the laboratory and not as general methods for contraception /26/.

1.3.13 Cycle-regulation:

A regular menstrual cycle would evidently be a great asset to NBC practitioners. Further research work on the physiological, psychological and other factors influencing the cycle's couse and length is certainly needed. An interesting but speculative idea is proposed by Lacey /27/ under the name 'Lunaception': She suggests exploring the possibility of synchronizing/regulating the cycle by sleeping under a variable light source (similar to the moon's light).

1.4 Some proposals for bio-electronic solutions

1.4.1 General comments:

In 1.3 we briefly explained the various measurable parameters which permit the detection of ovulation time. The most reliable and precise method , viz the hormonal analysis of plasma for determining the LH surge by radioimmunoassay is invasive and not available for home use. Simple non-invasive methods like BBT and cervical mucus viscosity measurements, remain unreliable so far due to the influence of various physiological variations on the measured parameters and also due to the high degree of motivation required by such methods. Therefore, there is urgent need for simple and reliable bio-electronic solutions in the field of NBC. Such bio-electronic solutions may have 3 objectives:

1. to simplify the use of existing methods of ovulation detection,
2. to introduce new methods with improved sensors, to measure the parameters mentioned in 1.3, with greater accuracy and precision,

3. to improve the reliability of existing methods by applying electronic signal processing techniques.

In this section we will describe various electronic solutions for estimating the ovulation time, which appear to be promising:

1.4.2 Temperature measurement

Basal body temperature (BBT): At present , the BBT method is widely used by NBC practitioners. BBT has the inherent disadvantage of detecting only the post-ovulatory phase. Furthermore, it involves the ordeal of daily temperature recording. The use of a clinical mercury thermometer with a high time constant (>5 minutes) to reach a stable temperature, brings additional unreliability to the method. For reliable detection of the BBT rise, WHO /3/ has recommended as 'thumb rule' a minimum of 0.2°C rise for 3 continuous days over the previous 6 consecutive days. However, even this rule can fail, if a woamn has a slight fever for 3 days. To overcome these limitations, we suggest the use of an adaptive algorithm, incorporated in an electronic BBT thermometer /2B/. Thereby, we define pre- and post-ovulation temperature thresholds and probable fertility interval depending on the adaptivly updated data of, say, the previous 3 menstrual cycles as shown in fig. 1.4. T_l and T_h are, respectively, the pre-and post-ovulation phase average temperature records of the past 3 menstrual cycles.

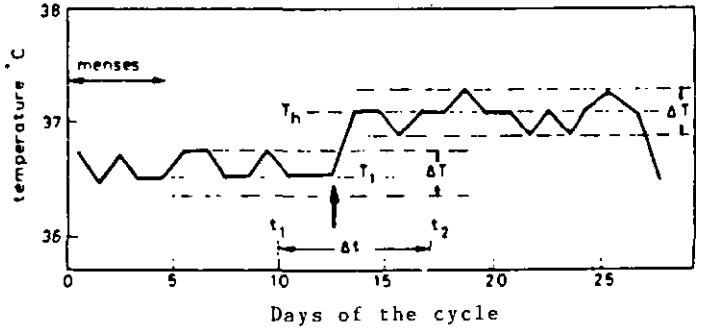

Fig. 1.4 Adaptive algorithm proposed for improved basal body temperature (BBT) recording and analysis.

The temperature margin of ΔT, around T_l and T_h, sets the limit of temperature levels acceptable as normal. Similarly, a temperature-level transition time interval Δt around the mid-cycle can be defined. In fig. 1.4, t_1 and t_2 are, respectively, the earliest and the latest expected day of the temperature-level transition (↑1.3.1). If the measured temperatures are within these defined thresholds, the cycle is considered to be normal and the ovulation detection is reliable, otherwise the user is warned of the unreliability of the instrument in that particular cycle. With commercially available microprocessors, all these functions as well as adaptive signal processing can be incorporated in a small electronic BBT thermometer, to detect the post-ovulatory phase much more reliably than the existing method.

Differential skin temperature (DST): A further improvement on temperature measurement can possibly be obtained by measuring skin temperature distribution over a few hormonally sensitive/insensitive areas of the body. Such interesting spots can be localized by contactless thermometry or more precisely by means of infrared therrmography (IRT). One can expect some parts of the breasts, vagina, etc... to reach higher temperatures than other areas because of hormonal, chemical and vascular activity during ovulation /29/. Absolute skin temperature being a function of ambient temperature, it cannot be of any significant importance. To overcome this problem, we have introduced the principle of differential skin temperatue (DST) measurement, involving e.g. the measurement of temperature difference between two points, one corresponding to a vascularity sensitive area (dynamic part) and the other to a vascularity insensitive area, on the body skin surface.
This differential skin temperature (DST) should be independent of ambient temperature, and hence the measurement of DST may have a significant importance. This new hypothesis of DST measurement has been further explained in detail, in chapter 3.

1.4.3 Cervical mucus viscosity measurement

Motivated women can predict the ovulation time sufficiently in advance by observing their cervical mucus viscosity. However, due to variations in the degree of change in mucus viscosity from cycle to cycle, the intuitive estimation of ovulation time, based on mucus observation, so far remains unreliable.
Measurement of mucus viscosity is difficult with the available commercial viscometers, due to the small volume of mucus. A recent development of an electromechanical tuning fork viscometer /30/ could be extended to

measure mucus viscosity. A miniature viscometer using a piezoelectric quartz tuning fork or a ceramic tuning fork instead of a mechanical tuning fork can be developed for mucus viscosity measurement. Normally, a torsionally vibrating quartz crystal in the form of a tuning fork would be an excellent choice. The torsionally vibrating crystal has resistive and reactive components in its equivalent elctronic circuit. When the crystal is immersed in the test fluid the static interelectrode capacitance dominated the reactive component. So the measurement of reactive impedance can be correlated with the characteristics of the liquid /31/. But a miniature quartz tuning fork cannot oscillate in the liquid at a low frequency due to its physical structure and size. It also acquires a high series impedance supressing the oscillations. Quartz crystals thus appear to set difficult problems for miniature viscometer development. We have overcome this problem by using ceramic tuning forks with a resonant frequency of 3 KHz. The principle of the operation is to measure the damping factor of the oscillation in correlation with the viscosity of the fluid. The damping factor is defined as the time required for the signal to reach (1/e)th of its original amplitude. The block diagram of the system is as shown in fig. 1.5a.
The piezoelectric crystal is excited with a sharp high energy impulse, to bring the crystal into its fundamental oscillating mode. Due to the high mechanical stress of the fluid media, the oscillation is dampened exponentially with a time constant τ, inversely proportional to the viscosity of the fluid.

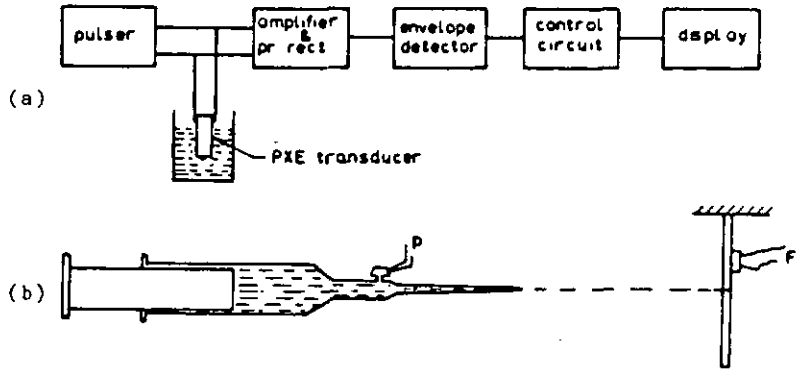

Fig. 1.5 Block schematic of: (a) ceramic transducer viscosity meter and (b) capillary type viscosity meter.

At the receiver, an amplifier and a precision rectifier convert these signals into high level unipolar signals. The envelope detector and the control circuit determines the time constant T of the signal and display the measured viscosity directly. The ceramic sensor and the associated electronic circuits could be miniaturized so as to be incoporated within a mucus extractor /32/ to measure the viscosity of the mucus directly at the vaginal opening, to avoid any temperature effects on the measurements.

Another alternative solution for the measurement of mucus viscosity has been suggested by Stauffer /33/ using two pressure transducers and a capillary. The principle of this method is to correlate the pressure applied on the liquid to obtain a known force on the hitting target with its viscosity. The system to be used insuch a measurement is shown in fig. 1.5b.

1.4.4 Bio-potential measurement

So far, the research in ovulation detection has been restricted to the direct observation of the potential difference between two points (say A and B) and to correlate $V_{ab}(t) = V_a(t) - V_b(t)$, with the ovulation time /20/. The main difficulties found in this method are:

1. the points of observation have not yet been found optimally,
2. body injuries and other physiological interferences will influence the potential measurement giving rise to false alarms.

So, bio-potential measurement at its present state of development is not suitable for birth control purposes. We however, wish to propose that there may certainly be scope for further research in observing bio-potential changes with respect to ovulation timing, through the understanding of the detailed potential distributions on the surface of the body over the whole menstrual cycle of a woman. Once such data are available, adaptive signal processing together with localized multiple-point potential measurement could perhaps be used to estimate ovulation time. The imaging of potential distributions can be referred to as "potentiography".

Until today, there is no technique available to display potential images directly, as in the case of temperature. However, with the physical-contact switched electrodes in contact with the skin one can possibly obtain such images. The switched electrodes would be in the form of matrix semiconductor sensor arrays with a multiplexed accessing in two ordinates. The block schematic of such a system and of a hypothetical bio-potential image are shown in fig. 1.6.

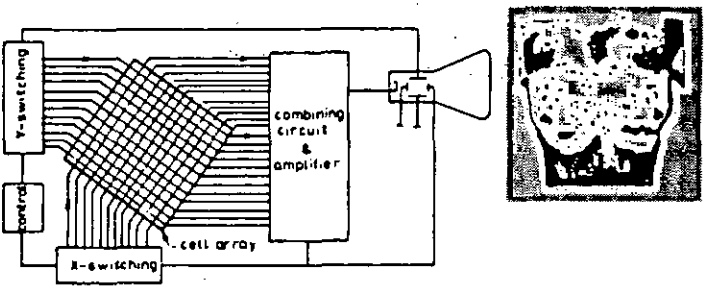

Fig. 1.6 Switched electrode 'bio-potential' imaging system and an hypothetical biopotential image.

1.4.5 Follicle explosion detection

Reliable follicle explosion detection gives the precise time of ovulation. One can detect the follicle explosion by an acoustic or ultrasonic method.

Acoustical method: Two very sensitive miniature microphones mounted on the two ovaries pre-localized by uterosonography may be able to detect the acoustical signal of follicle explosion. To avoid interference with other ventricular noises, the signal can be processed further to select a predefined spectrum only and to perform a geometrically-selective correlation. The size of the microphones and their sensitivity will be a limiting factor in the system's size and its performance.

Ultrasonic method: The limitation of the passive acoustical system could be overcome using an ultrasonic system. The principle of the Doppler technique, as used in foetus heart rate monitor and blood flow detector can be extended for follicle explosion detection using two transducers, one on each ovary.

The follicle explosion method could be an excellent solution only for inferility problems, in timing the artificial insemination.

1.4.6 Chemical and hormonal measurement:

Test papers: Chemically treated test papers, which change colour as a result of chemical concentration, have of late been introduced to measure the chemical activity in mucus and saliva /27/. But the absolute level of chemical concentration varies from one woman to another and also form one cycle to another for the same person. In fact, only relative changes are supposed to indicate the menstrual cycle status.

Therefore, chemically treated test papers are not generally applicable in estimating the menstrual cycle status, unless a way is found to combine them with an electronic instrument to determine the degree of change in chemical activity.

Chemically sensitive electronic devices (CSED): Recently, a new type of semiconductor devices called chemically sensitive electronic device (CSED) have been developed /34,35/. These devices provide an electric signal proportional to the chemical activity on the device interface. Such electric signals could be processed electronically as desired, making CSEDs more interesting for biological studies. CSEDs in the form of CHEMFETs with a suitable chemically selective membrane as their gates are generally being developed to analyse chemical concentration in a solution.
The principle of construction and operation of a CHEMFET is shown in fig. 1.7 /36/.

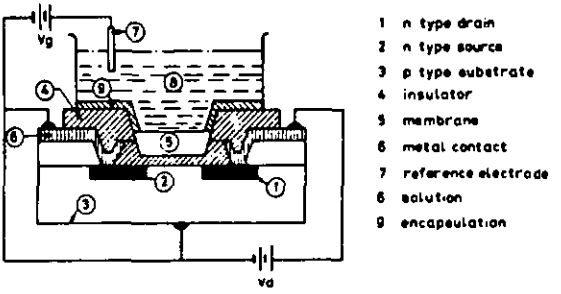

Fig. 1.7 Construction principle of CHEMFET /36/.

The solution to be analysed is placed in contact with the chemically selective membrane of the FET. The solution-membrane interface acts as an electrical resistance and the potential developed across the interface is related to the ionic activity on the interface. Because of the field effect, the drain current is varied proportional to the gate potential. Now, the electrical signal proportional to the chemical activity can be further processed in a conventional manner.
Thus, CHEMFETs can be used to measure pH values and possibly with further improvement in the technology, they could be used to measure hormone, protein and enzyme concentrations.

pH measurement: Though there is no significant change in pH, either in plasma or in urine over a menstrual cycle (fig. 1.3), some gynaecologists expect the uterine fluid to have a significant pH change during the ovulatory period /17/. This could be easily measured with a miniature CHEMFET or a simple gate-controlled diode (GCD), placed in the uterus. The pH characteristics of these CSEDs have already been proved for precision and repeatabiliity. However, such pH sensors in the uterus could be expulsed as in the case of IUDs, making pH measurement in the uterus a speculative method only.

Hormone concentration: The LH surge is a well-established reference for ovulation detection and is used in all the performance measurements of other methods of ovulation detection. Therefore, the development of a simple method to measure LH concentration will constitute a breakthrough in the field of ovulation detection.
The actual knowledge of CSEDs extended in the future to immunoreactive measurements (similar to those applied to RIA analysis) can perhaps give a simple solution for measurement of the LH concentration. If the chemically sensitive membrane is replaced by a specific anti-body membrane, the interfacial immuno-reaction of the antigen hormone (like FSH, LH) with the anti-bodies in the FET membrane will result in a drain potential varying according to the degree of antigen-antibody activity. But for the timebeing, it is not known how to re-activate the antibody interface layer so as to make a FET re-usable after a test. If CHEMFETs with a re-activatable antibody interface layer for immuno-reaction are developed, an excellent device could be found in such an "IMMUNOFET" for measuring any antigenic hormone concentration.
In theory, the antibody could be either natural or synthetic, depending on the type of antigen hormone to be analysed.

Enzyme/protein analysis: CSEDs can also be used to analyse enzymes, proteins, etc... with a suitable membrane to have an ionic activity, which gives rise to corresponding drain current variation. At the Twente University in Holland, tests are made to measure the albumin concentration in a compound. The threshold sensitivity achieved so far is in the order of 6 mg per litre of solution /26/.
The albumin concentrtion in the mucus is about 10µg per litre, which corresponds to a factor of a thousand times less than the sensitivity achieved so far.

1.5 Choice of a suitable parameter for electronic ovulation detection:

After looking into the various measurable parameters that characterize ovulation and into the techniques involved in their electronic measurement, a comparative study was done to choose the most suitable parameter. Except for body temperture all other parameters pose, when measured daily, either aesthetic problems or technical problems. Therefore, temperature measurement particularly as a differential measurement has been chosen in the study of ovulation detection. The details of this study are elaborated in the following chapters.

CHAPTER 2

This chapter presents a basic physics of thermokinetics. The reader can skip this chapter without losing any continuity for the main body of the thesis. The matter of this chapter is available in any standard physics textbook treating thermokintica, in view of human body temperature regulation.

2. HUMAN BODY TEMPERATURE AND ITS REGULATION

2.1 Basic physical phenomena

Temperature is an arbitrary scalar unit of measuring a thermal state of a body.

The study of heat transfer is called thermokinetics /42/. Heat flow is a function of temperature gradient between the points considered. Thermal equilibrium is the state in which there is no transfer of heat. With the existance of a thermal (temperature) gradient, there exists heat flow. Heat flow can occur by conduction, convection, evaporation and radiation, until thermal equilibrium is reached.

2.11 Conduction: Conduction is defined as the flow of heat through physical contact of molecules. Rate of heat flow by conduction is given by eq. 2.1:

$$H_{cond} = \frac{k}{x} \cdot (T_2 - T_1) \qquad (2.1)$$

where T_2 and T_1 are higher and lower temperatures (°C) and k is thermal conductivity of the media (W/m°C).

2.12 Convection: Heat flow through the movement of molecules is called convective heat flow. The rate of heat flow by convection is given by eq. 2.2:

$$H_{conv} = h_c \cdot (T_2 - T_1) \qquad (2.2)$$

where h_c is the convective coefficient and is in general a function of (T_2-T_1).

2.13 Radiation: Every object with a temperature more than absolute zero (0 K), radiates electromagnetic (EM) energy in all wavelengths. Heat transfer by radiation mainly occurs in wavelength region between 10^{-7} and 10^{-4} meters. The whole EM spectrum has been arbitrarily classified into few groups as shown in Fig. 2.1 /41/.

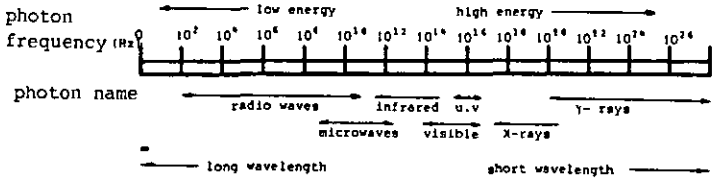

Fig. 2.1 Commonly used classification of electromagnetic (EM) spectrum into distinct wavelength bands and corresponding photon names.

A black body is an ideal type of heat radiator (emissivity=1), whose radiant flux is the maximum obtainable at any wavelength for a body at a fixed temperature.

2.14 Planck's law: The spectral radiant energy of a black body at a particular wavelength is a function of temperature and is given by Planck's law:

$$W(\lambda) = \frac{2\pi hc^2}{\lambda^5\left[\exp\left\{\frac{hc}{\lambda kT}\right\}-1\right]}\cdot 10^{-6} \qquad (2.3)$$

where $W(\lambda)$ = spectral radiant emittance (watts/m^2 μm)
c = the velocity of light (3×10^8 m/sec)
h = Planck's constant (6.6×10^{-34} joule sec)
k = Boltzmann's constant (1.4×10^{-23} joule/K)
T = the absolute temperature (K) of the black body
λ = wavelength (m)

Fig. 2.2 shows that the spectral radiant power increases with temperature and that the maximum radiation will be in the infrared (IR) region of the EM spectrum.

2.15 Wien's law: The wavelength at which maximum energy is radiated can be calculated by Wien's formula:

$$\lambda_{max} = \frac{2898}{T} \qquad (2.4)$$

where λ is in μm and T is in K.

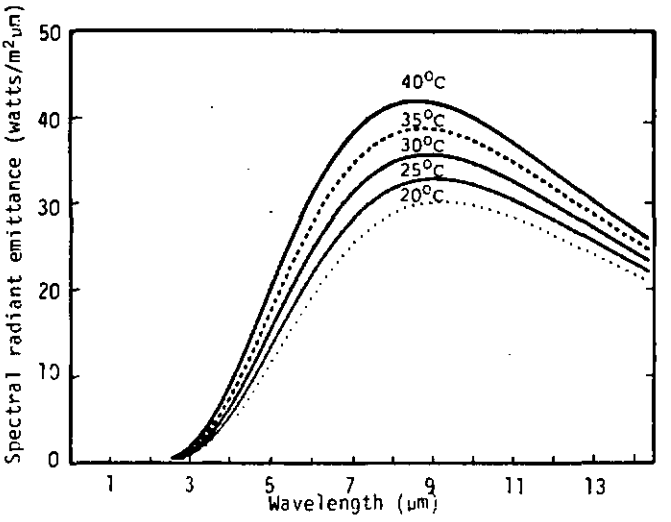

Fig. 2.2 Spectral radiant emittance of a black body as a function of wavelength and temperature, as obtained by Planck's law.

2.16 Stefan-Boltzman's law: Total energy emitted by a blackbody (ε=1) is proportional to the fourth power of its temperature and is given by the Stefan-Boltzman's law:

$$W_b = \sigma \cdot T^4 \tag{2.5}$$

where σ is Stefan-Boltzman constant (56.7×10^{-9} W $m^2 K^{-4}$).

2.17 Emissivity: In most of the cases, objects are not black bodies. They can have varying physical characteristics of transparence, reflection and asorption for different spectral incident energy. According to kirchoff's law, the coefficient of absorption is equal to the coefficient of emission /43/. Thus different surfaces have different emissivity characteristics. The emissivity factor of an object is defined as the ratio of the object's emitted power to that of the radiated power from the black body (at a given temperature), and is given by the equation:

$$\varepsilon(\lambda)_o = \frac{W(\lambda)_o}{W(\lambda)_b} \tag{2.6}$$

substituting eq. 2.6 in eq. 2.5, we can write for the energy emitted by a surfce other than a black body as:

$$W(\lambda)_o = \varepsilon(\lambda) \cdot \sigma \cdot T^4 \tag{2.7}$$

2.2 Temperature of the human body

Body temperature is a consequence of the heat energy that is continually being produced as a by-product of metabolism. The inner body temperature, often called 'core temperature', is independent of external ambient conditions, though it is very sensitive to the body's physical work rate /44,45/. Each organ of the body produces a different amount of heat energy depending on its metabolic rate (oxygen consumption). However, the circulating system within the body's core keeps the core temperature at 37±0.5°C at different parts of the body /46/. In contrast to this constant core temperature, the skin temperature is a function of external ambient conditions. Skin temperature is controlled by anatomical physiological functions in such a way as to keep a balance between the metabolically generated heat within the body and the heat loss to the environment from the skin. Thus skin, the 'largest organ' of the human body, functions as a thermal interface between the inner core and the external ambient conditions.

Thermal receptors in the skin sense the temperature and transmit this information to the temperature regulatory glands situated near the hypothalmus glands /42/. Depending on the feedback, the temperature control agent adjusts the blood circulation in the peripheral tissues for bringing back the equilibrium. In effect, the average thermal conductance of the peripheral tissues may thereby be changed by a factor of 5 or 6 in passing between full vasoconstriction and full vasodilation of the blood vessels /45,47/. Skin transfers heat to the environment through radiation, evaporation and convection, radiation being the major factor. The emissivity of the skin is very nearly equal to 1 (0.989±0.01) /48/. Because of this constant value of emissivity, the skin temperature and infrared (IR) radiation can be easily studied together using Planck's law.

In a warm environment skin temperature is on an average 2°C lower, and in a cold environment it can be on an average as low as 6.5 °C lower than the core temperature. Fig. 2.3 shows the balance mechanism /46/ of heat in the human body. Fig. 2.4 shows the thermal emissivity and reflectivity characteristics of the human skin /48/. Fig. 2.5 shows measured temperatures at different parts on the skin surface /42/.

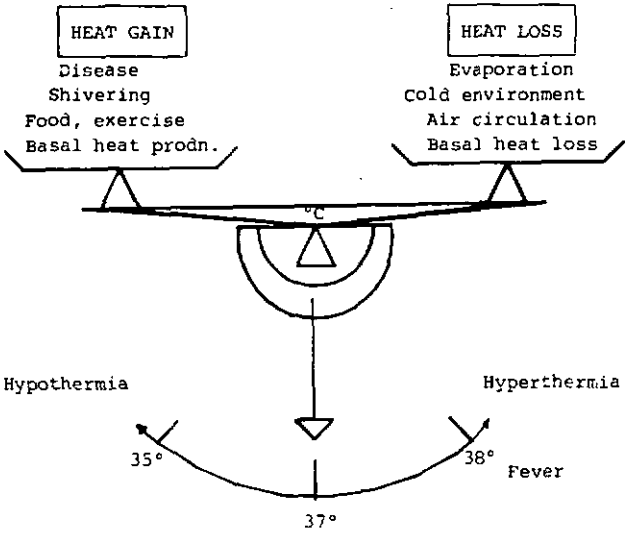

Fig. 2.3 Heat balance mechanism in the human body /46/.

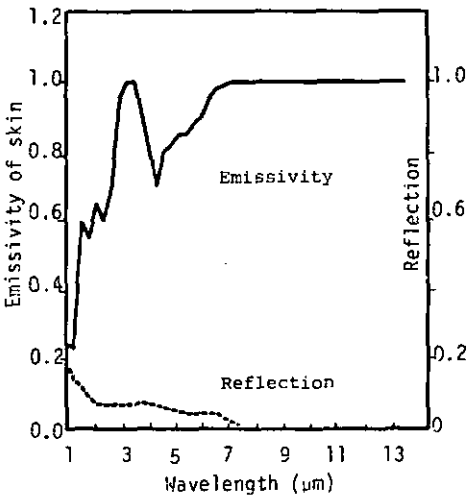

Fig. 2.4 Typical variation of emissivity and reflection coefficients of human skin in the infrared EM spectrum.

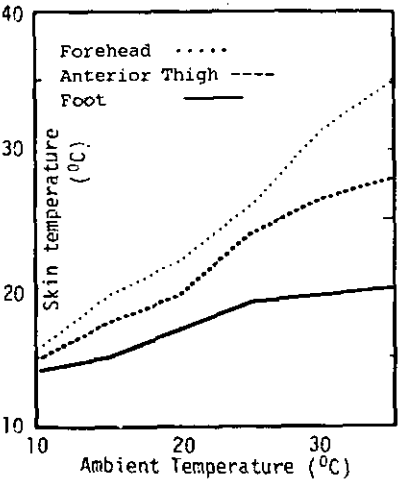

Fig. 2.5 Static local mean skin temperature estimates as a function of ambient temperature /42/.

2.3 Temperature regulation equations

The body is said to be in the thermal steady-state (thermal equilibrium) when the heat gained by the core through metabolism (tissue oxidation) is equal to the heat lost to the environment. In this case both core temperature and skin temperature will be constant with time. If one represents heat production by metabolism by H_m and heat lost to the environment by H_l, then

$$H_m = H_l \qquad \text{for thermal equilibrium.}$$

where H_l is the sum of heat losses due to conduction (K), convection (C), evaporation (E) and radiation (R).

In a transient condition the steady state is not reached and the heat is stored in the body (there can be positive storage, i.e: heat gain ; or negative storage, i.e: heat loss).
The heat storage (S) can be represented by the equation /42/:

$$S = mc \cdot \frac{dT}{dt} \tag{2.8}$$

where m = mass and c = specific heat.

2.4 Hypothermia

Hypothermia is defined as the condition in which the core temperature falls cosiderably below the normal core temperature during rest in a thermoneutral environment /42/.
Hypothermia generally occurs as a result of external cold stress. In such a case, heat loss to the environment will be higher than the metabolic heat production ($H_m < H_l$). The thermal regulating system of the body counteracts the cold stress through the physiological reaction of vasoconstriction, limiting the blood flow to peripheric tissues. This reduces the heat transfer from core to skin with a corresponding fall in differential temperature between the skin and the environment and thus reducing the heat loss. If the cold stress is more than the physiological compensation that can be achieved by vasoconstriction, the body is bound to produce more heat for thermal neutrality and this corresponds to the shivering of the body.

2.5 Hyperthermia

Hyperthermia is defined as the condition in which the core temperature rises considerably above the normal core temperature during rest in a thermoneutral environment /42/.

Hyperthermia generally occurs as result of external heat stress due to increase in environmental temperature. In such a case, heat loss from the skin to the environment is reduced ($H_m > H_1$), due to the lower differential temperature between the skin and the environment. As the metabolic heat production cannot be decreased, the thermal regulating system of the body counteracts the heat stress through the physiological reaction of vasodilation, increasing the blood flow to the peripheric tissues. This increases the heat transfer from the core to the skin, thereby raising the temperature difference between the skin and the environment to increase the heat loss so as to reach a thermal steady state.

If the heat stress is more than the physiological compensation that can be achieved by vasodilation, the sweating mechanism will start functioning. Sweat glands secrete the sweat and secretion further increases with the rise in environmental temperature. By this mechanism, the skin is cooled to keep up a high rate of heat transfer from core to skin and more heat is lost to the environment by evaporation, in addition to normal convection and radiation losses.

2.6 Basal body temperature

Basal body temperature (BBT) refers to the core temperature measured in the morning hours after a good sleep, in comfortable ambient conditions. Metabolic heat production, in such a cordition is mainly due to basal functioning of the cells, organs, respiratory and circulatory systems of the body /44/. Other parameters influencing the core temperature are : time of the day (circadian rhythm), menstrual cycle status in case of women (circatrigintan rhythm) and age.

Circadian rhythm: Core temperature shows a cyclic change over 24 hours time (a day) and such changes are referred to as the circadian rhythm. So, for useful measurement of BBT, time factor is important and suitable correction should be provided /49/.

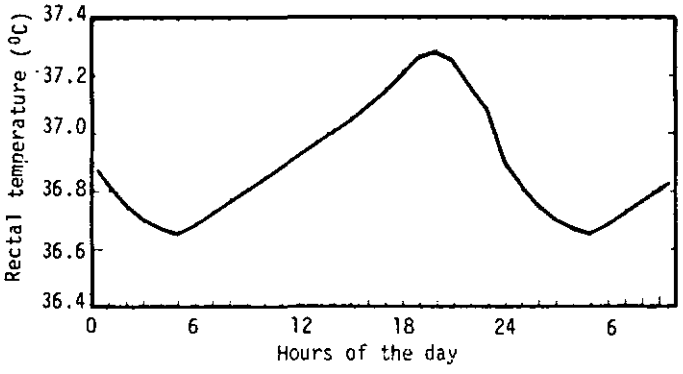

Fig. 2.6 Typical circadian rhythm of core temperature /42/.

Circatrigintan rhythm: Core temperature changes corresponding to hormonal effects controlling the menstrual cycle are referred to as the circatrigintan rhythm. Two principal hormones that influence the body temperature are estrogenic hormones in follicular phase and progesterone hormone in leutal phase of the menstrual cycle. Estrogenic hormones have the characteristic of increasing the blood flow /4/, particularly in the genetic organ like vagina and endocrine target organ like breasts (mammary glands). Due to this increased blood flow, heat transfer from core to skin increases with a corresonding skin temperture change in those areas. However, no change in the core temperature due to estrogenic hormones has been observed (except that there is a drop of 0.1 to 0.2°C in BBT on the day of the peak LH surge; this drop has so far no explication). On the other hand, the progesterone hormone in leutal phase is thermogenic in nature and raises the core temperature by 0.3 to 0.5°C. This rise in BBT is currently being used in estimating the post-ovulatory infertile phase of the menstrual cycle.

CHAPTER 3

This chapter presents our hypothesis of 'differential skin temperature (DST)' measurement for ovulation detection; it forms the basis for following chapters.

3. TEMPERATURE MEASUREMENT

3.1 Basal Body temperature measurement

Basal body temperature (BBT) is defined as the body core temperature, measured in a thermally neutral condition corresponding to a thermal equilibrium at the skin interface. Normally, the human body will be in a thermal equilibrium in the morning after a good sleep, in thermally comfortable ambient conditions. Thus, BBT can conveniently be referred to as the body temperature measured in the morning after a good sleep. BBT measurement reflects the cellular organ activity corresponding to chemical and hormonal reactions. Metabolism is also a function of time during the day and so BBT also shows the circadian variations as given in Fig.2.6. For useful information to be obtained from BBT, the measurement should be done in regular hours of the morning. Otherwise corrections to the measurements should be made /49/. BBT can be measured at several sites (rectum, vagina or mouth). The measurements generally change constantly but differ slightly from one another /42,46/. BBT values recorded at different sites by a motivated volunteer and corrected for the circadian variation /49/ are shown in Fig. 3.1.

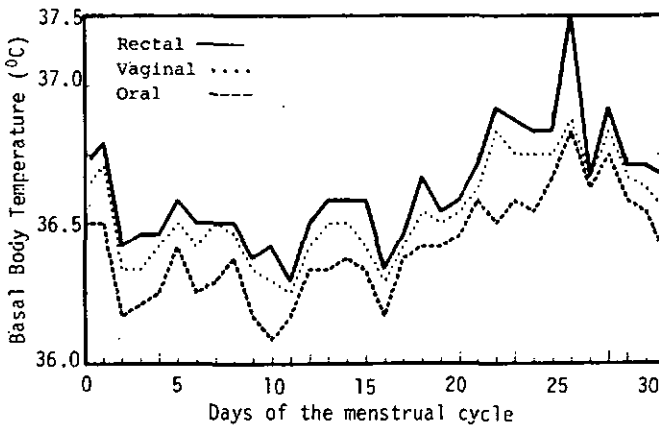

Fig. 3.1 BBT recording obtained from a volunteer over a menstrual cycle; measurements were done at three different sites: a) rectum, b) vagina and c) oral.

In the ovulatory menstrual cycle BBT shows a clear biphasic pattern and so BBT is well accepted as a measure of hormonal activity in determining the status of the menstrual cycle. The progesterone hormone rises in the leutal phase of the menstrual cycle; as this hormone is thermogenic in nature, the core temperature also rises by 0.3 to 0.5 °C. This rise of BBT, over the values obtained during the previous days of the cycle confirms the rise in plasma progesterone level and hence it indicates the beginning of the post-ovulatory infertility phase of the menstrual cycle.

3.2 Skin temperature measurement

Thermal properties of the human breast

The breast skin surface temperature has been studied as a function of the underlying pathological, physiological changes in the body /52-55/. The breast skin surface temperature is a function of core temperature, blood circulation, underlying tissue pathology and environmental thermal conditions. Therefore, breast skin temperature also has circadian, circagnitan changes for given ambient conditions. Thermographic mapping of breast temperature shows a wide degree of temperature distributions over the breast skin surface. Such a thermal distribution image is called a "breast thermogram" and is generally obtained by detecting infrared radiation emitted from the skin surface, by suitable scanning techniques (see chapter 6, for details).

Average breast temperature has been observed to rise during the pre-ovulatory phase /56/ and this rise has been attributed to the bloood circulating in the cutaneous blood vessels rather than to tissue conduction /57/. Estrogen hormone and in particular 17-β estradiol hormone induces a higher vascularity in the endocrinological target organs like breasts /54/. This has been confirmed with studies /58/ made, involving the external injection of estrogen steroids. This estradiol-induced vascularity (increased blood flow) transfers more heat to the skin surface above the cutaneous blood vessels than in other parts where the heat transfer is only due to tissue conduction (avascular areas); thus the average breast temperature increases by a few tenths of a degree C. However, these studies were made in controlled clinical conditions, in such a way that the ambient temperature did not influence the skin surface temperature measurement. To overcome the influence of ambient temperature, differential skin temperature measurement on the breast skin surace is proposed in this thesis.

3.3 Differential skin surface temperaure measurement: An hypothesis

Human breast skin surface temperature measured in basal condition varies as a function of tissue conduction and cutaneous blood flow through capillary action. During the menstrual cycle of a woman, the blood flow in the breast region is observed to vary as a function of hormonal concentration in the plasma. Hence, we can expect the different levels of vascularity and corresponding change in thermal distribution over the breast's skin surface during the menstrual cycle.

The follicular phase of the menstrual cycle has the least hormonal activity and so will have less vascular activity. During this phase, the thermal distributions over the breasts can be expectd to be in the form of isothermal rings, corresponding to heat flow through tissue conduction only as shown in Fig. 3.2a.

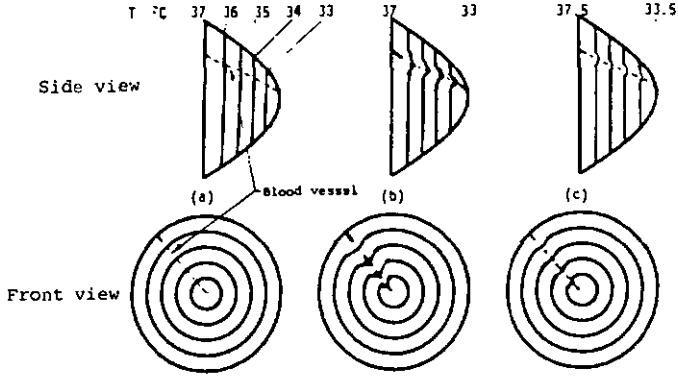

Fig. 3.2 Hypothetical temperature distribution on the breast's skin surface, over the different phases of the menstrual cycle.
a) avascular condition, corresponding to the follicular phase,
b) vascular condition, referring to the ovulatory phase, and
c) moderately vascular condition, corresponding to the leutal phase.

The ovulatory phase of the menstrual cycle involves the peak hormonal activity. Estrogen hormones in particular increase the blood flow in the cutaneous blood vessels and hence disturb the isothermal thermal distributions over the breasts, in those particular regions with cutaneous blood vessels. The hypothetical thermal distributions with superposed thermal maps due to estradiol-induced vascularity are shown in Fig. 3.2b.

The post-ovulatory phase has both estrogen and progesterone hormones present in the plasma. The progesterone hormone is thermogenic in nture and hence raises the body temperature by few tenth's of a degree. At the same time the tissue conduction coefficient increases /54/, thereby increasing the skin temperature also. Estrogen hormones have lesser influence in vasodilation of the blood vessels in this phase /57/. Therefore the thermal distributions on the breast skin surface will be similar to those during the follicular phase with small distortions and with a relatively higher thermal level as shown in Fig. 3.2c.

Based on the above observations, we can interpret the thermal distributions over the breast's skin surface as follows: Isothermal rings corresponds to the tissue conductive temperature distribution (minimum blood flow) and any distrotions of these rings supposed to be caused by vascular activity (increased blood flow).

Measurement of the temperature difference between these distorted temperature areas corresponding to dynamic temperature spots (caused by estradiol-induced vascularity) and undistorted isothermal ring areas corresponding to static temperature spots should hence reflect estrogen hormonal activity in the body. With this prinicple, we make an hypothesis to correlate the temperature difference measured to the estrdiol hormone concentration and hence to estimate the ovulation time.

Our hypothesis states that the temperature difference measured between a 'dynamic point' referring to the vascular sensitive temperature area with cutaneous blood vessel and a 'static point' referring to the avascular temperature area without any cutaneous blood vessel correlates with the estradiol hormone concentration in the plasma and hence with the ovulation time.

We call the temperature difference measured between a 'dynamic point' and a 'atatic point' as differential skin aurface temperature (DST) henceforth.

Because of differential measurement principle, the influence of ambient temperature on the DST measurement will be insignificant.

Selection of dynamic and static temperature areas for DST measurement has a major role in establishing the significance of DST measurement as

an indicator of hormonal response and hence as a parameter for advance detection of ovulation timing. Telethermographic infrared imaging can be used to detect reliably, the dynamic temperature spots and the static temperature spots over the menstrual cycle.

Based on the above hypothesis of DST measurement for ovulation detection, a detailed study is carried out to verify the significance of DST through clinical experiments, mathematical modeling and computer simulation of hypothetical breast thermograms and detailed computer-assisted image analysis of thermograms. All these points are explained in the following chapters.

CHAPTER 4

This chapter presents the details of the clinical tests conducted and the results thereby obtained. The results presented in this chapter have been published in the following publications:

"Determination of fertility interval with ovulation time estimation using differential skin surface temperature (DST) measurement."
Fertility and Sterility, Vol. 41, No. 5, May 1984, pp. 771-774.

"Correlation study of differential skin temperature (DST) for ovulation detection using infrared thermography."
Proc. of ISMII'82 Berlin Conference, 1982, pp. 129-131.

4. CLINICAL EXPERIMENTS AND RESULTS

4.1 Infrared Thermography

Human skin has the radiation characteristics that correspond approximately to those of a black body, in the infrared (IR) range of 2 to 40 µm wavelength, as explained in §2.2. Therefore, the temperature distribution on the skin can be well studied by detecting the infrared radiation from the skin surface. Temperature measurement with sensors in contact with the skin (like thermistors, thermocouples or transistors), disturb the thermal equilibrium on the skin interface. Also, it is very difficult to obtain the temperature distribution over the interested area with a high spatial resolution, when measurements are done with contact sensors of a finite size. The problems of disturbing the thermal equilibrium and that of limited resolution due to the size of sensors can be overcome by remote thermal scanning of the interested area. However, IR radiation undergoes high attenuation in the atmosphere except in the two atmospheric IR windows with the wavelength ranges of 2 to 5.6 µm and 8 to 14 µm /41/, which are therefore commonly used in remote thermal scanning. The peak IR radiation from the human skin occurs at a wavelength of around 9.7 m corresponding to a skin temperature of 300 K, according to Wien's law /42/. So, in our clinical experiments we have used a thermography system (AGA 782) that is sensitive in the wavelength range of 8 to 14 µm. The detailed description of 'AGA 782' infrared tehrmography (IRT) system is given in chapter 6.

4.2 Selection of Volunteers

The principle interest of our study being the detection of ovulation for natural conception/contraception among healthy and regularly menstruating women, the selection of volunteers in the first phase of the experiment, was done among non-pharmaceutical contraceptive users only . Six volunteers in the age group of 20 to 35 years who were healthy, regularly menstruating and interested in the practice of natural contraception, took part in this investigation. One of the volunteers was breast-feeding her baby. This person was included to observe the temperature cycle as a function of lactation.

In the second phase of the experiment, 10 volunteers were chosen irrespective of their contraceptive methods in use. They included 3 pill users, 3 natural birth control (NBC) practitioners , 3 intrauterine device (IUD) users and one without any particular method in use (she had no sexual relationships with the opposite sex). This choice was allowed us to study the effects of various contraceptive methods in practice.

4.3 Experimental protocol

All the volunteers who took part in this experiment were briefed about the difference between ionizing and non-ionizing radiation type of medical imaging. This we felt necessary to make it clear to the volunteers that no EM energy is being transmitted through their breasts while thermal scanning, and hence there is no side-effect of any sort, as in the case of Mammography. This enabled the volunteers to participate in the experiment with a high degree of motivation without any anxiety or hesitation.

The volunteers took their BBT before waking up from the bed every morning, and noted down remarks on the time of measurement, on any long journies made, drugs consumed, etc... These remarks were called for, to improve the interpretation of the BBT records later on. They were asked to lead a normal life, without being overly consious about the experiment. They came to the hospital in the early hours of the morning (between 7:30 a.m and 9:00 a.m) without consuming any drinks/food (so as to maintain very nearly a basal state of metabolism), on the predefined days of the menstrual cycle. These defined days being: once in three days between days 1 and 11 (follicular phase), every day between days 12 and 18 (the generally expected period of ovulation), and then once in two days until the end of the menstrual cycle (leutal phase).

Once they came to hospital, they relaxed for 15 minutes bare-breasted for temperature stabilization and then posed their breasts for IR thermographic scanning in arms raised position as shown in Fig. 4.1. Then contact temperature measurement was done at few selected points. Later on volunteers gave 10 ml of blood samples, which were stored centrifuged and analysed later on for plasma hormonal concentration to obtain the reference ovulation time.

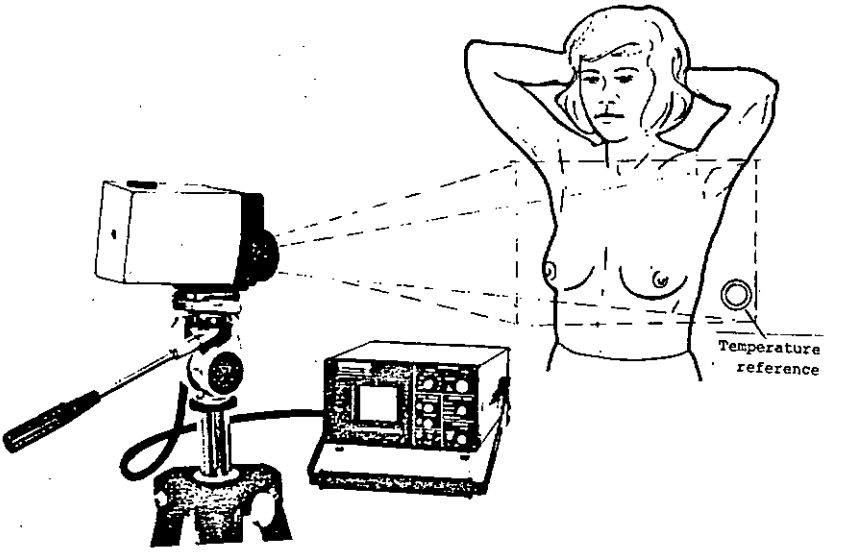

Fig. 4.1 Infrared imaging of breasts in arms-raised position, as adopted during our clinical tests.

4.4 Infrared imaging procedure and video recording

The infrared thermography system was installed in a spacious room with normal central heating. The room temperature was observed to vary between 19°C and 23°C on different days of the experiment. No special attention was taken to regulate the room temperature more precisely. The walls were observed not be to have any IR reflecting surface that could disturb our measurements.

Volunteers, after arriving in the hospital rested in a room next to the IRT imaging room, bare-breasted for about 15 minutes. This was necessary to bring back the metabolic rate to approximately that of the basal state and to obtain temperature stabilization in the new environment /59/. After the expected temperature stabilization, they stood in front of the IR camera at a distance of 1.5 metres and posed for thermal imaging in a hands-raised position, to confirm with the recommended procedure /41/. The operator took care not to interfere himself with

the detected IR radiation and thus create artifacts in the IRT image (e.g. the case when he stands behind the camera and thus providing a reflecting media).

The reference object with black body characteristics (emissivity =1) was situated next to the volunteer (at the same distance of 1.5 metres) and the reference temperature was set to the mean temperature of the breasts. Thermal level of the IRT system was adjusted to obtain this reference temperature as '0' isotherm on an IRT image when scanned. Thermal range was always set to '5' so that there would not be any saturation levels appearing in the IRT image. Breasts were scanned for front and side views, for better analysis of temperature distribution on the breasts. The hard copy of the IRT image was recorded on a polaroid film and stored with proper identification of the volunteer and date of the record.

The composite video signal from IRT system was recorded on the video magnetic tape for computer-assisted image analysis to be carried out later on. Thermal settings of the IRT system (thermal range and level) were noted for quantitative analysis of the breast thermogram.

4.5 Contact temperature measurement

Based on the IRT image, a few points were located for contact temperature measurement. Fig. 4.2 shows the points so selected: 'a' is a vascularly sensitive point (which we call 'dynamic point': situated over the cutaneous blood vessels in the area of the areola), 'b' is a point on the sternum and 'c' is a point just below the breasts. Both 'b' and 'c' are supposed to be static points corresponding to the avascular area. Measurement was done with a precise electronic thermometer (Ultrakust, model 4012). The temperature difference (DST) between 'a' and 'b' and between 'a' and 'c' were calculated.

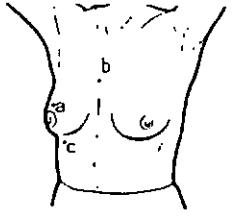

Fig. 4.2 Points of temperature measurement with a contact-sensor thermometer.

4.6 Serum collection and Storage

Blood samples of 10 ml was collected on each day of the IRT investigation. They were centrifuged for 5 minutes at approximately 1000 g pressure within 10 minutes of sample collection and the plasma was stored at -20°C. Each tube containing the plasma sample was properly labelled to provide correct identification of the volunteer, date of extraction and the maximum time within which, the hormonal assays should be carried out for correct results.

4.7 Radioimmunoassay

Plasma samples stored during the experiment were sent for hormonal assays at the end of the duration of the experimental. The assays were conducted for 17-β estradiol, Leutinizing hormone, Follicle stimulating hormone and progesterone hormones. The peak day of LH surge was taken as a reference for ovulation time estimation /5/.

4.7a Methods used in the radioimmunoassay: All RIA methods essentially depend on a reaction between a labelled hormone (e.g. ^{125}I standard hormone) and antibody specific to the hormone.
The reaction can be written in the form:

Labelled hormone (F) + hormone antibody ↔ labelled anigen-antibody complex (B)

+

Unlabelled hormone

↕

Unlabelled antigen-antibody complex

The ratio between labelled hormone bound to antibody (B) and the free ^{125}I labelled hormone (F) falls progressively in proportion to the increase in the concentration of the unlabelled hormone. The ratio B/F is plotted against the hormone content of the standard hormone. From the plot, actual concentration of the specific hormone is determined. The plasma samples of the volunteers stored during the experiment were analysed using DAB/PEG method /50/, which is a standard RIA method with 'Serono diagnostics' company /50/, who analysed our samples.

4.8 Results

Observations on one of the volunteers, who was breast-feeding her baby were discontinued after few days of observation, because of the random temperature changes observed on her breasts.

Breast thermograms of one of the volunteers as observed by AGA IRT system are shown in Fig. 4.3 (as typical examples of menstrual cycle dependent breast thermograms). Thermogram 'a' with a few isothermal rings (in a graded grey scale) confirms our expectation of temperature distribution on the surface of the breasts, through tissue conduction. These isothermal rings get distorted over the following days due to the estradiol-induced vascularity as observed in the thermograms 'd','e' and 'f'. After the day of ovulation, vascularity due to estradiol is again minimum and the pattern of isothermal rings is again observed in the breast thermograms, as can be observed in thermograms 'g' and 'h'. However, post-ovulatory thermograms have a higher mean temperature compared to the pre-ovulatory phase thermograms, because of increased level of plasma progesterone which is thermogenic in nature.

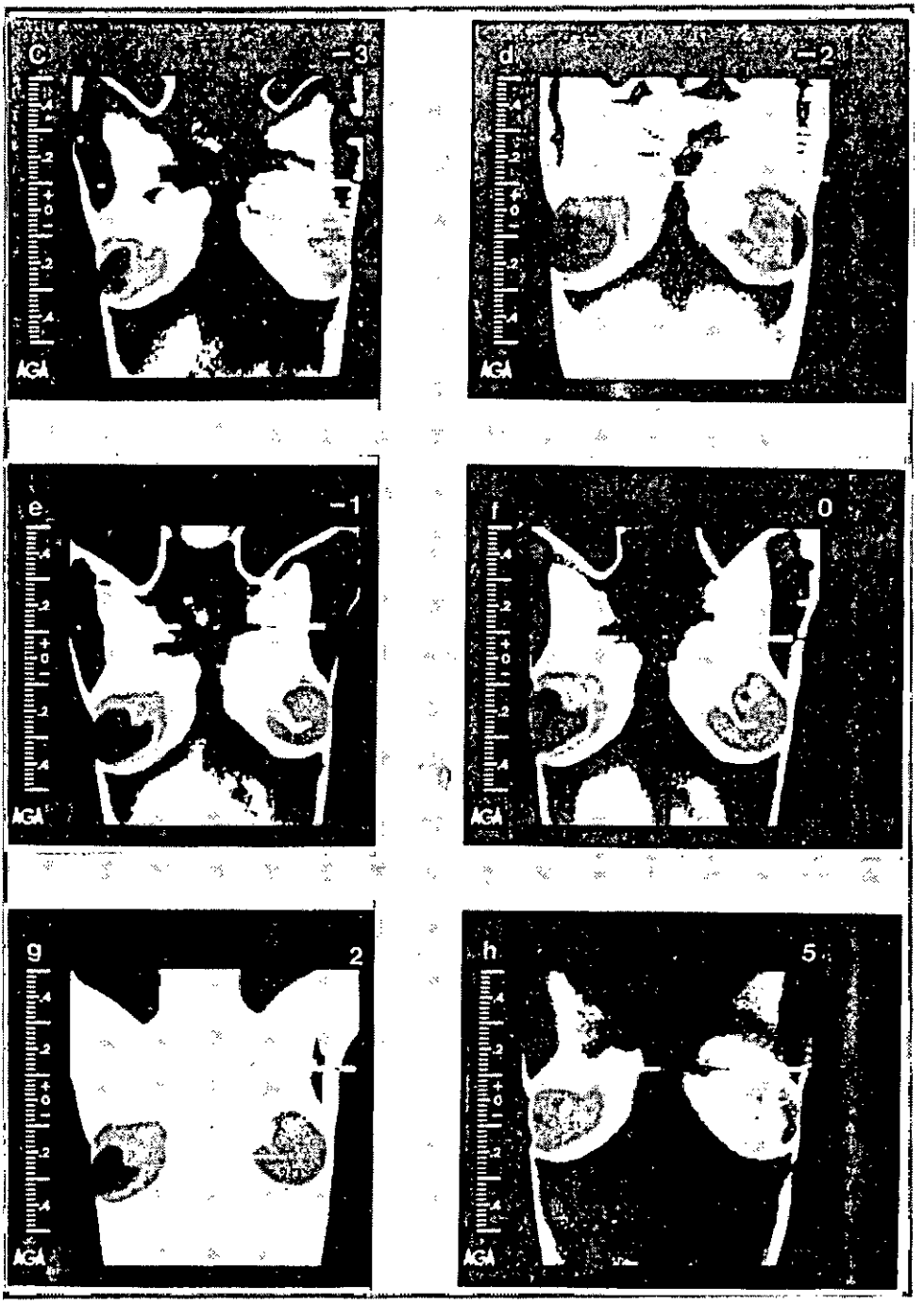

Fig. 4.3 Menstrual-cycle dependent breast thermograms of one of the volunteers: Numbers on the image represent the day of the menstrual cycle counted with respect to the day of LH surge.

Individual data of each of the volunteers were analysed for their completeness or proper validity. Those which were incomplete or not valid due to irregular physiological conditions as observed on the BBT records of the volunteers were eliminated and not used during the further analysis. Individual data collected on the hormonal concentrations, on DST and on BBT are presented in Appendix A.

The mean DST between point 'a' and 'b' (i.e., $T_a - T_b$), the BBT, and the hormonal variations over a menstrual cycle, averaged for ten volunteers, are as shown in Fig. 4.4. Only the middle part of the menstrual cycle

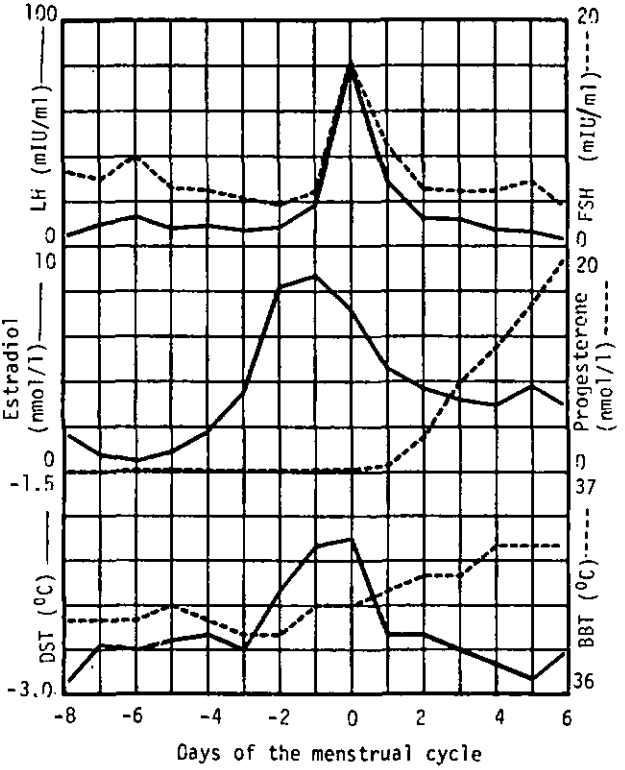

Fig. 4.4 Variation of hormone concentration in the plasma (LH and FSH at the top, estrogen and progesterone in the middle), BBT and DST (bottom) during the middle part of the menstrual cycle. The data plotted are the average of the data obtained from 10 volunteers, who were all non-pharmaceutical contraceptive users.

was complete with respect to data and hence the plotted results are restricted to the middle part of the menstrual cycle only. Day '0' represents the day of the leutinizing hormone surge, a reference value, obtained by standard radioimmunoassay. It can be seen that between days -3 and -1, estradiol (E_2) curves rose concurrently. The degree of rise in DST was related to the level of E_2 in the individual volunteers and the correlation between them was significant as can be seen in table 1. Student's 't' distribution was used in the statistical analysis (for obtaining mean, standard error mean (SEM), standard deviation (SD) and correlation coefficient (r) as shown in tables 1 and 2) of the data collected and in calculating the significance of the DST measurement /90/. Formulae used in this analysis are explained in Appendix B.

Table 4.1 : Individual volunteer's data in the middle part of the cycle.

Volunteer	E_2 (10 nmol/l)		DST (T_a-T_b)°C		Corr. coefficient (r)
	Mean	SD	Mean	SD	E_2- DST
B.S (Ne)	0.21	0.17	-2.82	0.51	0.94
G.R (Ne)	0.47	0.31	-2.77	0.62	0.63
M.N (Ne)	0.49	0.41	-2.62	0.40	0.86
K.P (Ne)	0.58	0.58	-2.44	0.51	0.86
C.B (Ne)	0.33	0.37	-2.35	0.47	0.88
P.C (Be)	0.44	0.25	-1.24	0.39	0.69
S.T (Be)	0.61	0.28	-1.32	0.50	0.82
L.N (Be)	0.98	0.53	-1.40	0.39	0.56
Y.V (Be)	0.52	0.24	-1.26	0.42	0.81
B.C (Be)	0.3	0.13	-1.58	0.29	0.88
8.D*(Be)	0.70	0.89	-1.35	0.41	0.61

* This volunteer is not considered in fig. 4.4, due to insufficient data

[Note: The volunteers of Neuchâtel participated in the basal condition, whereas the volunteers of Bern participated during their working hours, in the experiment. This may be the reason for the difference in the degree of sensitivity in DST between these two sets of experiment.]

The changes in DST were significant ($P << 0.02$, calculated with respect to day 0), compared with the BBT variations. The individual and mean statistical analysis comprising E_2, DST and BBT are given in tables 1 and 2. The BBT records were corrected for circadian variations before the statistical anlaysis.

Table 4.2 : Mean E_2, B8T and DST during the middle part of the cycle.

DAY	E_2 (10 nmol/l)		B8T (^{0}C)		DST (^{0}C)		P <
	Mean ± SEM	SD	Mean ± SEM	SD	MEAN ± SEM	SD	
-5	0.34 ±0.09	0.27	36.36 ±0.07	0.25	-2.0 ± 0.28	0.85	0.001
-4	0.42 ±0.07	0.21	36.47 ±0.07	0.23	-1.92 ±0.20	0.63	0.001
-3	0.51 ±0.07	0.23	36.49 ±0.05	0.15	-2.08 ±0.17	0.54	0.001
-2	0.74 ±0.12	0.37	36.45 ±0.05	0.17	-1.62 ±0.17	0.54	0.001
-1	0.84 ±0.14	0.45	36.43 ±0.07	0.23	-1.41 ±0.22	0.77	0.005
0	0.79 ±0.12	0.40	36.45 ±0.06	0.19	-1.30 ±0.24	0.81	-
1	0.53 ±0.15	0.44	36.60 ±0.04	0.14	-1.81 ±0.22	0.69	0.001
2	0.39 ±0.11	0.34	36.70 ±0.05	0.16	-1.92 ±0.19	0.63	0.001
3	0.29 ±0.05	0.15	36.74 ±0.06	0.19	-2.03 ±0.26	0.77	0.001
4	0.18 ±0.05	0.10	36.82 ±0.03	0.10	-1.60 ±0.28	0.57	0.001
5	0.22 ±0.08	0.13	36.78 ±0.03	0.11	-1.53 ±0.22	0.39	0.001

SEM = Standard Error Mean, SD = Standard Deviation

Fig.4.5 shows the curves of DST, BBT and hormonal levels obtained with one of the volunteers (typical case).

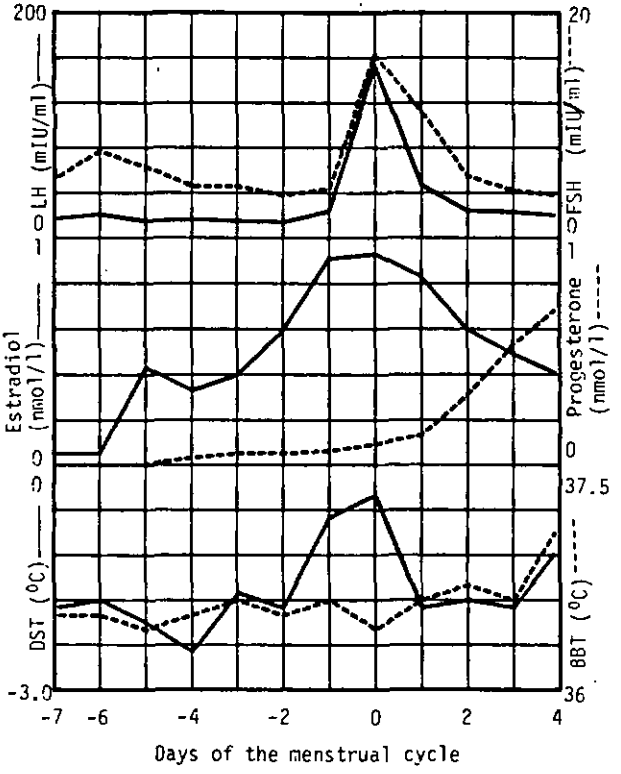

Fig. 4.5 Hormonal levels, BBT and DST as measured with one of the volunteers in the middle part of the menstrual cycle.

The DST and BBT variations over the middle part of a menstrual cycle for a particular volunteer who had mild fever for one day during the observation cycle are plotted in Fig. 4.6. It can be seen that the BBT change due to fever is not reflected in the DST curve of the same volunteer. This indicates that in at least one case DST was not affected by transient physiologic changes. This could prove to be a significant advantage of the DST as compared with the BBT.

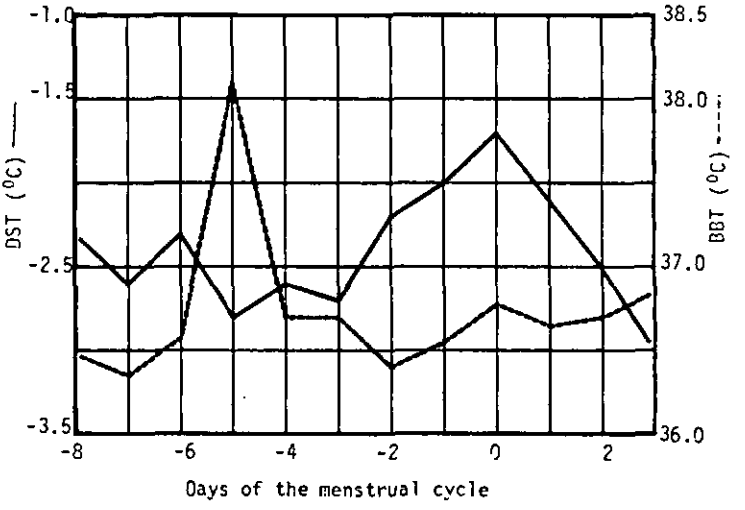

Fig. 4.6 BBT and DST values measured with a volunteer who had mild fever over one day in a particular cycle.

The hormonal assay of plasma of one of the volunteer showed the anovulatory cycle. The corresponding BBT, DST and the hormonal levels are plotted in Fig. 4.7. It can be observed from the figure that careful analysis of DST chart can indicate the anovulatory cycle without the need of hormonal analysis of the blood samples.

The DST and BBT averaged for all 3 pill users did not have any systematic and significant variations over a menstrual cycle. The mean of DST and BBT averaged for all 3 pill users are as shown in Fig. 4.B. This data confirms other researchers' results that there will be no significant change in breast temperature among pill users /29/.

We did not observe any particular special effect of an intrauterine device on the breast temperature among the users of this mechanical contracetive.

The temperature distribution changes were observed (by IRT) to be almost symmetric on the two breasts, and hence thermometric measurements were done only on the right breast.

All temperature measurements so far described refer to the contact thermometric measurements. The breast thermograms recorded on the video magnetic tape during the clinical experiment are analysed later on with in-house developed computer assisted thermography (CAT) system. The details of the CAT system, image processing features and the results based on computer-assisted analysis of breast thermograms are given in chapter 6.

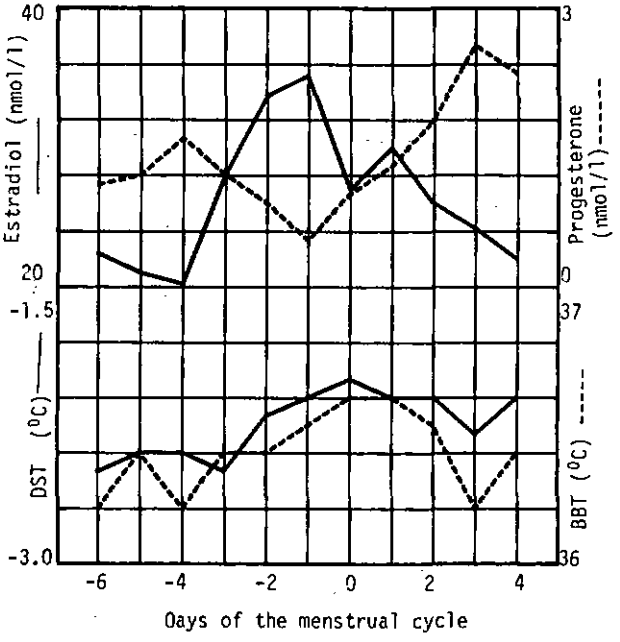

Fig. 4.7 Bormonal levels in the plasma , BBT and DST values measured with a volunteer, with whom the ovulation was not confirmed by RIA analysis of plasma samples (i.e: the cycle was anovulatory).

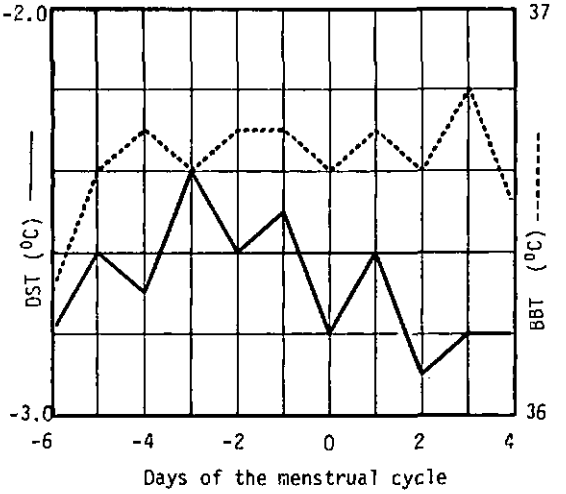

Fig. 4.8 BBT and DST variations with pill users over a menstrual cycle. The data plotted is the average of the data obtined from 3 pill users.

4.9 Discussion

The DST behaviour observed can be explained as follows: referring to Fig 4.2, point 'b' is in a vascularly insensitive area, and T_b threfore provides a 'static' temperature. Point 'a' lies over a vascularly sensitive area, and so T_a represents a 'dynamic' temperature. During the early follicular phase, there is no strong vascular action, and T_a remains low. T_b being always higher than T_a, $(T_a - T_b)$ is low (and negative). During the pre-ovulatory phase, the vascular activity reaches a peak corresponding to E_2 activity, and T_a increases due to convective heat transfer, increasing $(T_a - T_b)$ to its peak value (however, negative). In the post-ovulatory phase, the 'static' temperature T_b increases due to the increased level of progesterone, resulting in a lower value $(T_a - T_b)$ once again.

If the experiments are conducted with pregnant, lactating and aged (beyond menopause) women, results similar to those obtained with oral contraceptive users (i.e., no significant varaitions in DST over the menstrual cycle) can be expected /29/.

A remark that might have some importance for tropical countries may be appropriate here. If one makes similar thermometric studies in hot environmental conditions, where the ambient temperature is higher than the body temperature, the inverse action should take place. The convecting blood flow basically takes away heat, and hence a cooling effect should be observable at point 'a' in Fig. 4.2. Even in this case we speculate that the proposed DST method holds good because of its 'dynamic' measurement principle. This hypothesis remains to be confirmed.

When the ambient temperature is of the order of 37 °C, the sensitivity of DST will be small and may pose problem to correlate with the hormonal levels and hence with ovulation time.

CHAPTER 5

This chapter presents a simple mathematical modeling and computer simulation of hypothetical breast thermograms, to explain the temperature variations on the breast's skin surface over the menstrual cycle. Most of the matter contained in this chapter was presented as a conference paper at the International Thermography Congress in Lucern, under the title:

"Menstrual cycle related breast thermograms: Mathematical modeling, computer simulation and experimental verification."

The same paper has been published in an International Journal " Infertility ", Vol. 8, pp 235-248, 1985 later-on.

5. MATHEMATICAL MODELING AND COMPUTER SIMULATION

5.1 Mathematical Modeling: Introduction

In general, heat transfer processes in biomaterials are the result of complex interactions between tissue conduction, tissue perfusion (involving capillary blood flow as well as arterial and venous blood flows) and tissue metabolism. Biomaterials being antisotropic and inhomogeneous in nature, the understanding of complicated heat transfer phenomena in biomaterials becomes difficult /60/.

In thermal modeling of a biological system, simplifications are generally applied with respect to material homogeneity, metabolism, tissue perfusion rates and the boundary conditions. These simplificatons allow one to represent the actual physical or physiological situation, by mathematical equations in the form of partial differential equations. Based on these simplifications, the temperature of the material as a function of space and time can be represented by applying the first law of thermodynamics. The resulting equation will be in the form of

$$\frac{\partial T}{\partial t} = \alpha \cdot \nabla^2 T \qquad (5.1)$$

where T is the instantaneous temperature and is the effective thermal diffusivity ($\alpha = k_{eff}/\rho \cdot c$ where k_{eff} is the effective thermal conductivity, is the specific density and c is the specific heat of the material).

This simple model is valid only for specific conditions: no blood flow, absence of tissue metabolism and isotropic medium.

To improve the modeling towards a real situation, Pennes /61/ separated the heat production into metabolism and tissue perfusion, resulting in eq. 5.2.

$$\rho c \cdot \frac{\partial T}{\partial t} = k \cdot \nabla^2 T + h_m + h_b \qquad (5.2)$$

where h_m = rate of tissue heat production = constant

h_b = rate of heat transfer from blood to the tissue

$h_b = w_b c_b (\gamma - 1)(T_{ts} - T_{ar})$; w_b = rate of blood flow

; c_b = specific heat of blood

; T_{ts} = tissue temperature
; T_{ar} = arterial blood temperature
; γ = equilibrium constant ($0 < \gamma < 1$)
$=0$; *for equilibrium*

If there is a difference in arterial blood temperature and venous blood temperature, eq. 5.2 can be modified to obtain eq. 5.3 /60/:

$$\rho \cdot c \cdot \frac{\partial T}{\partial t} = k \cdot \nabla^2 T + h_m + h_b - h_{ta} \cdot A_a \cdot (T_{ts} - T_{ar}) - h_{tv} \cdot A_v \cdot (T_{ts} - T_v) \quad (5.3)$$

where T_v is venous blood temperature, h_{ta} and h_{tv} are heat transfer coefficients from artery and vein to the tissues, A_a and A_v are surface areas of arterial and venous veins respectively.
Many investigators improved on Pennes' model to incorporate other physiological parameters in the calculation while modeling the thermal regulation of a complete human body /63-65/ or of a single part of the body /62/.

Based on Awbery's /66/ physical thermal modeling for hidden point and line sources, Draper and Boag have calculated the skin temperature distribution by considering the hidden heat sources as point sources (ex: tumour) or line sources (ex: veins) /67/.

5.2 Modeling of breast thermograms

Our interest is to analyse and understand breast thermograms as a function of the menstrual cycle. Therefore throughout our analysis thermal equilibrium is assumed and the principle variables are the hormonal changes and their effects /70/.
The breasts possess tissue heterogeneity and complex vascular patterns; therefore, a number of assumptions have to be made before we can establish a mammary thermal model that allows for simple mathematical treatment.

5.2.1 Thermal aspects

In the absence of big blood vessels, the heat flow H in the mammary tissues can be described by Fourier's law /68/:

$$H = - k_{eff} \cdot \vec{g}\text{rad } T \quad (5.4)$$

Where k_{eff} represents the thermal conductivity coefficient including the capillary heat transfer.

When the rate of heat production and the rate of heat loss are equal, eq. 5.2 reduces to another Fourier equation /60/:

$$\nabla^2 T = \frac{\rho c}{k_{eff}} \cdot \frac{\partial T}{\partial t} \qquad (5.5)$$

Since, during rest the change in temperature with time is absent, we have a simplified equation by setting eq. 5.5 to 0:

$$\nabla^2 T = 0 \qquad (5.6)$$

Eq. 5.6 is called the Laplace equation.
In this condition of equilibrium, the heat balance equation according to Newton's law of equilibrium can be applied at the skin interface:

Heat gained by the skin by transfer of heat from the core =
Heat lost to the environment from the skin surface

5.2.2 Geometrical aspects of breasts

The tissue structure between the skin and the core is assumed to be made up of three layers as shown in Fig. 5.1. The core is assumed to be a plane (y= 0) and normal to bell-shaped breasts; the temperature of this plane would be equivalent to the rectal temperature (36.5°C to 37.0°C).

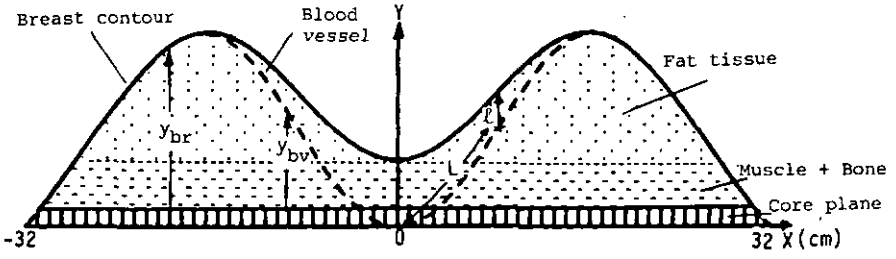

Fig. 5.1 Tissue structure of breasts assumed in mathematical modeling of breast thermograms. Values of constants assumed are: a=16, b=140, and c=200.

The geometrical shape of breasts is assumed to follow eq. 5.7:

$$y_{br}(x) = \exp\frac{-(x + a)^2}{b} + \exp\frac{-(x - a)^2}{b} \qquad (5.7)$$

where x and y_{br} are geometrical co-ordinates of breast, as shown in Fig. 5.1. Similarly, the main blood vessels in the breasts are assumed to follow the path $y_{bv}(x)$ given by eq. 5.8:

$$y_{bv}(x) = \exp\frac{-(x + a)^2}{c} + \exp\frac{-(x - a)^2}{c} \quad ; \; -a < x < a \qquad (5.8)$$

a, b and c in eq. 5.7 and eq. 5.8 define the size of the breasts and the path of the blood vessels.

5.3 Heat transfer equations

Skin receives heat from the core by thermal conduction through the tissues and by thermal convection through blood circulation in the veins. At the same time, skin looses heat to the environment by thermal convection through surrounding air, by thermal radiation and by evaporation. In the thermal equilibrium condition, heat gain and heat loss at the skin interface being equal, the skin temperature can be calculated by the heat balance equation.

5.3.1 Heat loss and thermal constants

The principle factors in heat loss are heat loss due to radiation and heat loss due to free convection. Both of these are proportional to the temperature difference between the skin surface temperature (T_s) and the ambient temperature (T_a), provided ($T_s - T_a$) is small /69/. Thus, the heat loss from the skin obeys Newton's law:

$$H = (T_s - T_a) \cdot E \qquad (5.9)$$

where E is called 'surface conductance' and is made up of radiative, convective and evaporative components, the latter however, being small in comfortable ambient conditions.

$$E = E_{rad} + E_{conv} + E_{cond} + E_{evp}$$

a) Heat loss by radiation: The net heat loss by radiation, from the skin surface at temperature T_s to the environment at temperature T_a, is given by Stefan-Boltzman's law,

$$H_{rad} = \sigma \cdot \varepsilon \cdot (T_s^4 - T_a^4) \qquad (5.10)$$

If $(T_s - T_a)$ is small eq. 5.10 can be simplified to

$$H_{rad} = 4 \cdot \sigma \cdot \varepsilon (T_s - T_a) \cdot T_m^3 \qquad (5.11)$$

where $T_m = (T_s + T_a)/2$ is the mean temperature of the emitting media and receiving media. Rearranging eq. 5.11 in the form of eq. 5.9 and assuming $\varepsilon = 1$ for the skin, we can write:

$$E_{rad} = 4 \cdot \sigma \cdot T_m^3 \qquad (5.12)$$

In comfortable ambient conditions E_{rad} varies between 5.8 $W/m^2\,°C$ and 6.2 $W/m^2\,°C$ /69/. For our calculation E_{rad} is assumed to be constant and equal to 6.0 $W/m^2\,°C$.

b) Heat loss due to convection: It is generally hard to estimate the convective heat loss due to the varying local contours of the body and to the air movement around the body, etc... However, a simplified empirical formula /69/ provides an estimate of convective heat loss in terms of the equivalent air thickness "h" of still air, which would allow the same heat transfer by conduction alone as actually occurs through the moving boundary layer by convection. We thereby write:

$$H_{conv} = \frac{k_{air}}{h} \cdot (T_s - T_a) = E_{conv} \cdot (T_s - T_a) \qquad (5.13)$$

The value of $E_{rad} = k_{air}/h$ around the breasts in comfortable ambient conditions varies between 4.0 $W/m^2\,°C$ and 5.0 $W/m^2\,°C$. The mean value of 4.5 $W/m^2\,°C$ for E_{conv} is taken as a constant for the calculation.

The total heat loss is a sum of losses due to radiation, convection and evaporation. We assume E =12.5 $W/m^2\,°C$ as a constant /69/. E represents the total surface conductance. It includes E_{rad} = 6.0 $W/m^2\,°C$ and E_{conv} = 4.5 $W/m^2\,°C$ as well as a remaining value of 2 $W/m^2\,°C$ that accounts for the losses due to evaporation and conduction.

5.3.2 Heat gain and thermal constants

Heat gained by the skin surface is through tissue conduction and by convection through the blood flow in the principle veins. Applying (as an approximation) Newton's law of heat transfer, we can calculate the skin temperature. The thermal constants for the materials that interest us here are given in Table 5.1 /60,69/.

Table 5.1 : Thermal properties of materials

Material	k[W/cm·°C]	ρ[gm/cm]	c[J/gm·°C]
Still air	$2.3 \cdot 10^{-4}$		
Skin	$3.8 \cdot 10^{-3}$		
Muscle	$4.2 \cdot 10^{-3}$	1.27	3.8
Fat	$2.1 \cdot 10^{-3}$	0.92	2.3
Blood	$5.06 \cdot 10^{-3}$	1.06	3.8

5.4 Effects of hormones on thermal physiology

The principle hormones of the menstrual cycle are estradiol (E_2), leutinizing hormone (LH), follicle stimulating hormone (FSH) and progesterone (P). Estradiol hormone induces higher blood flow in the endocrinological organs like mammary glands /4,29,54,57,58/;this we denote as 'estradiol-induced vascularity'. This phenomenon has been tested by external induction of estradiol in the plasma and observation of a subsequent riae in blood flow upto 2.5 times the normal flow rate /58/. This rise in blood flow causes more heat transfer to the upper layers of the breast through convection. So, a few skin surface areas with cutaneous blood vessels have a higher temperature than the neighbouring areas where there are no cutaneous blood vessels. This, in fact, can be observed on the breast thermograms.

LH and FSH have no influence on the thermal physiology. But progesterone hormone, whose concentration rises in the leutal phase of the menstrual cycle, has thermogenic properties /5/; it so increases the core temperature by 0.3°C to 0.5°C. This rise in core temperature also increases the skin temperature through tissue conduction, an effect that can be observed on the breast thermograms.

The above effects of hormones are considered in the following mathematical analysis of breast thermograms.

5.5 Phases of the menstrual cycle

5.5.1 Follicular phase of the menstrual cycle

The follicular phase of the menstrual cycle is characterized by minimum hormonal concentration in plasma and hence by minimum estradiol-induced vascularity. In this avascular condition the principle heat flow from core to skin is through thermal conduction which includes heat exchange by capillaries. Considering conductive heat from a point source on the plane y=0, (at the point on the plane y=0, normal to the point under consideration on the skin surface), we can write the heat balance equation for thermal equilibrium at the skin surface as

$$\frac{(T_c - T_s)\cdot k_{eff}}{y_{br}(x)} = E\cdot(T_s - T_a) \qquad (5.14)$$

where E is the total surface coductance constant governing heat loss to environment

$$E = E_{rad} + E_{conv} + E_{cond} + E_{evap}$$

and

$$\frac{k_{eff}}{y_{br}} = \Sigma\frac{k_i}{y_i}$$ is the total tissue conductance governing heat transfer from the core to the skin; k_i and y_i being effective thermal conductivity and thickness of the i^{th} layer.

(In our calculation the values of constants used are: T_c = 36.5 °C, $k_{muscle} = 4.2\ 10^{-3}$ W/cm, $k_{fat} = 2.1\ 10^{-3}$ W/cm, and $E = 12.5\ 10^{-4}$ W/cm).

Rearranging eq. 5.14, we have

$$T_s(\text{avascular}) = T_{sav}(X) = \frac{T_c\cdot\frac{k_{eff}}{y_{br}(x)} + E\cdot T_a}{\frac{k_{eff}}{y_{br}(x)} + E} \qquad (5.15)$$

T_{sav} is calculated as a function of ambient temperature and plotted for different values of y_{br} in Fig. 5.2.

The corresponding temperature ($T_{sav}(x)$) line profile drawn across the mamelons (line x-x in the fig.) for a given value of T_a is as shown in Fig. 5.3.

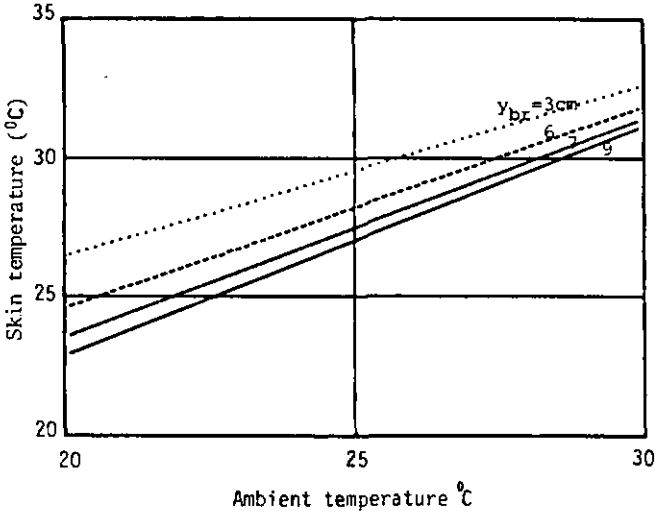

Fig. 5.2 Skin temperature as a function of ambient temperature and depth of the heat source.

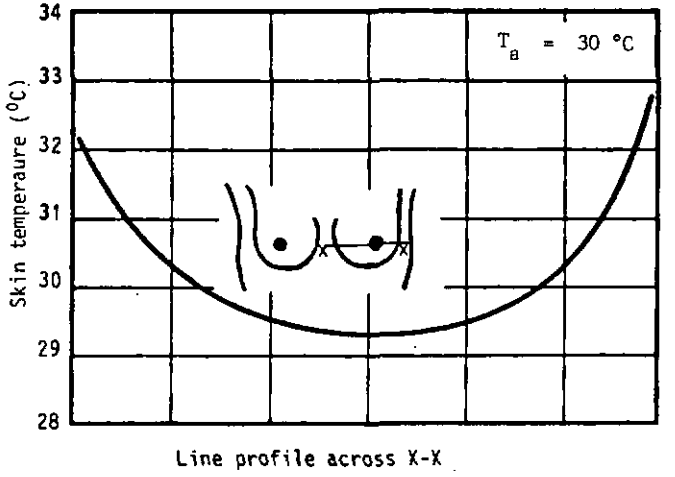

Fig. 5.3 Breast skin temperature line profile, over an x-x axis, passing through the mamelons. (for breast size see fig. 5.1)

5.5.2 Pre-ovulatory phase of the menstrual cycle

The pre-ovulatory phase of the menstrual cycle is characterized by a peak concentration of estradiol (E_2), leutinizing hormone (LH) and follicle stimulating hormone (FSH). Estradiol induces more vascularity by increasing the blood flow particularly in the areas sensitive to estrogenic hormones, including the mammary glands /54,57/.

The heat flow from the core to the skin is now by convection through blood flow and thermal conduction by the tissues. Heat flow by convection is proportional to the rate of blood flow in the veins. Starting from the arterial system (with temperature T_{ar}), blood looses heat on its path to the surrounding tissues until its temperature is equal to that of the tissues and gains thereon from the tissues to reach the venous system with temperature almost equal to T_{ar}.

The convective heat flow is given by the equation:

$$H = \rho \cdot c \cdot v_b \cdot \frac{dT}{dx} \tag{5.16}$$

where ρ = specific density of blood (gm/cm),
c = specific heat (J/gm.°C),
v = rate of blood flow (cm/sec.),
and $\frac{dT}{dx}$ = temperature gradient (°C/cm)

Considering the temperature gradient to be constant in the blood vessel, during the thermal equilibrium condition, we can calculate the temperature of the blood:

$$T_{bl}(x) = T_c - L \cdot \frac{dT}{dx} \tag{5.17}$$

where $L = \int_0^x \sqrt{1 + \left(\frac{dy_{bv}}{dx}\right)^2}\, dx$ is the length of the blood vessel from the artery (see Fig. 5.1).

The thermal gradient in the blood stream being smaller (k_{blood} = 5.06 10^{-3} W/cm) than in the fat tissues (k_{fat} =2.1 10^{-3} W/cm), the temperature around the blood vessel is higher during the vascular condition than in the avascular condition. The line heat source corresponding to the blood vessel can be considered as a series of point sources /67/. Each of these point sources will have a temperature $T_{bl}(x)$ calculated by eq. 5.17. The heat transfer from these point sources towards the skin is higher (due to the higher temperature gradient) than the heat

transfer towards the internal core. It is clear that each point source will basically have an effect on the whole temperature distribution on the skin. As there are many point sources to be considered on a single blood vessel, the whole calculation of the combined effect of these point sources becomes complicated. In fact, Draper and Boag /67/ have calculated the skin temperature distribution due to a single point source and even that step is quite involved. Their results are reproduced in Fig. 5.4 and one sees that the temperature falls-off rapidly with the offset distance.

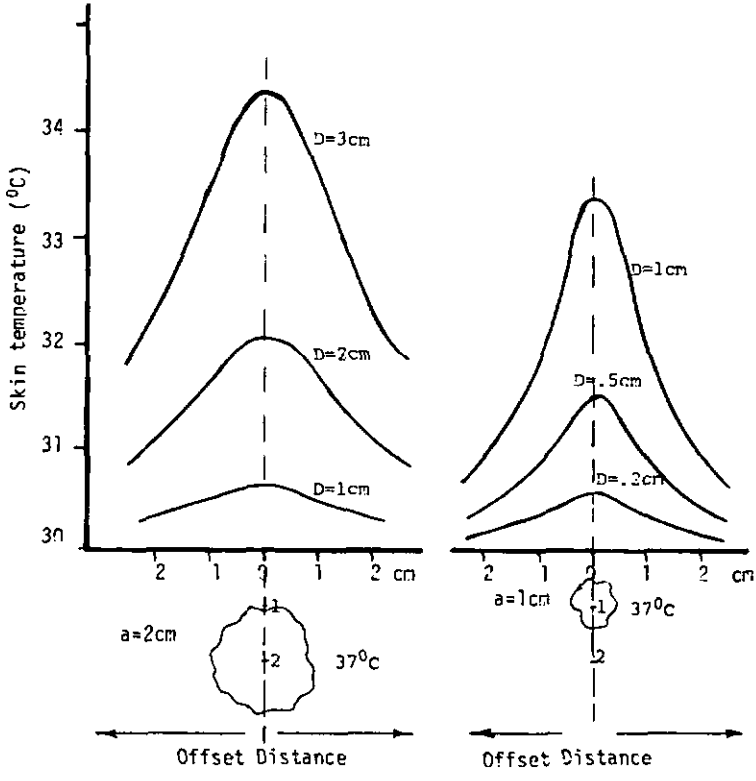

Fig. 5.4 Skin temperature distributions for a point source of diameter D and temperature of 37 °C, with centres at various depths a, as calculated by Draper and Boag /67/. Temperature profiles plotted are with a superimposed thermal gradient of 3 °C/cm. Assumed values of constants are:
T_s=30 °C, T_a=20 °C, E=12.5 W/cm².°C, and k =4.2.10⁻³ W/cm.C.

In our calculation, we have followed a much simpler procedure, which actually amounts to a crude approximation.

We assume that the skin temperature at any point 'A' on the breast is influenced only by the point source 'B' lying immediately below the skin point in a direction normal to the plane y=0 (Fig. 5.5a).

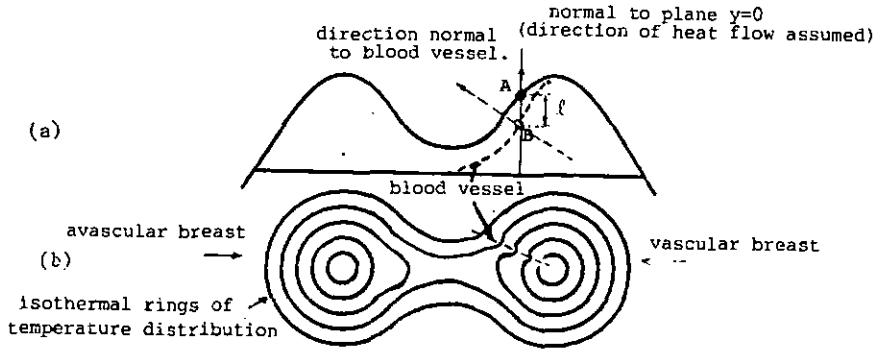

Fig. 5.5 Principle of approximation used for calculating skin temperature over the cutaneous blood vessel:
a) sectional view of breast with and without cutaneous blood vessels (left and right breast respectively)
b) thermal distribution: expected breast thermogram from our model..

As there are only few blood vessels in the breast region distributing the blood flow to the capillaries, temperature at points on the skin surface away from those just above the blood vessels falls off rapidly as shown in Fig. 5.4.

Fig. 5.5b shows qualitatively the isothermal diagram of a breast, as one can expect with a cutaneous blood vessel (see also observed thermograms presented in 4.6).

With the above approximation, we are able to determine, in a simple manner, the temperatures of the skin points that are lying immediately above the assumed blood vessels.

To obtain numerical results, we have assumed further that the direction of heat flow is only in the direction normal to the plane y=0, independent of the distance of the point on the skin surface considered from the point source. This is not unreasonable, as the upper parts of the breasts are colder than the lower parts, the maximum heat transfer between the blood vessel and the skin will certainly be in a direction somewhat between the direction normal to the plane y=0 and the direction normal to the blood vessel. The temperature on the skin surface due to

the heat source can now be determined by an equation similar to eq. 5.15:

$$T_s(\text{vascular}) = T_{sv}(x) = \frac{T_{bl}(x).\frac{k_{eff}}{\ell} + E.T_a}{\frac{k_{eff}}{\ell} + E} \qquad (5.18)$$

where $\ell = y_{br}(x) - y_{bl}(x)$ and $T_{bl}(x)$ follows from eq. 5.17.

The calculated temperature now represents the temperature on the skin point, where $T_{sv}(x)$ corresponds to the temperature at the point on the skin surface above the cutaneous blood vessel and k_{eff} is the conductive heat transfer coefficient as a function of vascularity.

The actual temperature prevailing at a given point is certainly a superposition of heat flow from the core plane and from the point heat sources on the blood vessel. In order to simplify our computation, we have introduced a further approximation:

$$T_{seff}(x) = \text{Max}(\, T_{sv}(X),\, T_{sav}(x)\,) \qquad (5.19)$$

Fig. 5.6 shows the calculated breast skin temperature above the cutaneous blood vessels for different levels of normalised vascularity.

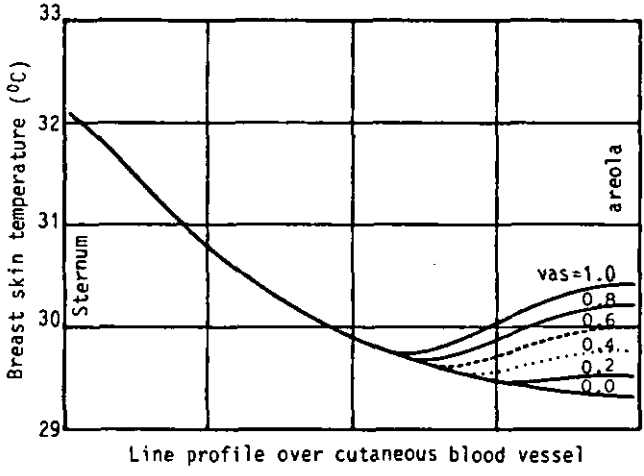

Fig. 5.6 Calculated breast skin temperature above the cutaneous blood vessel, for different vascularity levels (rate of blood flow is assumed to reach 4 times the normal flow at the peak vascularity level).

Fig. 5.7 shows the calculated skin temperature difference between dynamic temperature points (referring to the vascularly-induced temperature) and static temperature points (corresponding to the tissue conductive temperature), as a function of normalised vascularity: These plotted curves of "differential skin temperature (DST)" refer to a temperature difference between the dynamic point (x,y_{br}') and the static point at $(x= 0,y_{br})$ corresponding to the sternum.

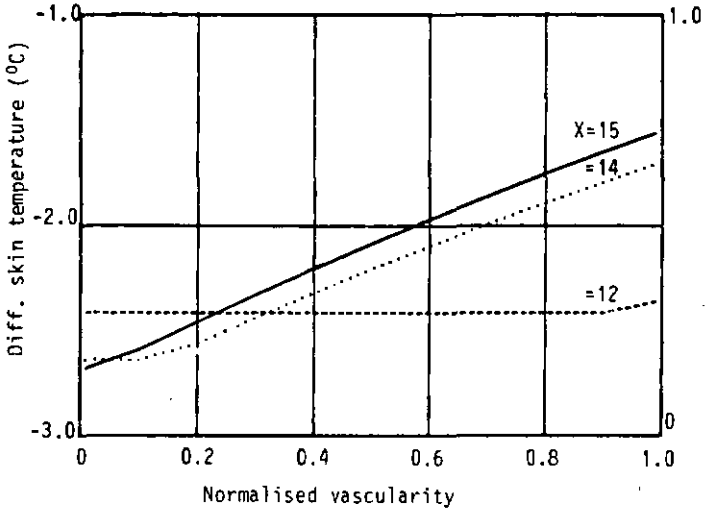

Fig. 5.7 Calculated differential skin temperature (DST) on the breast. DST is obtained by subtracting the skin temperature above the sternum (static temperature point) from the temperature of a point above a cutaneous blood vessel (dynamic temperature point).

[Nomalised vascularity= Level of vascularity w.r.t. maximum vascularity]

In Fig. 5.7 we can observe a direct correlation between vascularity and the calculated DST values. As a next step, it would be interesting to see if we can establish a link between the DST values and hormonal concentrations, especially estrogen. In fact, many investigators /4,29,54,57/ have shown that estrogen compounds produce increased blood flow. Verzini et al /29/ have measured urine estradiol and relative vascularity level in breasts over a menstrual cycle; these measurements are shown in Fig. 5.8. From this data we can extrapolate the change in vascularity due to estradiol. The data thus extrapolated is given in Fig. 5.9.

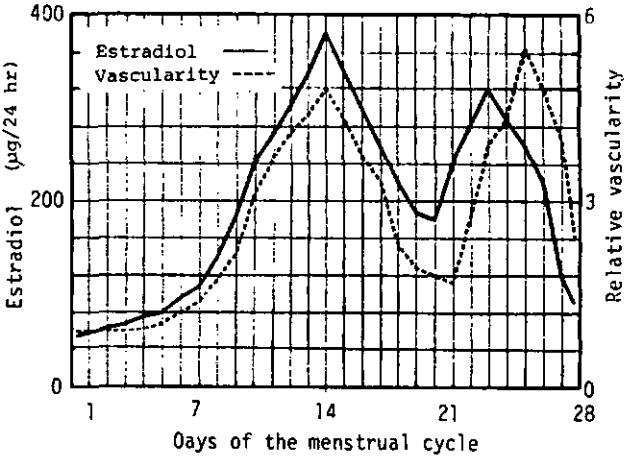

Fig. 5.9 Urine estradiol and relative vascularity levels in the breast over the menstrual cycle as published by Verzini et al /29/.

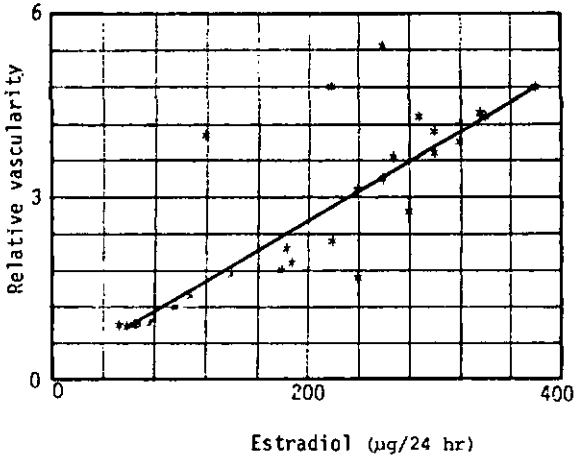

Fig. 5.9 Relative vascularity level in the breast as a function of urine estradiol concentration, extrapolated from the data of Verzini et al /29/ as given in Fig. 5.9.

By comparing the curves of Fig. 5.6 with the curves of Fig. 5.9, we can establish a correlation between estradiol and DST, in the pre-ovulatory phase of the menstrual cycle.

5.5.3 Leutal phase of the menstrual cycle

The leutal phase of the menstrual cycle is characterized by a drop in the estradiol concentration in the early post-ovulatory phase, followed by a rise in the thermogenic progesterone hormone. Estradiol hormone rises again in the middle part of the leutal phase. Skin temperature can be calculated for corresponding vascularity levels using equations (5.15) to (5.18), that now correspond to the second peak in DST (now we have $T_c = 37°C$, due to the increased level of progesterone). However, the DST peak in this phase is not as pronounced as the DST peak in the pre-ovulatory phase. This is due to the increased conductance of the tissues because of the higher progesterone level: the latter is in fact also supposed to restrict the vasodilation /54,57/. Before the following menstruation, both estradiol and progesterone fall back to low levels.

5.6 Computer simulation of breast thermograms

Based on the mathematical equations of the previous section, hypothetical thermograms were simulated on our PDP 11/60 minicomputer. Fig. 5.10 shows computer-simulated breast thermograms compared with typical clinical breast thermograms obtained at different days of the menstrual cycle. The temperature line profiles superposed on the images demonstrate dynamic temperature shifts at points just over the cutaneous blood vessels.

Numbers -3, -1, 2 and 9 on thermograms represent days of the menstrual cycle, the day numbered as 0 being the day of ovulation.

Hypothetical thermograms (Fig. 5.10a) are obtained with the assumption of three blood vessels situated symmetrically in both of the breasts. This assumption, however, represents a particular case only.

The temperature fall-off from the point on the skin surface above the cutaneous blood vessel is assumed to follow an exponential law /69/:

$$T_x = T_p \cdot (1 - \exp(-\beta X)) \qquad (5.20)$$

where T_x is the temperature at any point 'x' away from point 'p', T_p is the temperature at point 'p', just above the blood vessel, is temperature fall-off constant (β=0.2/cm, so chosen as to fit the observed clinical thermogram), and 'X' is the distance between point 'p' and 'x'.

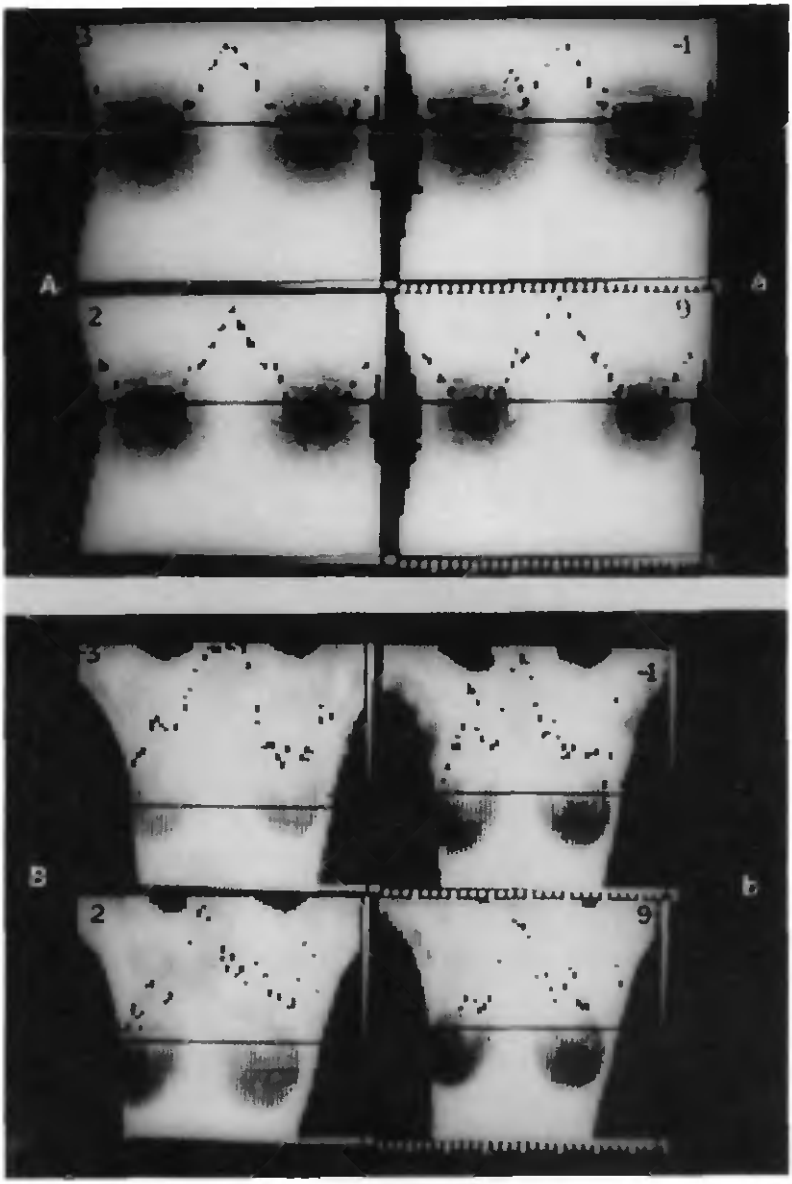

Fig. 5.10 (a) Hypothetical and (b) clinical thermograms over a menstrual cycle, with superimposed temperature line profiles.

5.7 Discussion

Our assumptions of the breasts having a bell-shaped geometrical profile may not always be true. However, looking at the side view of breasts of young women in hands-raised position, one can see the profile of typical breasts to be bell-shaped as assumed by us.

The convective heat transfer through blood is very nearly equal to or less than the conductive heat transfer in muscle or bone. So, the exact path of the blood vessel near the core plane is not important. Blood vessel path in the fat tissues can be varied in our model by varying the constant 'c' and thus the assumption made here for the blood vessel path is realistic. Awbery and Draper have arrived at mathematical equations for estimating the heat flow from a point source and a line heat source for semi-infinite media. In their calculaion, they need to know the thermal power of the point source, which is very difficult to calculate. In the method we adopted in calculating the effect of a point source on the skin surface temperature, we need to know only the temperature drop in the blood vessel. The application of Newton's heat balance equation, thereon at the skin interface will provide us approximate skin temperature directly, without the need of complicated numerical integration (however, our method is based on crude approximation).

The thermal surface conductance E, defined as the sum of heat loss coefficients, is generally not constant, but rather a function of skin contour, air flow, humidity and ambient temperature. E varies between 10 10^{-4} W/cm and 15 10^{-4} W/cm. However, in normal indoor basal conditions a value of 12.5 10^{-4} W/cm is quite a realistic figure.

The delay observed on the measured curves (but not on the calculated curves) between plasma estradiol concentration and DST is due to the fact that the effect of estradiol in vasodilation and the corresponding increased blood flow has a time constant of around 6 to 12 hours. Further, there is a thermal time constant involved in heat transfer to the skin due to thermal capacitance and thermal resistance of the tissue media. Therefore, the total delay observed by us between the estradiol peak and the DST peak, of about 12 to 24 hours is understandable; this delay is, however, absent in our calculation of skin temperature. Disturbing peaks on the experimental DST curve (in the previous chapter) are probably due to the difference in ambient temperature and changes in the metabolic rate at the time of IRT imaging.

CHAPTER 6

In this chapter, the details of the commercial AGA Infrared Thermography (IRT) equipment and the computer-assisted thermography system developed by us to interface with the AGA equipment are presented. The summary of this chapter can be found in a paper titled:

"Computer-assisted thermography (CAT) and its application in ovulation detection."
Proc. of ISMII'84 Arlington (Virginia, U.S.A) Conference, July 1984, pp. 459-464.

The details of the circuit hardware and the software programmes associated with our computer-assisted thermography system are available in the form of a technical report of the Institut de Microtechnique, Université de Neuchâtel:

"Computer-assisted image analysis: application in thermography." Report, Institut de Microtechnique, Report No. IMT 155 EC 02/85.

6. COMPUTER ASSISTED IMAGE ANALYSIS

6.1 Introduction

Electronic imaging of objects in various EM wavelengths is well known, ever since the advent of cathode ray tubes (CRT), to visualize the various aspects of the object's surface thus mappped. With the development of semiconductor technology for signal processing, various new modalities of imaging have found applications both in medicine and industry. Imaging methods basically employ radiation in one of three modes: transmission, emission or scattering, as indicated in Fig. 6.1 /72/. Methods indicated at the top are generally used for industrial applications and those shown at the bottom are normally used in diagnostic medicine.

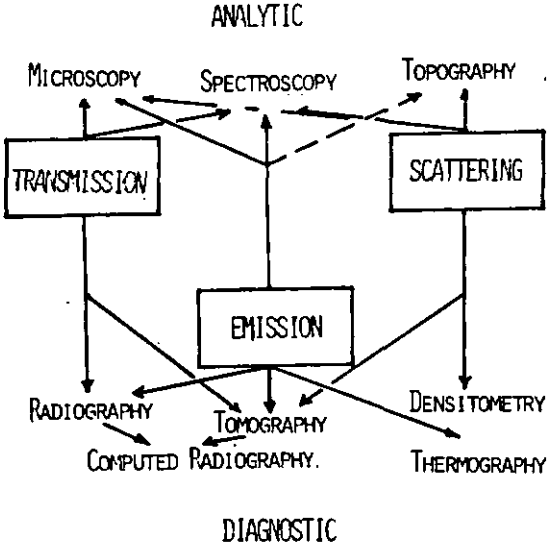

Fig. 6.1 Analytic and diagnostic imaging methods based on transmission, emission and scattering /72/.

Simple imaging through two-dimensional scanning and mapping on a CRT will not always be sufficient for proper utilisation of the information contained in the image; this is due to limitations like:

1. only limited data can be collected in real time,
2. interpretation of the image in a particular context is difficult because various parameters have to be considered,
3. only limited analysing features can be built into the circuit hardware,
4. only visual analysis of the image is possible.
5. processing of the image is extremely difficult and so limited in use, etc...

These problems are presently being overcome with digital signal processing based on microprocessors; the latter provide a powerful tool for information processing. Thus, at present generally all imaging systems have 'digital image processing (DIP)' associated with signal acquisition, quantization (digitization), storage of digital data in a large memory/disc, retrieval of this data as well as signal processing in real or processor time /78/.

6.2 Thermal imaging

Here, we concentrate on thermal imaging only. Thermal imaging depends on the external detection of emitted infrared radiation from the object's surface. The IR radiation thus detected gives information about the surface temperature distribution as a function of the emissivity of the surface (corresponding to a surface with a depth of about 1 mm and with a spatial resolution of 1 mm, at IR wavelengths) /41/.
The picture displaying the temperature/isotherm distribution of the surface is called a thermogram.

6.3 Infrared Thermography system

In our study of breast thermograms related to menstrual cycles we have used the infrared scanning system AGA 782 (AGA., Sweden). This system employs a cryogenically-cooled photon detector to obtain a high quality IR image with high immunity towards noise /41/. For scanning of the object's surface, the principle of refractive scanning is employed. Scanning is achieved by two silicon octogonal prisms, one rotating in the horizontal plane to generate the line scan, and one rotating in the vertical plane to generate the frame scan. The object field, which is

focussed on to the central plane of the horizontal scanning prism by a germanium lens, is scanned by the AGA 782 system once every 40 ms, generating 100.25 lines per frame. A spatial resolution of 401 lines is then realised by interlacing four frames, so that the total number of resolvable elemental areas in the object field is scanned once every 160 ms. The optical system of the AGA 782 IRT system and the scanning format are shown in Fig. 6.2a and Fig. 6.2b respectively /73/.

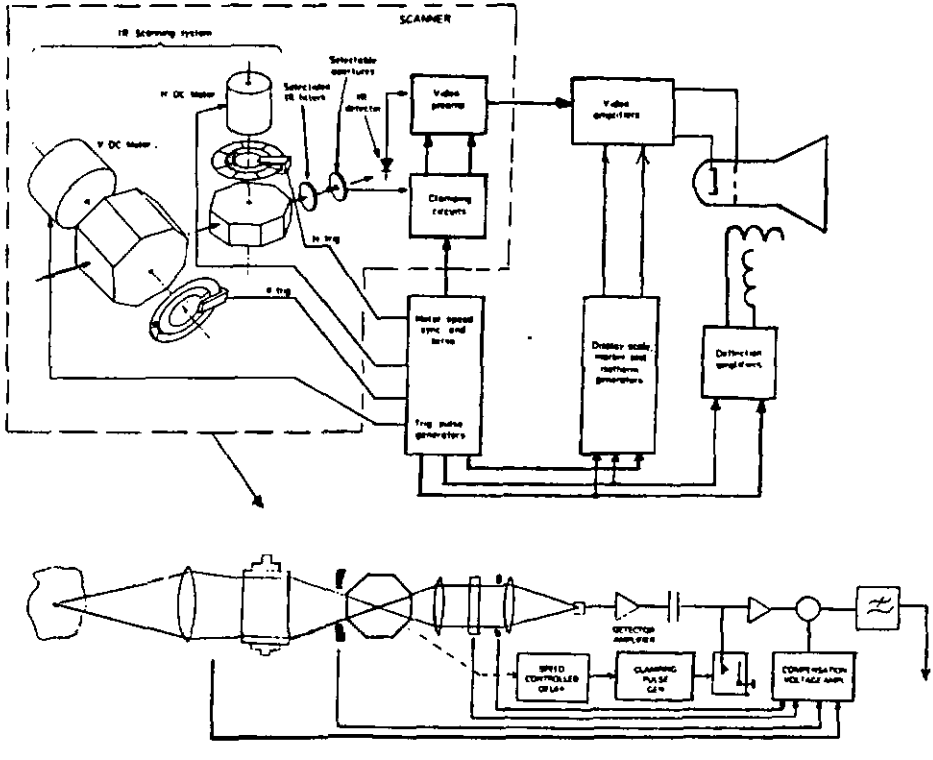

Fig. 6.2a Block diagram of the AGA 782 IRT equipment and details of its optical system used.

Though the thermogram has 401 lines per image, the active image area is only about 50% of the total area as shown in the Fig. 6.2b [the horizontal time scan is 300 s and the active frame time is 30 ms].

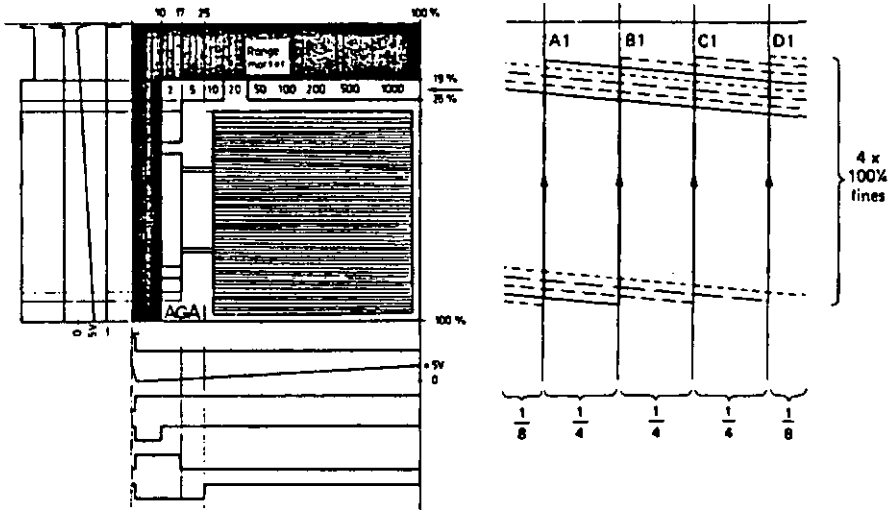

Fig. 6.2b Display format and frame interlacing scheme used in the ACA 782 IRT equipment.

The composite video signal of the thermogram is shown in Fig. 6.3; it includes the horizontal aynchronization signal (H), the vertical synchronization signal (V) as well as the direct-video aignal.

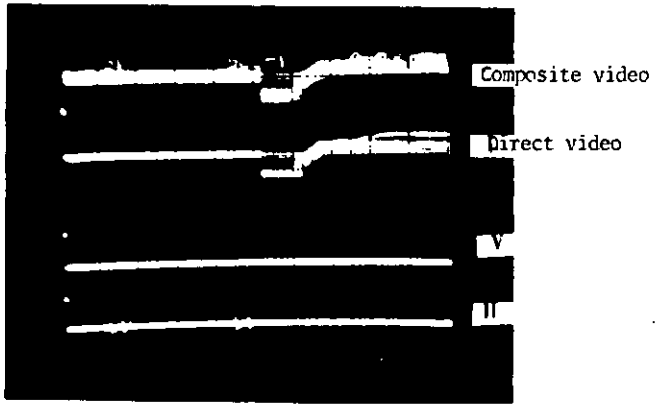

Fig. 6.3 Composite video signal (input) and decoded control signals of our computer-assisted thermography (CAT) system.

6.4 Limitations of the AGA 782 system

1. Thermograms obtained on the AGA monitor are too small [8cm x 8cm] for visual monitoring, and are not flicker-free.
2. Thermograms represent the photon flux proportional to the third power of temperature and so their units are non-linear. To read thermograms in a linear temperature scale one has first to refer to the conversion formula or to monograms supplied by the manufacturer.
3. Thermograms can be monitored only in black and white and the grading is done in a 6 level grey scale. This limits both quantitative resolution and visual discrimination of the thermal characteristics.
4. Thermograms obtained at different times cannot be easily correlated with each other due to different control settings during the experiment.
5. Thermal analysis of a dynamically changing process, has to be done in real time; otherwise one has to depend only on polaroid photos taken during the experiment itself, for later visual inspection and intetpretation.

6.5 Improvements needed in thermal imaging

1. For comparative study of a large number of thermograms (as in our case), immediate need will be the computer storage of the thermograms.

2. Easy retrieval of stored thermograms and display in a larger format, preferably on a TV monitor.

3. Transformation of thermograms from non-linear isotherm units into a linear temperature scale.

4. Normalization of thermograms with respect to control settings to enable quntitaive comparison of different thermograms.

5. Specific image analyzing features to suit the particular requirements.

6. Conversion of black and white thermograms into pseudo-colour thermogram to increase visual resolution and facilitate easier image interpretation /79/.

6.6 Computer-assisted thermography (CAT)

There are a few image processing systems available /74,75/ that are compatible to AGA IRT equipment. However, they are very expensive and even so, do not provide all the analysing features that we needed. Therefore, we developed on our own a 'computer-assisted thermography (CAT)' system to suit our particular specifications for analysing breast thermograms recorded on the video magnetic tape during the experiment as explained in chapter 4. This system is based on the in-house PDP-11/60 mini-computer and its peripheral device LAP-11 which has a 16 bit I/O port for data transfer /76/. The block schematic of the CAT system is as shown in Fig. 6.4.

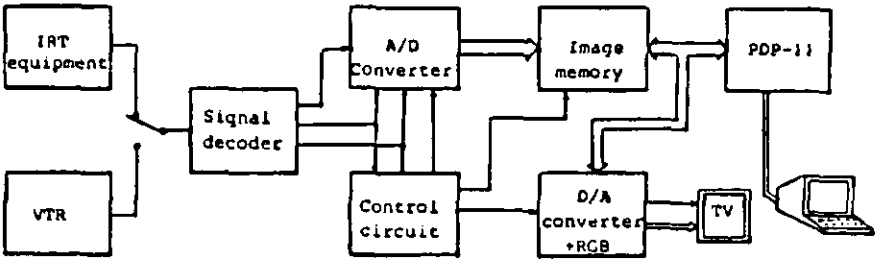

Fig. 6.4 Block diagram of our computer-assisted thermography (CAT) system.

6.6a Development of CAT system specifications

1. Computer interfacing of the AGA 782 IRT equipment should be possible both ON-line (field compatability) or OFF-line (video tape recorder compatibility).
-----Use of the composite signal from the IRT equipment and then generation of the horizontal (H), vertical (V) and direct-video signals in the CAT system for further signal processing.

2. Temperature resolution: 256 levels in a given dynamic range.
-----8 bit digital quantization of video signal.

3. Spatial resolution: thermogram should have a minimum of 128 x 128

pixels over the total image area (this is a compromise between the desire for good spatial resolution and the need to keep the memory capacity/costs low)
-----this corresponds to [128 x 128] pixels/thermogram or, in other words, each thermogram will have 16 kbytes [=128 x 128 x8] memory capacity to provide the desired spatial and thermal resolution.
-----use of two-interlaced frames with 64 lines/frame, with each horizontal line represented by 128 pixels.

4. pseudo-colour thermogram with 16 pseudo-colours, expandable in thermal scale.
----- suitable RGB tristimulus signal generation as a function of signal level and thermal range expansion.

5. Possibility to acquire an analog thermogram from the AGA equipment/VTR, digitize , store in the intermediate memory and display the digitized image on a TV monitor through software command.
-----suitable software and hardware development.

6. Transfer of digitized thermogram onto the computer mass storage for later-on analysis.
-----suitable interface between the hardware of the CAT system and the PDP-11/60 computer

7. Transformation of thermograms from non-linear isotherm units into a linear temperature scale and normalization as needed for correlating/ comparing of images.
-----suitable software development.

8. Various analysing features suitable for breast thermogram analysis.
-----suitable software development.

6.7 System Hardware

The system hardware is relatively complex due to the different timings that the specification calls for. We are in fact concerned with digitization of IR video signal and the data storage in AGA timing, transfer of this data onto the computer at the relatively slow processor timing and conversion of data in the image memory into the TV format video timing. The block schematic of such a hardware system is shown in Fig. 6.5.

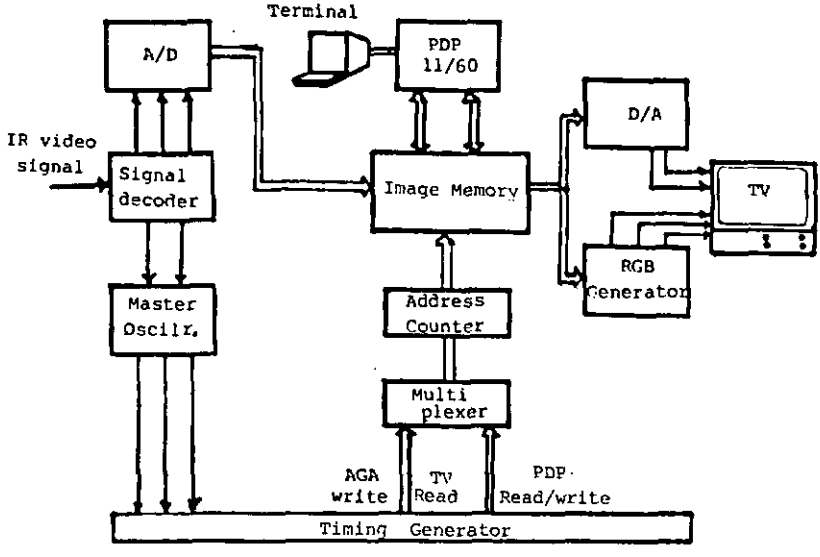

Fig. 6.5 Basic hardware block schematic of our CAT system.

However, the system of Fig. 6.5 is limited in use; it can in fact only be used for thermogram analysis. To improve the CAT system's flexibility and to make it compatible to accept images not only from the AGA IRT equipment, but also from other systems, particularly from the video TV format /77/, we have used the block schematic of Fig. 6.6 in our CAT system hardware.

The signal decoder generates horizontal (H), vertical (V) and direct-video signals from the input IR composite video signal. Direct-video signal thus generated is digitized in an 8 bit A/D converter at the rate of 400 KHz corresponding to 128 x 2.5 μs (this corresponds to 312 μs active thermogram line scan) and stored in the buffer image memory (8IM) of 16 Kbytes capacity, through selective address locations so as to interlace the two frames of thermogram properly . Each frame has 64 x 128 x 2.5 μs (this corresponds to 20.48 ms for an active thermogram). This is so chosen that only the active area of the thermogram scanning format in the AGA equipment is digitized. The stored data is read at proper timing corresponding to the TV standards and written into the intermediate image memory (1IM). At the same time it is converted into analog form to display the thermogram on a TV monitor.

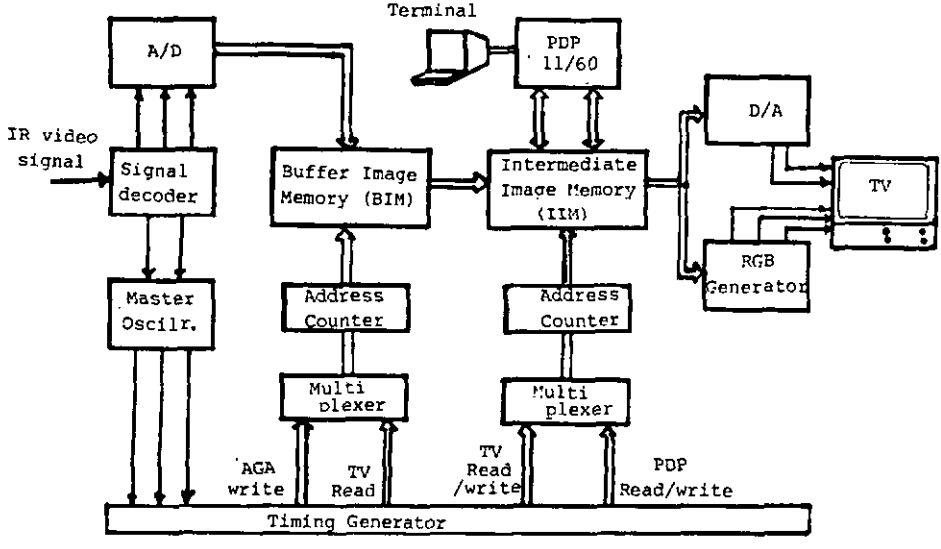

Fig. 6.6 Modified hardware block schematic as used in our CAT system.

Timing generator generates all the required timing signals. RGB generator generates the three tristimulus signals, at the proper impedance level, as a function of data to produce the pseudo colour thermograms. Thus, there is a provision to visualize the thermograms either in black and white (grey code) or in a 16 level pseudo-colour format. Table 6.1 shows the RGB signal scheme of the CAT system.

Table 6.1 : Pseudo-colour assignment scheme in CAT system

CODE	0 16	16 32	32 48	48 64	64 80	80 96	96 112	112 128	128 144	144 160	160 176	176 192	192 208	208 224	224 240	240 256
PSEUDO-COLOUR	BLACK	KAKI	BLUE	SKY BLUE	DARK GREEN	GREEN	LIGHT BLUE	CYAN	RED	ORANGE	MAGENTA	ROSE	REDDISH ORANGE	YELLOW	ORANGE PINK	WHITE

Communication between PDP-11/60 mini-computer and CAT system is done at the level of intermediate image memory (IIM). Data transfer between PDP and IIM is done row by row to reduce the computer time, at a relatively slow rate (2 KHz). When the CAT system is used for TV format digitization, the data transfer between digitizer and image memory is done at the high rate of 3 MHz. Thus, the modified scheme of CAT system is useful both for video and non-video format signals.
Once the image is stored in the computer , the further analysis of the image is now independent of the input image format; therefore the CAT system can be used for different applications.
The detailed circuit diagram of the CAT system hardware and the listings/descriptions of the associated software package for image analysis are presented in the internal report of the institute /80/.

6.8 Image processing software for CAT system

Image processing techniques have grown into a vast field in recent years. Digital image processing (DIP) systems vary in their complexity from simple algorithm implementations to very complex signal processing packages /78/
The principle goal of the CAT system is to implement simple image processing algorithms to suit the analysis of breast thermograms, with a little bit of additional flexibility to suit other, future imaging applications.
Throughout this chapter, images are represented in the form of a matrix [A] with its elements as $\{a_{i,j}\}$ in the form shown below:

$$[A] = \{a_{i,j}\} \quad ; \quad [(0,0) < a_{i,j} < (127,127)] \qquad (6.1)$$

where $\{a_{i,j}\}$ $(0 < a_{i,j} < 255)$ represent the grey levels of the referred pixel.

6.9 Image Processing features

Image processing features of CAT systems can be sub-divided into three groups: 1. Communication control between CAT system hardware and PDP computer; 2. Image acquisition and storage; 3. Pre-processing and analysis of images.
All these 3 groups are included in the principal 'MENU' features for selection of a particular mode by the operator. The 'MENU' of the CAT system is as shown:

MENU OF CAT

0. EXIT	1. CONTROL	2. ACQUISITION	3. STORE
4. LINEARIZE	5. DISPLAY	6. FILTERING	7. AREA STATISTICS
8. ISOTHERMS	9. ENHANCEMENT	10. X-Y PROFILE	11. HISTOGRAM
12. COMBINATION	13. ZOOM	14. X-Y ROLL	15. MULTIPLE IMAGE
16. MULTIPLE AREA ANALYSIS		17. LOW RESOLUTION PRINT	

Each of these 'MENU' features is explained briefly (without going into mathematical details) in the following section.

0. EXIT: This feature selects the termination of the programme.

1. CONTROL: Selection of this menu feature checks the communication between CAT system and PDP computer, and displays the control format image (linear grey image (Fig. 6.7a) or graded grey image (Fig. 6.7b)).

2. ACQUISITION: When the CAT system is connected either to the AGA 782 IRT equipment (ON-line) or to the video tape recorder in the play-back mode (OFF-line), thermograms can be acquired with a software command. With the selection of this menu feature the following steps are done:
a. acquired thermogram is digitized in an 8 bit A/D converter,
b. data is stored in the buffer image memory (BIM) at AGA timing,
c. data is transferred to the intermediate image memory (IIM) at video timing,
d. data in IIM is reconverted into analog form at video timing,
e. acquired thermogram is displayed on a TV monitor either in black and white grey code or in pseudo-color code (Fig. 6.7c).

3. STORE: With this menu feature, thermogram stored in IIM is transferred into mass-storage of PDP computer and stored in the form of an unformatted binary data image file.

4a. LINEARIZE: AGA 782 IRT equipment has a photon detector to detect thermal radiation. Thus, thermogram displayed on AGA monitor is a non-linear function of temperature, as already explained in sections 6.3 and 6.4.

The mathematical equation given by the manufacturer /73/ describe the isotherm units displayed, as a function of detection, system optics and ambient temperature:

$$I = \frac{P}{\exp(Q/T) - 1} \qquad (6.2)$$

where I = Isotherm units corresponding to the temperature T in K.
P,Q = Aperture constants of the IRT camera
(P=552855 and Q = 2994 , as given by the manufacturer)

Evaluating eq. 6.2 for T in °C yields eq. 6.3:

$$T = \frac{Q}{\ln(\frac{P + Q}{I})} + 273.15 \qquad (6.3)$$

Following eq. 6.3, linearization of thermograms is done by our software (Fig. 6.7d).

4b. NORMALIZATION: Thermograms registered at different times have different control setups each time. Hence, the visual comparison of images is not straightforward. To make interpretation of IR images much easier and more uniform, linearized images are normalized with respect to a reference temperature observed at certain physiologically less sensitive skin surface areas (in our case normalization is done with respect to the skin surface above the sternum).
The normalization function can be written in the form :

$$[B] = m \cdot [A] + c \qquad (6.4)$$

where [A] is the original image, [B] is the new image, m is the thermal range manipulation factor and c is a normalizing constant.
Fig. 6.7e shows a normalized version of Fig. 6.7d.

5. DISPLAY: With the selection of this menu feature, the data of a selected thermogram in the computer image file is transferred into the IIM and further converted into a video analog signal to display the thermogram on the TV monitor. Display can be had either in grey code or pseudo colour code. A further choice is given to reverse the grey scale to produce a negative image (inverted mode), whose visual effect places a different emphasis on certain picture details /84/. The algorithm used is demonstrated in Fig. 6.8. The thermogram thus displayed has grey/colour code bar and grid markers (4th and 16th grids for both rows

and columns) superposed on the image for co-ordinate and thermal level observation of the interested area (Fig. 6.7f).

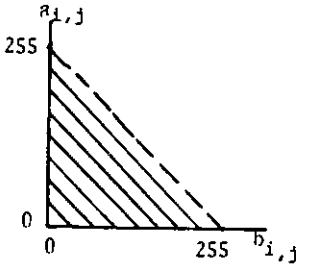

$$\{b_{i,j}\} = \{255 - a_{i,j}\}$$

Fig. 6.8 Computer algorithm for inverted image display

6. FILTERING: The filtering algorithm is generally used to improve the image characteristics with respect to sharpening (of blurred images) and smoothing of images (through noise reduction) /78/.

a. SHARPENING: Blurring is defined as the weakening of high spatial frequencies (corresponds to inability of the detector to follow fast input changes) relative to low spatial frequencies. This is due to optical limitations and the media involved. Sharpening of blurred images is generally done by using the Laplacian operator $\nabla^2 f$:

$$\nabla^2 f = \frac{\delta^2 f}{\delta x^2} + \frac{\delta^2 f}{\delta y^2} \qquad (6.5)$$

Here f corresponds to the grey scale value of the pixel considered. In the digital version, $\nabla^2 f$ is proportional to $(f - \bar{f})$, where $\bar{f}$ is local avearage of f /81/. By adding this derivative of grey level to the original image, the high frequencies are enhanced and the low spatial frequencies are unaffected: this deblurrs the original image (Fig. 6.7g)

b. SMOOTHING: Smoothing of images is done through noise reduction, based on local-order statistics /78/. In our software, we have used an 'out-range' noise cleaning algorithm as shown in Fig. 6.9.

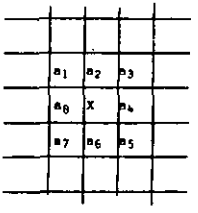

$$\text{If} \quad \frac{1}{8}\{\sum_1^8 a_i\} - \epsilon > X > \frac{1}{8}\{\sum_1^8 a_i\} + \epsilon$$

$$\text{Then} \quad X = \frac{1}{8}\{\sum_1^8 a_i\}$$

Fig. 6.9 Example of 'out-range' smoothing algorithm.

With this technique, each pixel is sequentially examined and if the magnitude of the pixel is greater or less than the average grey level of its immediate neighbours by some threshold level, it is replaced by an average value. Application of this algorithm is shown in Fig. 6.7h (smoothed image of 6.7d).

c. AVERAGING: If the image is clustered with high frequency noise (zero-mean gaussian noise is generally always present), an improvement in signal to noise ratio can be achieved by local averaging of each pixel with its neighbours /84/. The computer algorithm used in our software is shown in Fig. 6.10. The resulting action will be low pass filtering of the image (Fig. 6.7h produces Fig.6.7i (for local averaging over 3*3 pixels)).

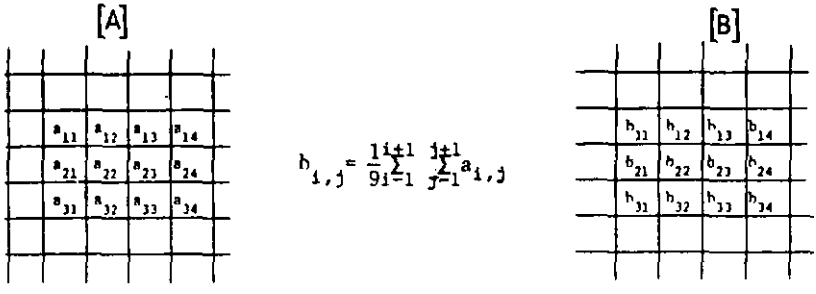

Fig. 6.10 Example of averaging algorithm.

d. HIGH PASS FILTERING: By subtracting the low pass filtered (averaged) image from the original image an high pass filter algorithm can be obtained. In our study this algorithm is used to obtain the vascular patterns of the breast as shown in Fig. 6.7j.

7. AREA STATISTICS: This menu feature calculates temperature statistics to obtain minimum (T_{min}), maximum (T_{max}) and mean (T_{mean}) values in a selected area of the image. It also provides the spot temperature ($T_{m,n}$) at the selected co-ordinates (m,n). The area borders chosen, as well as the full Thermogram are displayed on the TV monitor (Fig. 6.7k) and the statistics are displayed on the terminal.

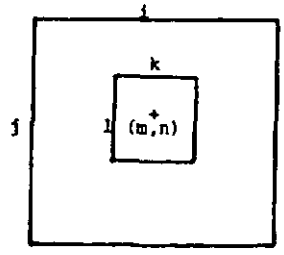

$$T_{min} = Min(a_{k,l})\frac{T_r}{255} + T_{Lmin}$$

$$T_{max} = Max(a_{k,l})\frac{T_r}{255} + T_{Lmin}$$

$$T_{mean} = \frac{\sum_k \sum_l a_{k,l}}{} \frac{T_r}{255} + T_{Lmin}$$

$$T_{m,n} = \frac{a_{m,n} \cdot T_r}{255} + T_{Lmin}$$

where T_r is thermal range and T_{Lmin} is thermal level

Fig. 6.11 Area statistics algorithm.

8. ISOTHERMS: With such a routine, all skin spots having a particular temperature can generally be 'zoomed' into a predefined grey level: this means that all these skin spots are assigned a grey level at the extreme range of the scale, so that they can be easily identified on the image. The algorithm used in our software is somewhat more complex. As shown in Fig 6.7 it allows for two whole ranges of grey levels, i.e. TH_1 (being the thermal range between L_1 and H_1) and TH_2 (being the thermal range between L_2 and H_2) to be 'zoomed', each to one of the extreme grey levels, i.e. to the black level (0) or the white level (255) respectively.

To clearly distinguish between these 'zoomed' (or 'highlighted') thermal ranges TH_1 and TH_2 and the rest of the image , all other grey levels are at the same time compressed into the reduced range between Q and (P+Q) as shown in Fig. 6.12.

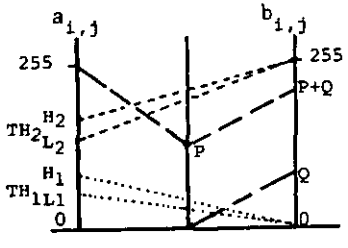

$$\{b_{i,j}\} = \{a_{i,j} \cdot \frac{P}{255} + Q\} \quad ; TH_1 \neq a_{i,j} \neq TH_2$$

$$\{b_{i,j}\} = 0 \quad ; a_{i,j} = TH_1$$

$$\{b_{i,j}\} = 255 \quad ; a_{i,j} = TH_2$$

Fig. 6.12 Example of the algorithm used for definition of isotherm contours.

Fig. 6.71 shows a thermogram with two isotherm contours (P=200, Q=100, L_1=60, H_1=70, L_2=200 and H_2=210).

9. ENHANCEMENT: In medical imaging, enhancement generally refers to the method of transforming the image grey scale to obtain statistically equally distributed levels ; it is used with the purpose of better fitting the image to the human eye /82/. This technique is useful as long as one is interested only in the qualitative features of the image /83/. However, in thermal imaging, one is interested also in quantitative analysis of the image and the above technique is therefore not applicable.

In our case, enhancement refers only to contrast enhancement /84/, and the algorithm used in our software is as shown in Fig. 6.13: By this algorithm temperature values lying in the range between Q and (P+Q) are given higher thermal resolution.

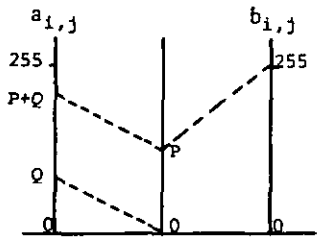

$$\{b_{i,j}\} = \{a_{i,j} - Q\} \cdot \frac{255}{P}$$

Fig. 6.13 Example of contrast enhancement algorithm.

In the enhanced image of Fig. 6.7m each colour represents 0.1 C against 0.25 C in Fig. 6.7f.

10. X-Y PROFILE: This menu feature selects the computer algorithm to plot temperature line profiles on selected X-Y axes. The profiles can be monitored on TV monitor (Fig. 6.7n) along with a geometrically compressed thermogram with the selected X-Y axes superposed, or they can be plotted on a paper for hard-copy reference.

11. HISTOGRAM: The histogram algorithm is used as a measure for determining the thermal asymmetry between two selected areas.: by selecting row and column widths, two areas corresponding to two breasts are chosen and the grey levels present in these two areas are distributed into 16 groups. The contents of these 16 groups are geometrically distributed over the selected row width, on a TV monitor as shown in Fig. 6.7o.

12. COMBINATION: This routine implements arithmetic functions. This function is used in the comparative study of test images with respect to an original image (images to be correlated should have the same position). With the selection of this menu feature, addition, subtraction and other arithmetic manipulations between two images can be done.

The 'combination' algorithm used in our software follows the equation:

$$\{d_{i,j}\} = p\cdot\{a_{i,j}\} + q\cdot\{b_{i,j}\} + c \qquad (6.6)$$

where $(a_{i,j})$ and $(b_{i,j})$ are the pixel values of the two images to be correlated at the point (i,j), c is a constant and $d(_{i,j})$ is the resultant pixel value in the new image. p and q are thermal range manipulation factors. Realisation of the high-pass filtering function is an example of this routine. The image of breast vascular patterns shown in Fig.6.7j is realised with p =1.0, q =-1.0 and c=30. [A] is the original thermogram matrix (Fig.6.7e), [B] is the low-pass filtered thermogram matrix (Fig.6.7i) and [D] is the high-pass filtered thermogram matrix.

13. ZOOM: The zoom routine provides geometrical transformation of images. A two dimensional geometrical transformation is defined by a pair of equations of the form:

$$X' = h_1[x,y] \qquad \text{and} \qquad Y' = h_2[x,y] \qquad (6.7)$$

which specify the new co-ordinates (x',y') as functions of the old ones (x,y). Since these new co-ordinates are generally non-integer, implementation of this algorithm by rounding of the co-ordinates, produces a new image with some pixels not represented: In this case, the new image will have different statistics compared to the original one.

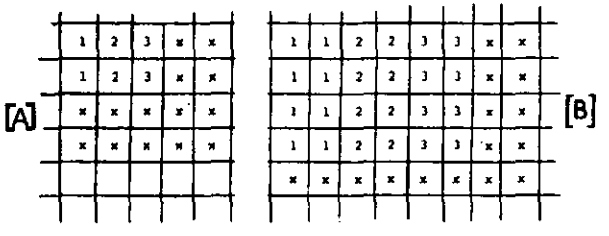

Fig. 6.14 Example of zoom algorithm (magnification=2).

However, for us it is essential that the pictorial statistics remain unchanged. Therefore our Zoom routine magnifies the selected portion of the image by integer horizontal and vertical factors. The computer algorithm used is demonstrated in Fig. 6.14.
Fig. 6.7p shows a magnified (2 x) image of the left breast portion of Fig.6.7e.

14. X-Y ROLL: This routine rolls the image by a selected number of rows and columns. This is useful in positioning of images for comparison. Using this routine along with the COMBINATION routine, an edge detection operation can be realised. The equation used in this function is:

$$\{b_{i,j}\} = c \cdot \{a_{i,j} - a_{i-1,j-1}\} - \{a_{i,j}\} \qquad (6.8)$$

Fig. 6.7q shows the result of the edge detection algorithm.

15. MULTIPLE IMAGE: This routine provides 4 images displayed together on the TV monitor (with reduced spatial resolution) for simultaneous visual analysis (Fig. 6.7r).

16. MULTIPLE AREA ANALYSIS: This routine is similar to the previously described 'Area statistics' routine; however, it determines the mean temperature (and not the statistical distribution) as a function of area. It is used for determining the importance of the area involved in DST measurement.

17. LOW RESOLUTION PRINT: This routine generates a low resolution picture of the thermogram by assigning an alphanumeric character of appropriate visual density to each grey level. These characters can be printed on a line-printer to form an hard copy of the image (of low resolution).

The coloured figures belonging to this chapter - namely figs 6.7/6.17/6.22 - are included at the end of this thesis.

6.10 RESULTS OF COMPUTER-ASSISTED THERMOGRAM (CAT) ANALYSIS

(NOTE: coloured figures are included at the end of the thesis)

The experimental protocol used in the investigation study to corelate the breast thermograms with the hormonal concentrations over the menstrual cycle with 10 volunteers is explained in detail in chapter 4. The breast thermograms recorded on a video magnetic tape during these experiments were transferred on to the PDP 11/60 computer using our CAT system hardware and software as explained in the previous sections. The stored menstrual cycle related breast thermograms were analysed with the various 'menu features' in our software so as to extract the dynamic temperature points, to study the degree of change in dynamic temperature, to make statistical analysis of temperature distributions, to find the effect of the area involoved in temperature measurement as a function of temperature sensitivity etc... The results based on this computer-analysis of breast thermograms are summarized below.

a. Breast temperature:

Average breast temperature as a function of menstrual cycle status has been computed by Smith et al. /33/, by measuring the temperature at a few points only on the breasts. With the application of CAT, we could measure actual breast temperature by computing the spot temperatures over all points on the breast. CAT-computed normalized breast temperature T_{br} is plotted as a function of the days of the menstrual cycle in Fig. 6.15. (The term 'normalized breast temperature' refers to breast temperature computed for a breast thermogram normalized with respect to temperature of sternum). BBT data of the same volunteers is also plotted for the purpose of comparison.

The peak differential T_{br} rise (T_{br} of one whole breast) occurs one or two days before ovulation, indicating the approaching ovulation. Further, it is interesting to note in Fig. 6.15 that there is no significant rise in differential T_{br} in the leutal phase. This result shows that the rise in absolute breast temperature computed by other authors /33/ is mainly due to the post-ovulatory rise of progesterone hormone concentration; it thus confirms their hypothesis that the local vasomotor effects due to estradiol are relatively less important in the leutal phase.

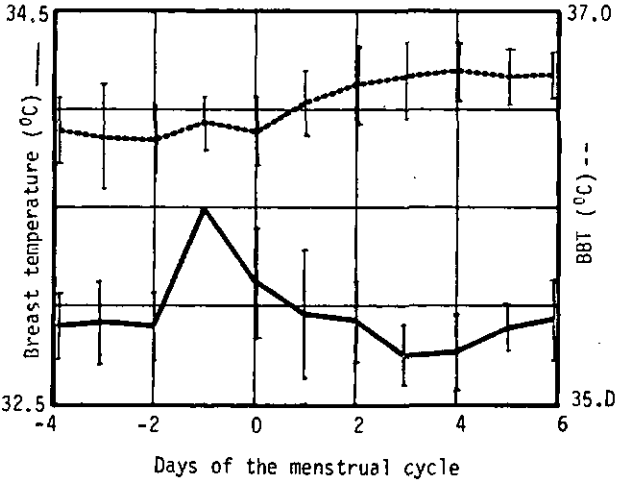

Fig. 6.15 Normalized breast temperature (T_{bn}) averaged over one whole breast, as well as basal body temperature (BBT) in the middle part of the menstrual cycle. The data plotted is the average (mean ±SEM) of the data from 6 non-pharmaceutical contraceptive users. Day '0' is the day of LH surge. [reference sternum temperature = 35 °C]
SEM= standard error mean.

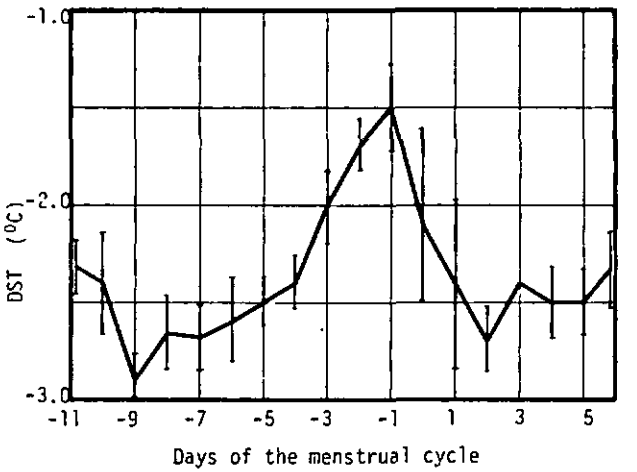

Fig. 6.16 Differential skin temperature (DST) measured on a small vascular area (9 sq. pixels) in the middle part of the menstrual cycle (mean ±SEM).

b. Spot DST measurement:

The average rise of differential breast temperatue T_{br} is only in the order of 0.6 C to 0.8 C in the pre-ovulatory period. However, with CAT, we could localize more precisely the vascularly sensitive dynamic temperature points and compute the differential temperature of these points with respect to the static or reference temperature point (in our case the sternum); thereby we obtain a more significant temperature peak before ovulation. Fig. 6.16 shows CAT-computed DST as a function of menstrual cycle days. The mean DST is obtained by averaging the data of six volunteers over one menstrual cycle.

The area of measurement is (3 * 3) pixels corresponding to approximately 15mm * 15mm of area on the vascular region over the breast.

The changes of differential temperature for vascularly sensitive dynamic temperature points can also be observed by means of X-Y profiles drawn across such points. IRT images (for days -3, -1, 0, +1 and +3 counted with respect to the day of LH surge: the latter is referred to as day 0) of a volunteer with corresponding line profiles and a typical isotherm distribution (between static and dynamic points) are shown in Fig. 6.17.

c. Offset-DST measurement:

One can find many dynamic temperature points on the breasts. The degree of change in DST at different points so located vary as a function of the depth and the distance of cutaneous blood vessels from the point of measurement on the skin surface as explained in chapter 5 /39,40/. We measured the temperature at different dynamic points (points 'a', 'b' and 'c' shown in the Fig.6.18a). In order to make the variations of DST clearly visible in a comparative way, we represent the measurements for these 3 points in the form of 'Offset-DST' curves. We define 'Offset-DST' as the difference between actual DST at the point measured and the peak DST measured at the same point over the same cycle. Thus, all 'Offset-DST' curves have their peaks at the same point. Fig. 6.18b shows 'offset-DST' curves for the points indicated, over a menstrual cycle for one of the volunteers as an example. The 'Multiple area analysis' routine of image processing software was used in computing DST at different points.

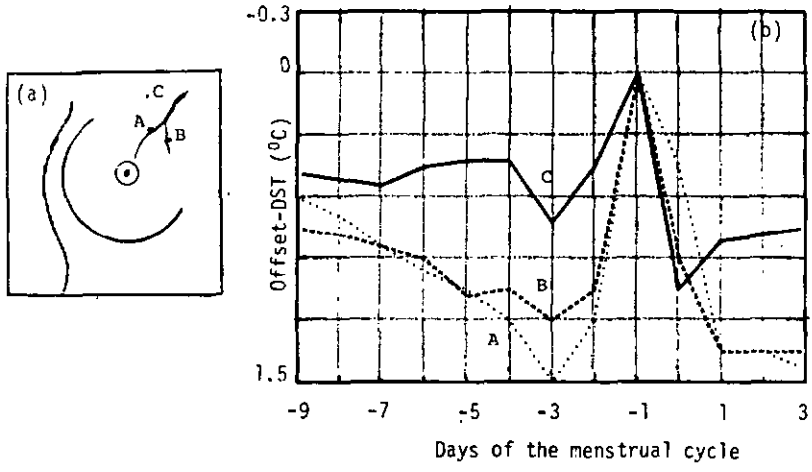

Fig. 6.18 (a) The dynamic points 'A', 'B' and 'C' selected for dynamic temperature measurement and (b) the corresponding 'Offset-DST' curves.

d. Area sensitivity:

Another variable involved in DST measurement is the area of the skin surface around the dynamic point covered in the actual temperature measurement. The area covered in the measurement of the static temperature point is usually less critical. The variation of DST values as a function of the measurement area involved (in square pixels) is shown in Fig. 6.19, as a typical curve. Note that the larger the area involved in meaurement, the lower the variation in DST. For ex: T_{br} of whole breast (Fig. 6.15) has less variation compared to the variation in spot DST (Fig. 6.16).

The sensitivity curve of Fig. 6.19 is of relevance in selecting the size of contact sensors in the design of electronic thermometer for ovulation detection (see Chapter 7).

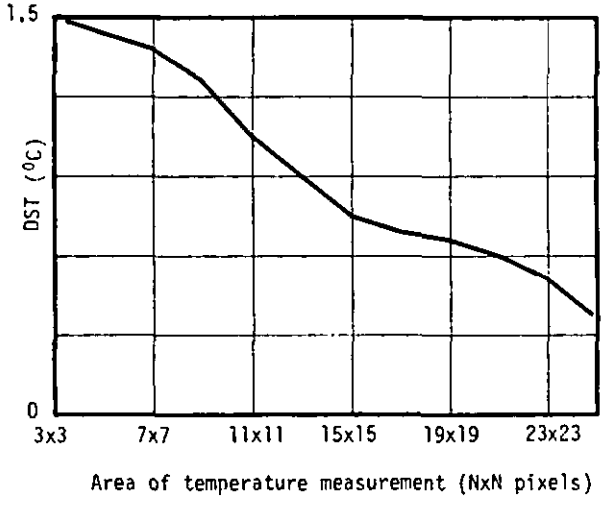

Fig. 6.19 DST curves plotted as a function of the area involved in temperature measurement. [10 sq. pixels= 2.5 sq. cm].

e. Histogram:

Temperature distribution over the breast's skin surface can be quantitatively seen by plotting this distribution as a histogram. We have selected different areas all located concentrically around a vascularly sensitive point (as shown in Fig. 6.20a).

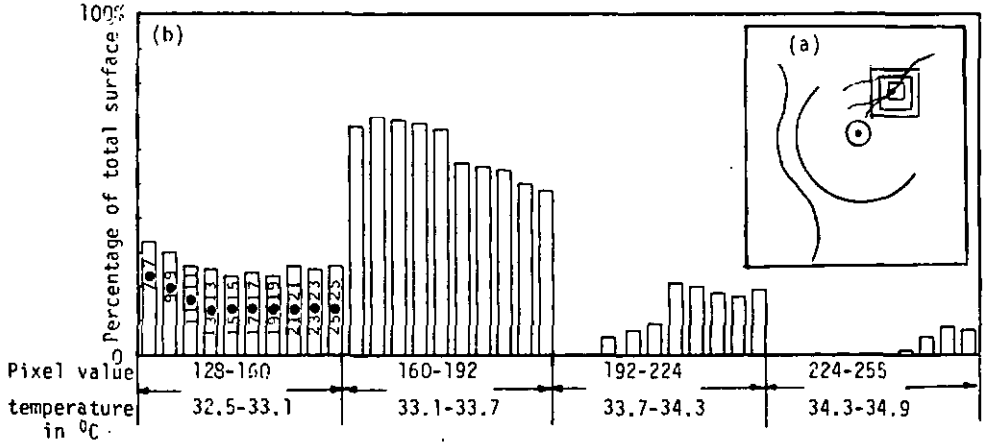

Fig. 6.20 (a) The areas chosen around a vascularly sensitive dynamic point and (b) the temperature distribution in each of these areas represented in the form of a histogram. A temperature range of 5 C is represented by binary values 0 to 255.

Histograms for each of these areas are shown in Fig. 6.20b. The data of Fig. 6.20b can be represented in an alternative form as in Fig. 6.21: Here we plot in function of the size of the concentric area selected, how much percentage of the totral surface does fall into a particular temperature range.

The mean temperature of the whole selected concentric area is also ploted in Fig. 6.21 (dashed curve).

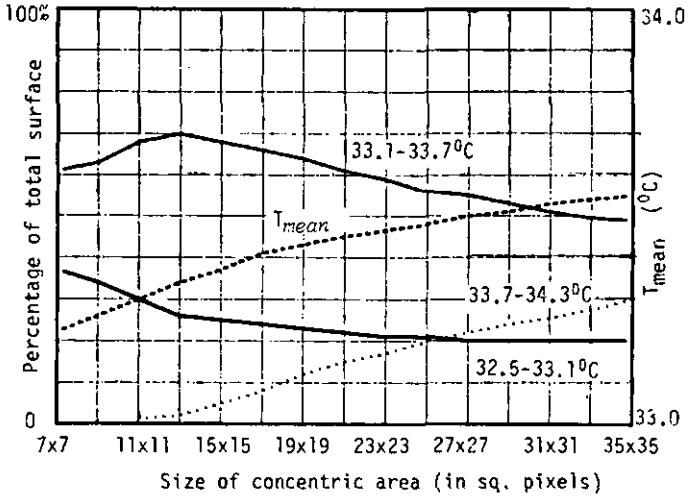

Fig. 6.21 Percentage of total surface falling in a given temperature range, and the mean temperature (T_{mean}) of the total area as a function of the area size chosen (Fig. 6.20a) around a vascularly-sensitive dynamic point.

f. Oral contraceptive users:

As explained in the chapter 4, we had a few oral contraceptive users in our experimental study. Image analysis of breast thermograms of these volunteers show very insignificant DST changes over the mensrual cycle. Fig. 6.22 shows a set of IRT images of an oral contraceptive user in the middle part of the menstrual cycle. Due to normalization of images with respect to the temperature of sternum, the relatively high absolute temperatures seen by thermometric mesurements do not show up in these computer images.

CHAPTER 7

This chapter presents the details of a digital thermometer developed for measuring both absolute and differential temperatures useful in biomedical applications.

7. ELECTRONIC THERMOMETER

7.1 Introduction

A correlation between breast thermograms and hormonal concentrations in plasma, over the menstrual cycle has been established in the previous chapters. Based on the analysis of breast thermograms, simple differential skin temperature (DST) measurement between a 'dynamic' temperature point and a 'static' temperature point has been shown to be sufficient to estimate ovulation time /28,70-71,85-86/.

There are many types of electronic thermometers availble in the market /87,88/ for bio-medical applications, replacing the conventionnal mercury thermometer. The advantage of an electronic thermometer is its faster measurement and its digital readout. However, in many situations one needs differential temperature measurement along with absolute temperature measurement (for ex: routine fallow-up checking in cancer therapy and vasomotor diceases). The BBT and DST measurement for ovulation detection also need absolute/differential temperature measuring thermometer. Thermometers measuring both absolute and differential temperature for bio-medical applications are not available commercially at low cost /87/. Higher cost of electronic thermometer is due to analog circuits involved in the circuit design (ex., wheatstone bridge followed by a pre-amplifier). For our field study, we developed a simple all digital thermometer to measure both absolute and differential temperature. We have called this thermometer 'FERTITHERM' to identify its principle application to fertility interval estimation with temperature measurement. The circuit design is aimed at low cost and suitability for integration into a single chip.

7.2 Thermometer specifications

Application:	Biomedical field,
Range of temperature:	25°C to 45°C
Accuracy of measurement:	0.1°C
Time constant:	30 seconds.

7.3 Choice of sensor

The selection of sensor is very important with respect to temperature sensitivity, linearity, precision and cost. Of the various possibilities, we considered semiconductor (diode and transistor), Thermistor (NTC), RTD (platinum resistance), thermocouples and quartz temperature sensors.

Table 7.1 provides the important characteristics of each of these sensors in brief:

Table 7.1 : Summary of contact temperature sensors and their characteristics

Device	Transduction principle	Linearity	Sensistivity	Precision	Cost	Remarks
Diode/ Transistor	Semiconductor V/I characteristics	Linear in a limited range	Low, less than 1 mv/°C	0.3°C	Low	Problem of drift, to be operated in linear region.
Thermistor (NTC)	Resistance (negtive temperature coefficient)	Easy to linearize in a limited range	High, upto 10% change of resistivity/°C	0.05°C	Low	Passive and reproducible characteristics
RTD (platinum resistance)	Resistance (positive temperature coefficient)	Linear	High	0.1°C	High	Linear characteristics
Thermocouple	Thermoelectric	Non-linear	High	0.3°C	High	Needs temperature compensation
Quartz	Piezoelectric	Linear	Small	0.001°C	High	Not readily availble for commercial use.

We chose the thermistor (NTC) for its high sensitivity, low cost and reproducibility characteristics.

7.3a Charactrization of thermistor:

The resistance vs temperature characteristics of a thermistor are generally written in the form /89/:

$$R_t = R_{t0} \cdot \exp(\beta \cdot (\frac{1}{T} - \frac{1}{T_0})) \qquad (7.1)$$

where R_t = zero power resistance at T K (t°C + 273.15)

R_{t0} = zero power resistance at T_0 K (t_0°C + 273.15)

β = thermistor material constant.

7.4 Linear thermistor resistance network design

Since the variation in the thermistor resistance with temperature is exponential, as described by eq. 7.1, it is necessary to linearize the 'resistance vs temperature' characteristics in the interesting temperature range. In our case, the thermal range considered is between 25°C and 45°C. Thermistor manufacturers generally provide the normalized resistance vs temperature characteristics and 'S' curves as shown in Fig. 7.1a and Fig. 7.1b /89/.

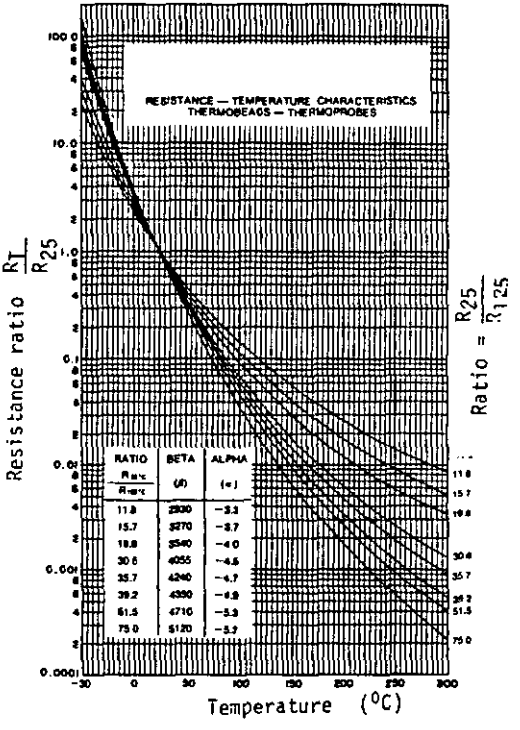

Fig. 7.1a Nominal resistance of a thermistor as a function of temperature

The linearized thermistor resistance network will be in the form shown in Fig. 7.2. Here R has to be suitably chosen to obtain good linearity characteristics vs temperature for the network /89/. The 'S' curves ($S = R_{25}/R$) shown in Fig. 7.1b can be used to obtain the best value of R for a specified thrmistor for a good linearity in the specified range.

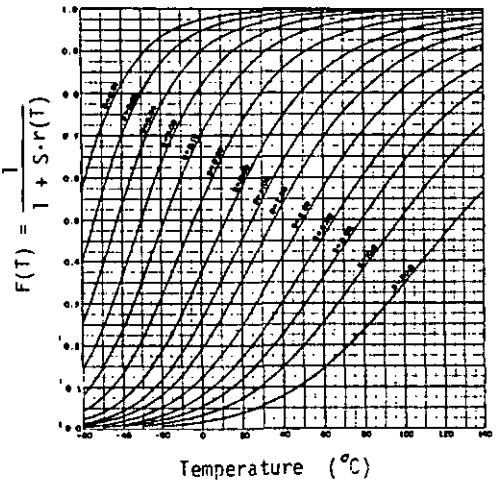

$$S = \frac{R_{25}}{R}$$

$$r(T) = \frac{R_T}{R_{25}}$$

Fig. 7.1b 'S' curves of thermistor as supplied by the manufacturer /88/.

We have choosen a Philips thermistor of type 'NTC 2322 624 22103' with 4.5% change/°C. For the range beteen 25°C and 45°C, 'S' value of 2.5 provides a good linearity. From Fig. 7.1b, we have a slope of the curve:

$$\frac{-R(F(45) - F(25))}{20} = -\frac{0.195\,R}{20} = -0.00975R \quad \Omega/^0C \qquad (7.2)$$

To obtain -40 Ω/°C, R = 40/0.00975 = 4102 Ω.
Since S= 2.5, R = 2.5x4102= 10255 Ω. So, we have choosen 10 k thermistor at 25°C. The equivalent (R_{eqv}//R) resistance at 25°C is 2.9 kΩ. To obtain the desired resistance value of 3.9 kΩ at 25°C for the linearized network, a series resistor R_s of 1 kΩ is added. So $R_{eff} = R_s + R_{eqv}$.

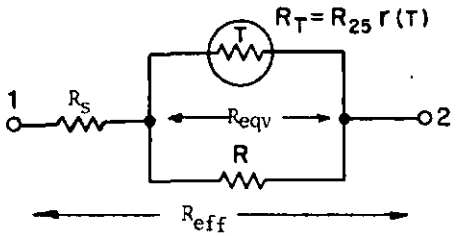

Fig. 7.2 Linear thermistor resistance network.

Fig. 7.3 shows original thermistor characteristics and that of linear network designed above with R_s = 1.0 kΩ.

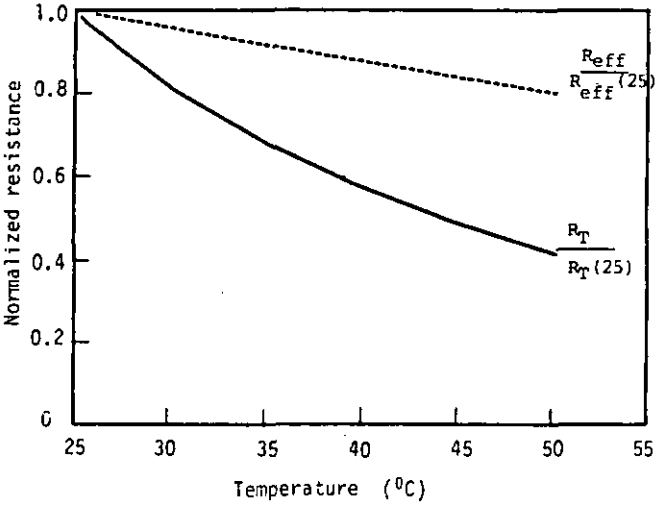

Fig. 7.3 Normalized resistance vs. temperature charcteristics of the thermistor (R_T) and of a linearized network (R_{eff}).

7.5 Design of the thermometer circuit

With the goal of realizing an all-digital thermometer, we effected the temperature to electrical signal conversion through a resistance-controlled pulse width modulator; here, the change in thermistor's resistance is converted into proportional pulse width. This is done using a monostable multivibrator. The block schematic of the thermometer circuit is as shown in Fig. 7.4.

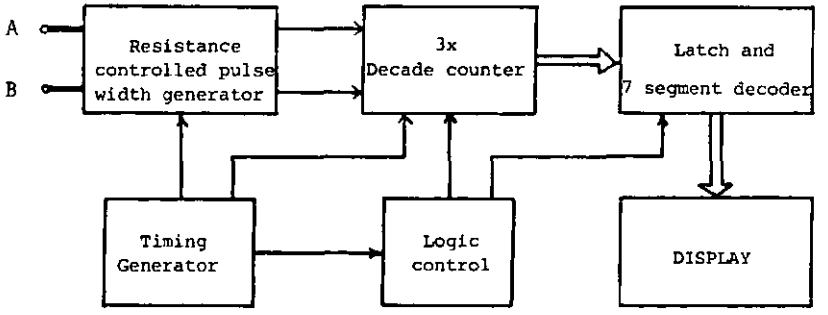

Fig. 7.4 Block diagram of our absolute/differential digital 'PERTITHERM' thermometer.

Since we are interested in measuring both absolute and differential temperatures, we designed our circuit basically to function in the differential mode. When an absolute temperature measurement is desired, one input is referred to ground reference (zero volts).

7.5a Principle of operation:

A pulse width proportional to the temperature, controls the number of clock pulses to be counted in a counter. Switching between UP-count and DOWN-count over one clock period generates a digital value corresponding to the resultant temperature at the end of a cycle; this value is displayed on a digital read-out. Inhibiting the DOWN-count operation provides an absolute temperature and UP/DOWN counting provides a differential temperature. The display is upgraded every 20 ms. So, this period of 20 ms has to cover two measurement cycles (one corresponding to UP and the other to DOWN counting), storage and display, and the counter clear cycle. This corresponds to 5 ms/operation. If we have to measure 50°C in 5 ms, with 0.1°C resolution, we need 500 counts/5 ms or a 100 KHz clock.

The linearized thermistor resistance network is so chosen, in conjunction with a low temperature coeficient capacitor, that a pulse width of 100 μs/°C is obtained as the output of monostable circuit.

7.6 Detailed circuit description

Fig. 7.5 shows the complete circuit diagram of the thermometer 'FERTITHERM'. The quartz-controlled master oscilator (CD4060) generates a 2.048 MHz, stable frequency. With a suitable divider chain (CD4060 and CO4040) a time base of 5 ms count period is generated. Measurement and display functions are completed in 4 such count periods. The monostable multivibrator (MM74c121) with a thermistor sensor 'A' in its RC network outputs a pulse width (Q_h) proportional to the temperature sensed by the sensor 'A'. The first count period is gated with Q_h to start UP-counting of input clock pulses (100 kHz) during Q_h. The 3 decade counters (MM74c192) count the input clock pulses; the contents after the end of Q_h stay unchanged until the next count command.

The second monostable multivibrator (MM74c121) outputs a pulse width (Q_l) proportional to the temperature sensed by sensor 'B'. The second count period is gated with Q_l to command DOWN-counting of the input clock pulses during Q_l. The contents of the counters at the end of the second count period represent the differential temperature measured with sensors 'A' and 'B'.

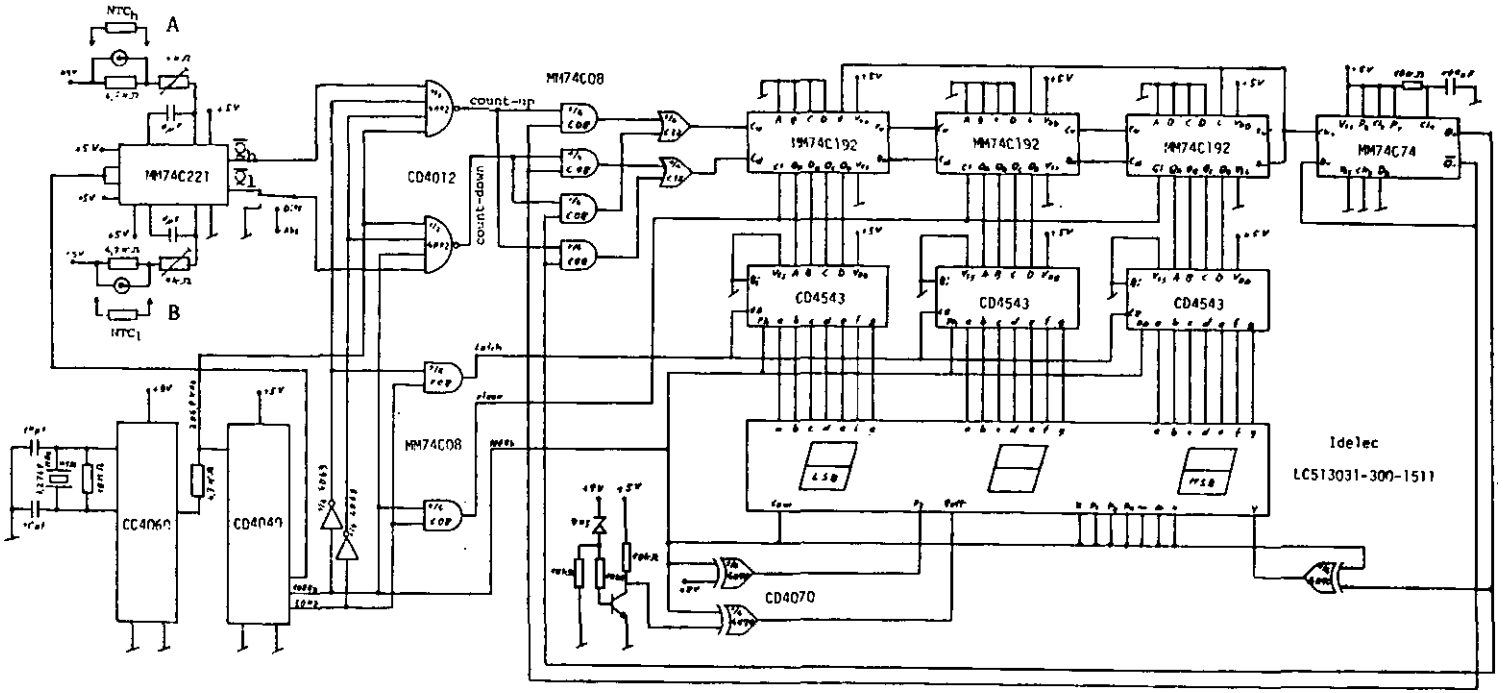

Fig. 7.5 Complete circuit diagram of the electronic thermometer 'FERTITHERM'.

If the DOWN-counting is inhibited during the second count period, the contents of the counters represent the absolute temperature measured with sensor 'A'.

During the third count period, data is stored and converted into 7 segment code (CD4542) to drive LCD display (Idelec type: LC513031-300-1511). During the fourth count period of the time base, the counters are reset to '0', to restart the measurement cycle once again.

The overflow from the counters drives a sign indicator, to display the sense of the differential temperature measured with respect to sensor 'A', i.e: $(T_A - T_B)$. A logic circuit is provided to inhibit the clock pulses in the absence of the input sensor probe or if the measurement corresponds to a temperature of more than 50°C. A two-way, two-pole switch controls the power and measurement mode. The waveforms related to above circuit are shown in Fig. 7.6. The complete hardware circuit is enclosed in a hand-held enclosure.

If the battery power is not sufficient for proper functioning of the circuit, an indicator on the LCD display warns the user, so that the battery can be replaced with a new one.

The thermometer functions with a standard 9 Volt battery.

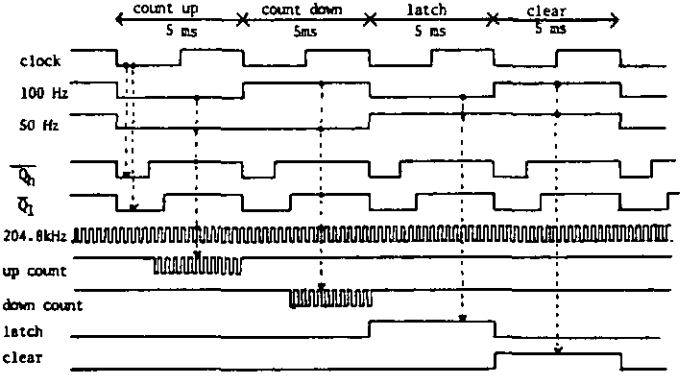

Fig. 7.6 Timing diagram of the thermomter circuit.

7.7 Results

Fig. 7.7 shows the prototype 'FERTITHERM' instrument based on the circuit shown in Fig. 7.5. A few such instruments are with some volunteers for measuring BBT and DST in home environment. BBT and DST data obtained by two volunteers with FERTITHERM are given in Fig. 7.8.

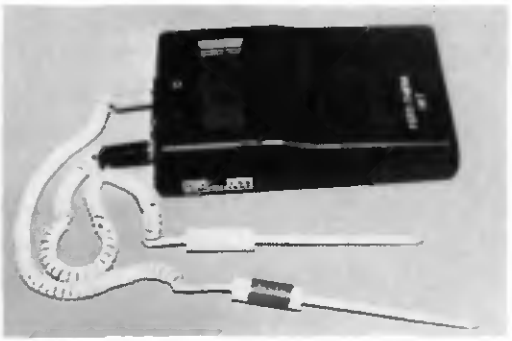

Fig. 7.7 Prototype model of 'FERTITHERM' thermometer.

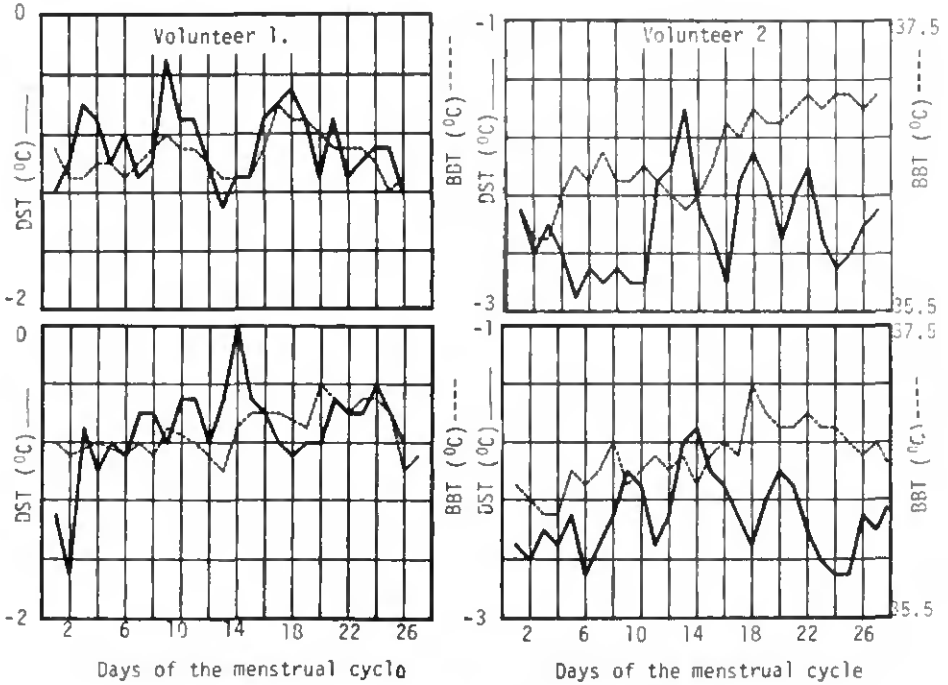

Fig. 7.8 BBT and DST measurements obtained in home environment using "FERTITHERM", by two volunteers.

The data obtained from these two volunteers shows that DST peaks in the middle part of the menstrual cycle as expected. However, they also have other peaks over the menstrual cycle. It is very difficult to draw definite conclusions based on only four such plots. However, we can foresee the problems yet unsolved for reliable application of DST measurement for estimating the fertile interval of the menstrual cycle in the home environment. The disturbances appearing in the above chart may be due to: the shift involved involved in locating the actual points of measurement, measurements done in a condition of thermal non-equilibrium, measurements done at different timings of the day and disturbing ambient conditions.

7.8 Discussion

The simple all-digital thermometer for biomedical applications will be useful not only for 88T and DST measurements, but also for other routine medical checkups. The performance of FERTITHERM thermometer has been tested for its repeatability and precision. The resolution of 0.1°c in the range of 25°C and 45°C is obtained with interchangable sensors. Precision and repeatability within 0.1°C is recorded with measurements done over 3 hours. The circuit could further be simplified with a single chip MK 50395 from MOSTEK company which has 6 decade counters and an inbuilt display decoder. Only a timing genearator and dual multi-vibrators as shown in our circuit design would have to be added.
FERTITHRM, however, has the disadvantage of a relatively high time constant of 30 seconds because of thermal mass of the sensor and the time constant of the thermistor itself. Further, a contact thermometer always disturbs the skin temperature to some extent, thus disturbing the thermal equilibrium over a considerable time: Therefore, a contact thermometer generally needs more than a minute's time for reading a stable temperature. The problems of large time constant and disturbance to skin thermal state by contact sensors can be avoided with non-contact temperature sensing (radiation sensing). Based on the principle of DST measurement 'ELTEC Instruments SA' (Neugutstrasse 4, 8304 Zurich, Switzerland) has developed a non-contact thermometer with pyroelectric sensors. The performance measurements of this 'ovulation detector' is yet to be done.

Conclusions

8. CONCLUSIONS

The relationship between the human reproduction and the menstrual cycle of a woman has been known since a very long time. Over the time, several methods of birth control, starting from primitive methods of contraception to highly reliable oral contraceptive methods have been developed. However, most of these methods are associated with aesthetic problems, technical difficulties or numerous side-effects to the human biological system. Therefore, a strong interest remains in natural birth control and in methods of ovulation detection.

There appear to be many possibilities like: mucus viscosity measurement, bio-potential measurement, hormonal analysis with solid-state sensors, temperature measurement, etc... However, all these measurements except temperature measurement involve complicated technical solutions or appear only as long term solutions. Therefore, we chose temperature as a parameter to continue our investigation and to develop a suitable method for estimating the ovulation time in advance.

The estradiol hormone being the principle hormone reaching its peak concentration in plasma before the ovulation, our interest was focussed around the effects of estradiol on the skin temperature. The estradiol hormone has the property of increasing blood flow (vascularity) in the genetic target organs like breasts and vagina. Based on this property of estradiol hormone, we proposed here, the temperature difference measurement between a vascularly-sensitive dynamic point and vascularly-insensitive static point on the breast's skin surface. Following this hypothesis of "differential skin surface temperature (DST)" measurement to estimate the ovulation time, a detailed study was done involving: clinical tests using infrared thermographic imaging of breasts over the menstrual cycle, mathematical modeling to explain the thermal aspects of the breasts, computer-assisted image analysis of thermograms and design and development of absolute/differential thermometer.

The results of this work show the validity of our hypothesis, when measurements were done in a basal thermal equilibrium condition. However, the number of volunteers being limited (15 volunteers only), the data obtained and statistics thereon may or may not be a true representation of a large population. So, there is a need to continue this investigation with a large number of volunteers, before

generalizing the hypothesis and before a commercial development of the DST method. Further, limited data obtained from some volunteers in a home environment reflect the problems involved in correct DST measurement with respect to localization of exact points, time of measurement, basal condition requirement, etc... Thus the present work has opened up new problems for investigation in human thermal physiology, and in particular as related to the menstrual cycle of a woman.

The problem of estimating the ovulation time in advance by a simple, non-invasive method for natural birth control through periodic abstinence cannot be fulfilled by the DST method. But DST can play an important role in solving infertility problems, as it provides the indication of forthcoming ovulation almost one day in advance, synchronously with that of the LH surge. Combining DST measurement with basal body temperature (BBT) measurement can provide higher reliability in determining the post-ovulatory infertile phase.

Further improvement in DST measurement can be expected with the use of non-contact temperature sensors with possible scanning for locating the dynamic temperature points automatically. However, this solution may not work out for economic reasons. Another possibility is to develop an array of silicon sensors in the form of a flexible film and multiplexed temperature measurement to localize the dynamic temperature points. This latter solution appears to be feasible with present-day technology. Further, this solution will also be useful in screening benign cancer patients and in the treatment of hyperthermia.

Appendix

APPENDIX - A

TABLE A-1 : Individual Data from the volunteers- LH concentration (mIU/ml)

Days	B.S	G.R	M.N	K.P	C.B	S.T	P.C	L.N	Y.V	B.C	B.D
-8	4.8		4.1								
-7	7.3	17.1			4.7						11.6
-6	5.0	21.1									9.5
-5	5.5	15.0	4.8	6.3			4.3	7.5			12.6
-4	6.0	16.4	4.2	6.8	4.9	3.8	9.2	8.6	4.0	9.4	
-3	6.9	15.0	3.9	7.2	2.6	6.8	8.8		5.8	8.6	10.2
-2	9.8	14.2	4.7	10.0	6.3	6.2	6.7	15.2	9.6	14.3	
-1	23.1	24.0	16.2	15.1	14.8	15.1	12.5	37.3	18.9	35.3	32.4
0	69.2	153.1	80.0	59.5	39.7	43.0	36.0	59.0	51.5	65.0	53.0
1	32.5	46.8	40.0	27.1	13.0	23.0	12.7	13.0	17.6		
2	12.3	24.1	8.2	9.6	7.2	6.2	8.5	6.3	5.8	28.2	
3	8.5	23.2	6.9	13.7	7.7	7.1	13.9		4.3	13.0	
4				8.3	6.2	11.4	6.1				
5				6.5		3.9	2.6				
6			1.3	4.6							
7				13.4	1.3	5.3	4.3				

TABLE A-2: Individual Data from the volunteers - FSH concentration (mIU/ml)

Days	B.S	G.R	M.N	K.P	C.B	S.T	P.C	L.N	Y.V	B.C	B.D
-8	7.4		6.1								
-7	7.5	5.2									8.1
-6	8.4	7.7									7.5
-5	6.3	6.3	3.2	5.0			4.2	5.3			8.7
-4	6.3	4.6	3.0	4.8	4.1	4.4	4.8	4.1	2.4	5.5	
-3	6.2	4.6	2.8	4.7	3.1	4.5	5.8		3.7	4.8	5.4
-2	5.2	3.8	2.3	4.9	3.4	4.2	4.7	7.1	5.1	6.4	
-1	7.4	4.3	4.1	4.2	4.5	8.1	5.4	11.5	6.4	10.4	8.0
0	27.2	16.3	14.0	11.7	13.2	21.0	15.1	17.5	17.6	19.6	13.7
1	13.3	11.3	7.0	9.5	6.6	9.8	4.4	6.5	9.3		
2	6.5	5.5	3.9	5.1	5.8	4.2	3.7	5.5	6.0	6.9	
3	7.4	4.2	3.1	4.1	5.7	5.3	3.4		2.4	6.1	
4				4.8	5.1	4.5	2.7				
5				5.8		2.7	2.1				
6			2.4	4.2							
7				4.9	2.0	2.2	4.2				

TABLE A-3 : Individual Data from the volunteers - Estradiol concentration (10 nmol/l)

Days	B.S	G.R	M.N	K.P	C.B	S.T	P.C	L.N	Y.V	B.C	B.D
-8	0.2		0.15								
-7	0.1	0.05			0.08						0.14
-6	0.05	0.05									0.19
-5	0.03	0.43	0.86	0.73	0.04	0.3	0.26	0.19			0.21
-4	0.18	0.33	0.61	0.68	0.25	0.39	0.33	0.27	0.89	0.32	
-3	0.28	0.4	0.49	0.71	0.87	0.26	0.50		0.94	0.33	0.35
-2	0.33	0.59	1.59	0.65	1.14	0.51	0.56	0.77	0.97	0.44	
-1	0.42	0.91	1.01	0.62	0.70	0.94	0.83	0.60	2.13	0.66	0.46
0	0.60	0.93	0.66	1.68	0.10	1.01	0.62	0.5	1.08	1.02	0.45
1	0.3	0.83	0.31	1.64	0.31	0.56	0.13	0.19	0.49	0.53	
2	0.12	0.60	0.19	1.30	0.29	0.40	0.08	0.12	0.37	0.43	
3	0.05	0.49	0.45	0.39	0.39	0.21	0.05		0.36	0.25	
4				0.20	0.30	0.20	0.01				
5				0.38		0.23	0.05				
6			0.27	0.32							
7				0.46	0.48	0.4	0.2				

TABLE A-4 : Individual Data from the volunteers - Progesterone concentration (nmol/l)

Days	8.S	G.R	M.N	K.P	C.B	S.T	P.C	L.N	Y.V	B.C	B.D
-8											
-7					0.08						
-6											0.51
-5	0.16				0.04		0.06	0.11			0.57
-4	0.16	0.13			0.04	0.41	0.16	0.18	0.31	0.50	
-3	0.19	0.05			0.25	0.41	0.16		0.25	0.70	0.77
-2	0.19	0.05			0.87	0.51	0.19	0.35	0.47	1.08	
-1	0.21	0.06	0.12		1.14	0.51	0.19	0.35	0.67	1.30	1.37
0	0.27	0.09	0.27	0..15	0.70	0.57	0.25	0.35	1.0	1.39	1.43
1	0.31	0.13	0.39	0.28	0.10	0.83	0.29	0.38	1.04		
2	0.42	0.31	0.67	0.44	0.31	1.20	0.41	0.64	2.58	2.00	
3	4.72	0.53	1.93	0.48	0.29	1.40	0.51		3.91	2.83	
4				0.74	0.39	1.62	1.27				
5				2.49		2.48	1.81				
6			6.43	3.2							
7				2.94	0.48	4.64	3.7				

TABLE A-5 : Individual Data from the volunteers - DST ($T_a - T_b$) (°C)

Days	B.S	G.R	M.N	K.P	C.B	S.T	P.C	L.N	Y.V	B.C	B.D
-8	-2.3		-3.6								
-7	-2.6	-2.8			-2.6						-2.1
-6	-2.3	-3.1									-1.8
-5	-2.8	-3.5	-2.7	-0.6	-1.8	-1.9	-1.1	-2.1			-1.5
-4	-2.6	-2.7	-3.0	-1.0	-1.6	-1.3	-1.3	-1.8	-1.9	-2.0	
-3	-2.7	-2.9	-2.7	-1.7	-2.6	-1.7	-1.5		-1.7	-1.8	-1.5
-2	-2.2	-1.7	-2.9	-1.1	-1.1	-1.2	-1.3	-1.3	-1.7	-1.7	
-1	-3.0	-1.4	-2.6	-1.3	-1.7	-0.5	-0.8	-1.2	-0.8	-0.9	-1.3
0	-1.7	-2.9	-2.7	-0.2	-1.4	-0.9	-0.6	-1.0	-0.9	-0.7	-1.3
1	-2.1	-2.8	-2.8	-1.9	-2.4	-1.7	-1.5	-0.8	-1.3	-0.8	
2	-2.5	-2.9	-2.8	-1.4	-2.4	-1.9	-1.2	-1.3	-1.5	-1.3	
3	-3.0	-2.1	-3.6	-1.6	-2.2	-1.0	-1.8		-1.4	-1.6	
4				-1.7	-2.3	-0.7	-1.7				
5				-1.9		-1.0	-1.7				
6			-3.5	-2.0							
7				-1.2	-2.5	-1.2	-1.4				

TABLE A-6: Individual Data from the volunteers - BBT (oral) (°C)

Days	B.S	G.R	M.N	K.P	C.B	S.T	P.C	L.N	Y.V	B.C	B.D
-8	36.5	36.4	36.6	36.4	36.6	36.6	36.4	36.6	36.4	36.4	36.3
-7	36.6	36.6	36.6	36.3	36.6	36.5	36.6	36.4	36.2	36.5	36.3
-6	36.6	36.4	36.7	36.4	36.7	36.4	36.7	36.5	36.1	36.5	36.5
-5	36.7	36.6	36.7	36.0	36.5	36.2	36.3	36.4	35.9	36.4	36.3
-4	36.6	36.7	36.8	35.9	36.5	36.4	36.5	36.6	36.3	36.5	36.4
-3	36.6	36.3	36.7	36.5	36.4	36.4	36.5	36.7	36.3	36.4	36.4
-2	36.5	36.5	36.7	36.5	36.6	36.3	36.4	36.7	36.1	36.3	36.3
-1	36.4	36.5	36.6	36.6	36.8	36.5	36.3	36.7	36.1	36.1	36.2
0	36.4	36.4	36.5	36.7	36.7	36.1	36.4	36.4	36.2	36.5	36.7
1	36.4	36.6	36.8	36.7	36.9	36.4	36.6	36.5	36.3	36.6	36.6
2	36.6	36.8	36.9	36.8	36.8	36.3	36.8	36.8	36.7	36.7	36.6
3	36.9	36.7	36.9	36.9	37.0	36.4	36.7	36.6	36.5	36.8	36.7
4	36.8	37.0	36.8	36.9	36.8	36.8	37.0	36.7	36.7	36.8	36.7
5	36.8	36.8	36.8	36.8	37.0	36.7	36.8	36.8	36.5	36.8	36.7
6	36.7	37.0	37.1	37.5	36.9	36.6	37.0	37.1	36.6	36.7	36.6
7	36.6	36.9	37.0	37.0	36.9	36.7	36.8	37.0	36.7	36.8	36.7

APPENDIX B

Formulae used in the statistical analysis of data

The number of samples to be analysed being less than 30, "student's" t distribution is more appropriate in the statistical analysis and tests of significance.

The formulae used in the statistical analysis of data obtained from the volunteers are:

$$\text{Mean} = \frac{\sum^{N} X_i}{N} = \bar{X}$$

$$\text{Standard deviation} = \sqrt{\sum^{N}(X_i - \bar{X})^2/N} = S_x$$

$$\text{Correlation coefficient} = \frac{\sum^{N}[(X_i - \bar{X})\cdot(Y_i - \bar{Y})/N]}{S_x \cdot S_y} = r$$

$$\text{Standard error mean} = \frac{S_x}{\sqrt{N}} = \text{SEM}$$

$$N = N_1 = N_2$$

where X_i and Y_i are data from the population sample group X and Y, N_1 and N_2 are number of samples in group X and Y respectively.

In calculating the significance of the data, "t" score is first calculated and then from the tables /90/ of "student's" t distibution, the confidence limit is read-out, for a particular degree of freedom.

The number of degrees of freedom = $(N_1 + N_2 - 2)$

$$\text{"t" score} = T = \frac{\bar{X} - \bar{Y}}{S\sqrt{(1/N_1 + 1/N_2)}}$$

where $$S = \sqrt{\frac{(N_1 \cdot S_x^2 + N_2 \cdot S_y^2)}{N_1 + N_2 - 2}}$$

References

References

1. Yen S.S.C : The human menstrual cycle in reproductive endocrinology; physiology, pathophysiology and clinical management.; Editors: S.S.C. Yen and R.B. Jaffe., W.B.Saunders Publ., 1978.

2. Simon and Schuster : Our bodies and ourselves.; New York, 1975.

3. WHO scientific group: Biology of fertility control by periodic abstinence.; WHO technical report No. 360., 1967.

4. Steinetz B.G : Secretion and function of ovarian estrogens.; Chapter 19 in ' Handbook of Physiology - Endocrinology II, part 1', pp. 439-466.

5. Moghissi K.S. : Prediction and detection of ovulation.; Fert. & Ster., Aug. 1980, pp. 89-98.

6. Seguy B. :Garcon ou fille a votre choix.; Mercure de France Publ., Paris, 1980.

7. Bio-self: Bioself Distributions S.A, 91, Rue de Geneve, 1126, Thonex, Switzerland.

8. Ovudate : ARES N.V., Geneve, Switzerland.

9. &Ovutestè& : Medical Electronics Trading, Hamburg, FRG.

10. Billings E.L, Billings J.J, Brown J.B, Burger H.G :Symptoms and hormonal changes accompanying ovulation; Lancet 1:282, 1972.

11. Dolack L.Sr. : Study confirms values of ovulation method.; Hospital Progress, Aug. 1978, pp. 64-78.

12. Woman's body: An owner's manual , Bantam Books, New York, 1979.

13. Chretien F.C, Ozenda B, Volochine B :Automatic device for measuring

the spinnability of cervical mucus in women ; Med. & Bio. Eng. & Comp., Nov. 1977, pp. 673-678.

14. Misweeney D.J, Sbarra A.J : Rapid ovarian hormone and ovulation test.; Obst. Gyn., Aug. 1965, pp. 201-206.

15. Abrams R.M, Kalra P.S, Wilcox C.J : Vaginal blood flow during the menstrual cycle; Am. J. Obst. Gyn.; Oct.15, 1978, pp. 396-400.

16. Borth R, Benoit H.J : Detection of preovulatory period using a vaginal probe in the home ; Contraception, Jan. 19B0, pp. 40-46.

17. Janata J., Kreiskrankenhaus, Kosching, BRD: Personal communication.

1B. Burr H.S, Musselman L.K : Bioelectric phenomenon associated with menstruation ; Yale J. Bio. Med., 1936, pp. 155-15B.

19. Burr H.S, Musselman L.K, Barton D, Kelley N.B : Bioelectric correlates of human ovulation ; Yale J. Bio. Med., Oct. 193B, pp. 155-160.

20. Ravitz L.J. : The detection of ovulation, Report, Ovutron Bulletin, 1977.

21. Poulson A.M, Carter G : Detection of ovulation by a method of change in finger- finger electropotential readings.; Contraception, Aug. 197B, pp. 39B-40B.

22. Spieler J.M., World Health Organisation, Geneve: Personal communication.

23. Blain J.A, Heald P.J, Mack A.E,Shaw C.E : Peroxidase in human cervical mucus during the menstrual cycle ; Contraception, June 1975, pp. 677-6B0.

24. Davis R.H, Balin H : Salivas Glucose: A useful criterion for determining the time of fertility in women. ; Am. J. Obs. Gyn., Jan. 15, 1973, pp. 2B7-2BB.

25. Diamant Y.Z, Polishuk W.J : Leukocyte alkaline phosphatase relative

score and basal body temperature as indicators of ovulation during menstrual cycles terminated by normal full term pregnancies.; Fert. & Ster., April 1979, pp. 64-72.

26. Bergeveld P., Twente University, Enschede, Holland: "Personal communication".

27. Lacey L. : Lunaception, L'Etincelle Press, Paris, 19B2.

2B. Rao K.H.S, Shah A, Ruedi B : Correlation study of differential skin temperature (DST) for ovulation detection using infrared thermography.; Proc. of ISMII'82 Berlin Conf., 1982, pp. 129-131.

29. Verzini L, Romani F, Talia B : Thermographic variations in the breast during the menstrual cycle., Acta Thermogr., Vol. 2(3), 1977, pp. 143-147.

30. Berger S.A, Chow F.W, Convidassamy G, Crooks L.E : A new electro-mechanical viscometer designed for biological fluids; IEEE Trans. on Biomed. eng. ; Vol. BME 25, N-1, Jan 1978, pp. 64-70.

31. Beukema G.J, Mellema J : Measuring system for complex shear modulus of liquids using torsionally vibrating crystals ; J.Phy. E: Sci. Instr., Vol. 14, 19B1.

32. Jondet M, Scholker R : A simple device for collecting human cervical mucus; Fert. & ster., Vol. 34, N-7, Jul. 19BO. pp. 72-33.

33. Stauffer B., Stanford Univeristy, Stanford, U.S.A : Personal communication.

34. Bergeveld P, DeRooij N : The development of chemical sensitive electronic devices; Report, Twente University of Technology, Enschede, Holland.

35. Haemmerli A, Janata J : Ion sensitive electrode for intracellular potassium mesurements.; Anal. Chem., Jul. 19BO, pp.1179-11B2.

36. Janata J, Humber R : Ion sensitive field transistors.; Ion sensitive electrode Review, Vol. 1, 1979, pp. 31-79.

37. Hilgers T.W, Abraham G.E, Cavanagh D : Natural family planning I .;

The Am. Col. Obs. & Gyn., Vol. 52, N-5, 1978, pp.575-582.

38. Hilgers T.W, Bailey A.J : Natural family planning II.; The Am. Col. Obs. & Gyn., Vol. 55, N-3, 1980. pp. 333-339.

39. Marshal J : A field trial of the basal body temperature method of regulating births.; Lancet, Jul. 6, 1978, pp. 8-10.

40. Marshal J : Cervical mucus and basal body temperature method of regulating births, Field trial.; Lancet, Aug. 1976, pp. 282-283.

41. Woodrough R.E : Medical infra-red thermography: Principles and practice.; Cambridge University Press, Cambridge, 1982.

42. Houdas Y, Ring E.F.J: Human body temperature: its measurement and regulation.; Plenum Pr., New York, 1982.

43. Rossel J : Physique Generale.; Neuchatel. 1971.

44. Houdas Y, Carette G : The physiology of Heat Production; in "Recent advances in Medical Thermography".; eds: Ring E.F.J and Phillips B., Plenum Pr. , 1984.

45. Clark R.P : 'Human skin temperature and its relevance in physiology and clinical assessment' in "Recent advances in Medical Thermography".; eds: Ring E.F.J and Phillips 8., Plenum Pr. ,1982.

46. Du Bois E.F: Human body temperature" in "Temperature- its measurement and control in science and industry".; Reinnhold pub., Paris, 1941.

47. Burton A.C : 'The operating characteristics of the human regulatory mechanism' in " Temperature-its measurement and control in science and industry".; Reinhold pub., Paris, 1941.

48. Gros Ch. et al: Les applications medicales de la thermographie infrarouge.; Acta electr., vol. 12, N-1, 1969.

49. Royston J.P, Abrams R.M : The adjustments of basal body temperature measurements to allow for time of waking.; Br. J. Obs. & Gyn., Vol. 87, 1980, pp. 1123-1127.

50. Brown J.B : Timing of ovulation.; Med. J. Austr., Vol. 2, 1977, pp. 780-783.

51. DAB/PAG method of RIA: Brochure, Serono Diagnostics S.A, 1267, Coinsins, Switzerland.

52. Nassar A.M, Smith R.El : Menstrual variations in breast thermal properties.; J. Appl. Phys., Vol. 39, N-5, 1975, pp. 806-811.

53. Simpson H.W, Wilson D et al: Thermorhythmometry of the breast: A review to 1981.; Biomedical thermology Congress, New York, 1982, pp. 133-154.

54. Smith R.El, Nassar A.M, May J.A, Hanson F.W : Anatomic aspets of mammary thermal menstrual rhythm.; Proc. Congress of Pharmacology, eds: Reinberg A. and Halberg F., Pergamon Press, Oxford, 1979, pp. 255-262.

55. Karochkin B.B, Kisenishsky A.M et al: Mammary glands' heating field of healthy women (thermography data).; Med. Radiol. (MOSK), Mar. 1977, pp. 31-38.

56. Nassar A.M, Smith R.El : Menstrual variations in thermal properties of the human breast.; J. Appl.Physiol., Vol. 39, N-5, 1975, pp. 806-810.

57. Smith R.El, May J.A, Nassar A.M : 'Breast temperature' in "Human Ovulation", eds: E.S.E. Hafez, North Holland Pub., New York, 1979.

58. Cecil H.C, Hannum J.A, Bitman J : Quantitative characterization of uterine vascular permeability changes with estrogen.; Am. J. Physiol., Vol. 211, N-5, 1966, pp. 1099-1102.

59. Gautherie M : Etude par thermographie infrarouge des proprietes thermiques de tissus humains ' in vivo'.; Rev. Franc. Etudes clin. et Biol., Vol. 14, 1969, pp. 885-901.

60. Bowman H.F, Cravalho E.G, Woods M :Theory, Measurement and Application of thermal properties of biomaterials.; Vol. 4, 1975, pp. 43-80.

61. Pennes H.H : Analysis of tissue and arterial blood temperatures in the resting human forearm.; J. Appl. Physiol., Vol. 1, N-2, 1948.

62. Mitchell J, Myers G.E: An analystical model of the counter-current

heat exchange phenomena.; 8iophy. journal, Vol. 8, 1968, pp. 897-911.

63. Peterson J.N, Seagrave R.C : An experimental and theoretical study of temperature regulation in the immersed dog.; IEEE Trans. on Biomed. Engg., BME-30, N-9, 1983.

64. Fan L.T, Hsu F.T, Hwang C.L : A review on mathematical models of the human thermal system.; IEEE Trans. on Biomed. Eng., BME-18, N-3, 1971, pp. 218-228.

65. Houdas Y: Modelling of heat transfer in man' in "8ioengineering, thermal physiology , and comfort".; eds: Cena K. and Clark J.A., Elsevier Publ., Amterdam, 1981.

66. Awbery J.H : Heat flow when the boundary condition is Newton's law.; Phil. Mag. Ser. 7, 1929, pp. 1143-1153.

67. Draper J.W, Boag J.W : Skin temperature distributions over veins and tumours.; Phys. Med. Biol., vol. 16, N-4, 1971, pp. 645-654.

68. Quenneville Y, Gautherie M, Gros Ch : Simulation physique et mathematique du transfert de chaleur dans les tissus mammaires cancereux.; Entropie, N-65, 1975, pp. 35-45.

69. Draper J.W, Boag J.W: The calculation of skin temperature distributions in thermography.; Phys. Med. Biol.,Vol. 16, N-2, 1971, pp. 201-211

70. Shah A, Rao K.H.S, Ruedi B, Magrini G : Determination of fertility interval with ovulation time estimation uaing differential skin surface temperature (DST) measurement.; Fert. & Ster., Vol. 41, N-5, 1984, pp. 771-774.

71. Rao K.H.S, Shah A : Natural birth control: A brief review and some bioelectronic solutions.; SADHANA, Proc. of INAS, Vol. 7, Part 1, 1984, pp. 73-89.

72. Jackson D.F : Imaging with non-ionizing radiations.; Vol. 2, Surrey University Press., New York, 1983.

73. AGA thermovision: Operating manual of 782 IRT system., AGA Infrared Systems AB, S-18211, Danderyd, Sweden.

74. Digital image processing system: AGA Infrared Systems A8, S-18211, Danderyd, Sweden.

75. Thermal video procesor system: Thermoteknix Systems Ltd. ,2-Fen Road, Milton, Cambridge CB4 4AD, England.

76. Hugli H : Systeme simple d'acquisition et d'affichage.; Internal report, IMT, 1982.

77. Arnoux C :Measure automatique de saut en longeur; Semester Project report., Inst. de Microtech., Neuchatel, 1982.

78. Pratt W.K : Digital Image Processing, John Wiley & Sons, New York.

79. Macovski : Medical Imaging.; Prentice-Hall Publ., Englewood, Calif., 1982.

80. Rao K.H.S :Computer-aasisted image analysis: application in thermography.; IMT Internal report No. EC 155 02/85, 1985.

81. Rosenfeld A :Image pattern recognition.; Proc. IEEE, Vol. 69, N-5, 1981, pp. 596-605.

82. Woods R.E, Gonzalez R.C : Real-time digital image ennhancement.; Proc. IEEE, Vol. 69, N-5, 1981, pp. 643-654.

83. Hugli H, Frei W : Real-time digital processing of color bronchoscopic images.; Proc. of SPIE conf. on processing of images and data from optical sensors.; Vol. 292, 1981, pp. 172-178.

84. Handbook of Image Proceesing: EYECOM, Spatial Data Systems. Inc.; 1979.

85. Rao K.H.S, Shah A : Menstrual cycle related breast thermograms: mathematical modeling, computer simulation and experimental verification.; Proc. Thermography Congress, Lucern, May 7-11, 1984.

86. Rao K.H.S, Shah A :Computer-assisted thermography and ita application in ovulation detection.; Proc. of ISMII'84 Arlington Conf., July 1984, pp. 459-464.

87. Biomedical thermometer: Ultrakust-Geratebau GMBH & Co., D-8375, Ruhmannsfelden, West Germany.

88. Digital Thermometer: Quarz AG, Othmarstrasse 8, 8034 Zurich.

89. Handbook of Thermistors: Thermometrics, Inc. , New Jersey 08817, U.S.A, 1983.

90. Spiegel M.R: Theory and problems of statistics.; Schaum's outline series, McGraw-Hill Book Co., New York, 1961.

ACKNOWLEDGEMENTS

This work was carried out at the institut de microtechnique of the University of Neuchâtel under the guidance of Professor. Dr. A.Shah, to whom I would like to express my gratitude for his encouragement and support.

The clinical experiments for this work were done at 'Hôpital des Cadolles', Neuchâtel and at 'Frauenklinik', Bern. My sincere thanks are due to Professor Dr. B. Ruedi and Dr. M. Walther who provided the above infrastructure and also accepted to be the members of the jury.

Further, I would like to thank Dr. E.F.J.Ring (Bath, U.K), Dr. W.Frei (Los Angeles, U.S.A), Prof. N. de Rooij (Neuchâtel) and Dr. J.Spieler (Washington D.C, U.S.A) for accepting to be the members of the jury and for their comments on my work.

I can't forget to thank all the volunteers, without whose help , this work was impossible to realise.

Finally, I express my thanks to all my friends and colleagues at the institut de microtechnique for their collaboration and help, during these past years. Equally, my appreciations are due to my wife, Girija, for her cooperation and patience during this difficult period.

This work was partly financed by 'Sandoz Foundation, Basel, Switzerland.'

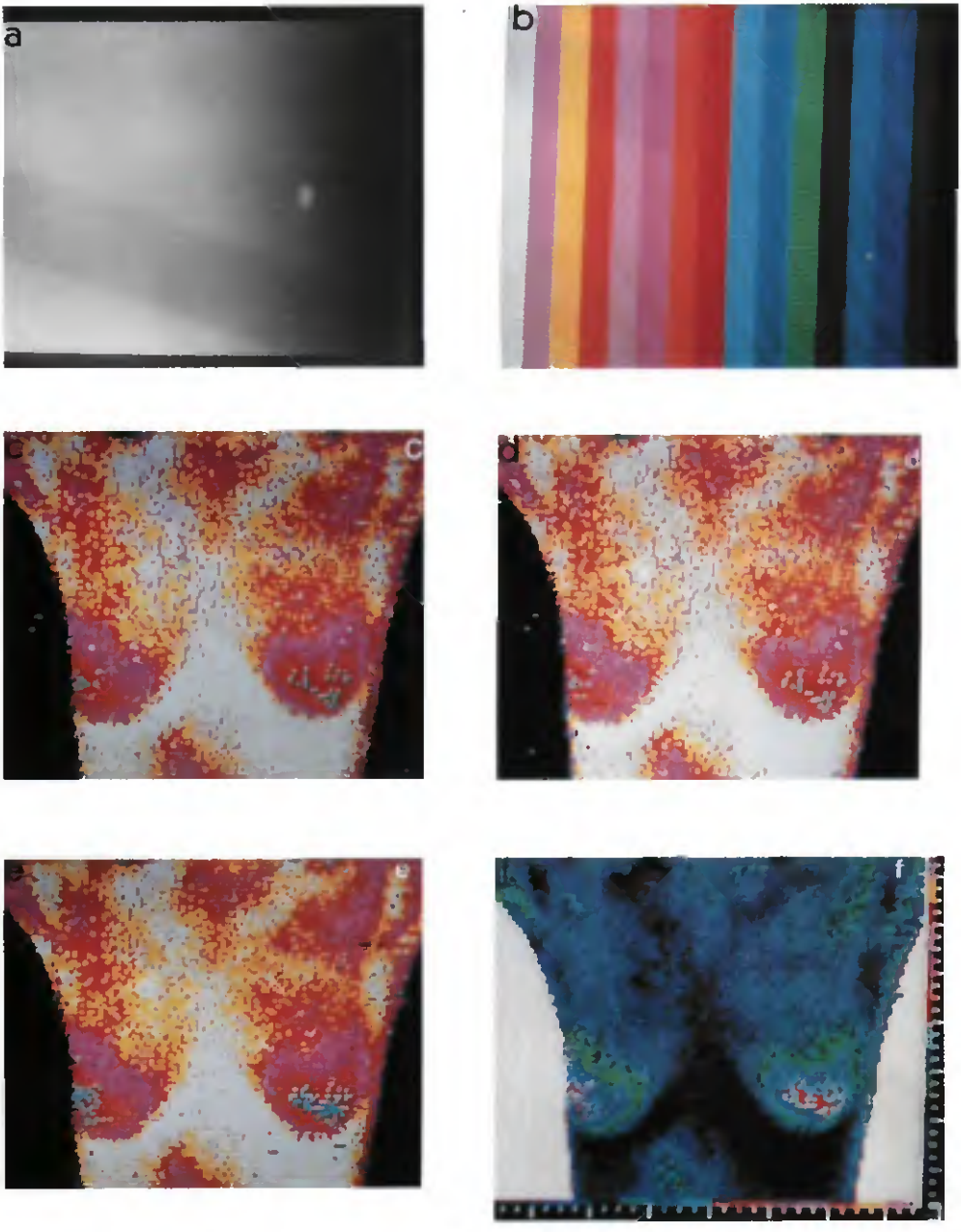

Fig. 6.7a-f Examples of the image analysis features included in the "MENU" of our CAT system software.

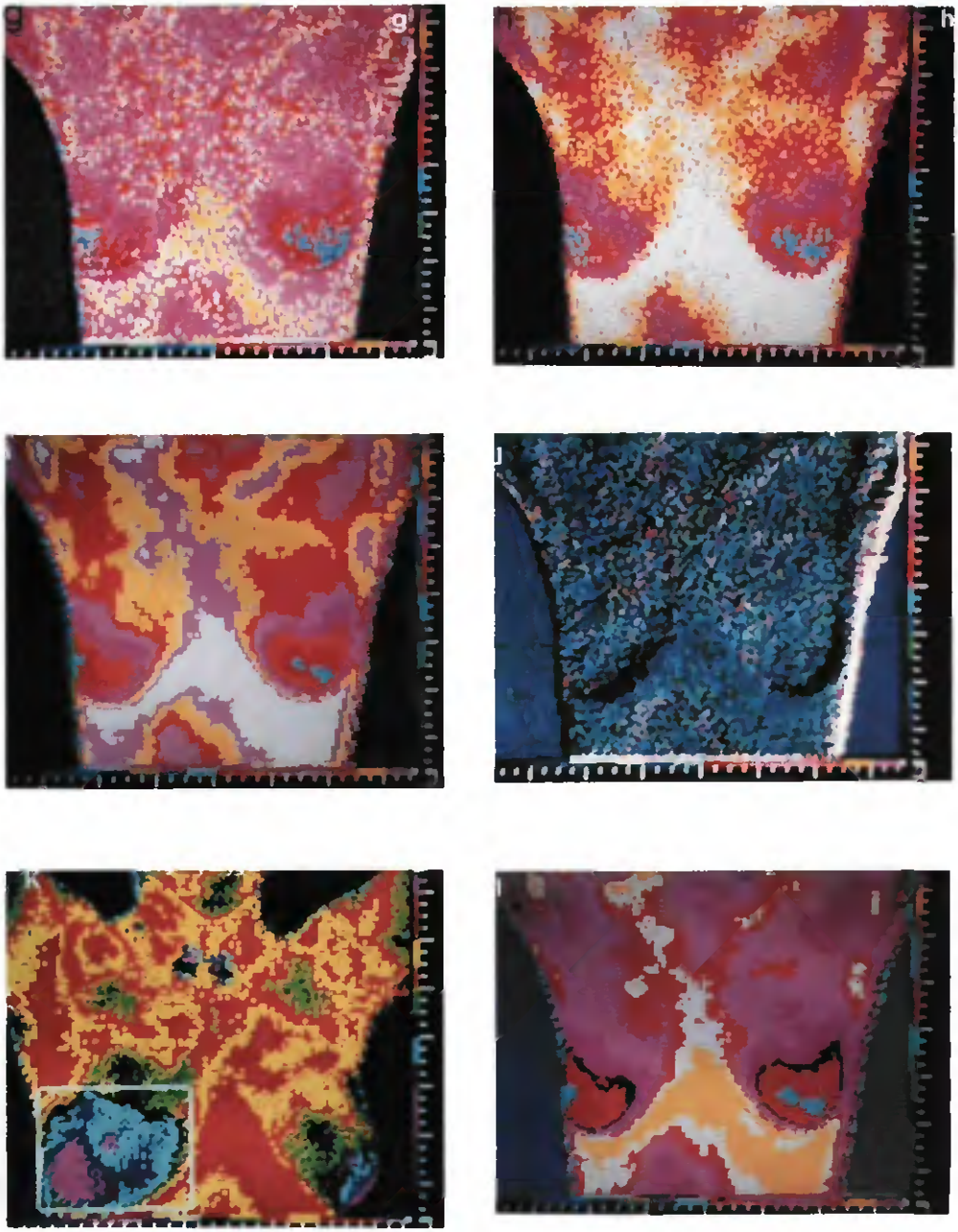

Fig. 6.7g-l Examples of the image analysis features included in the "MENU" of our CAT system software.

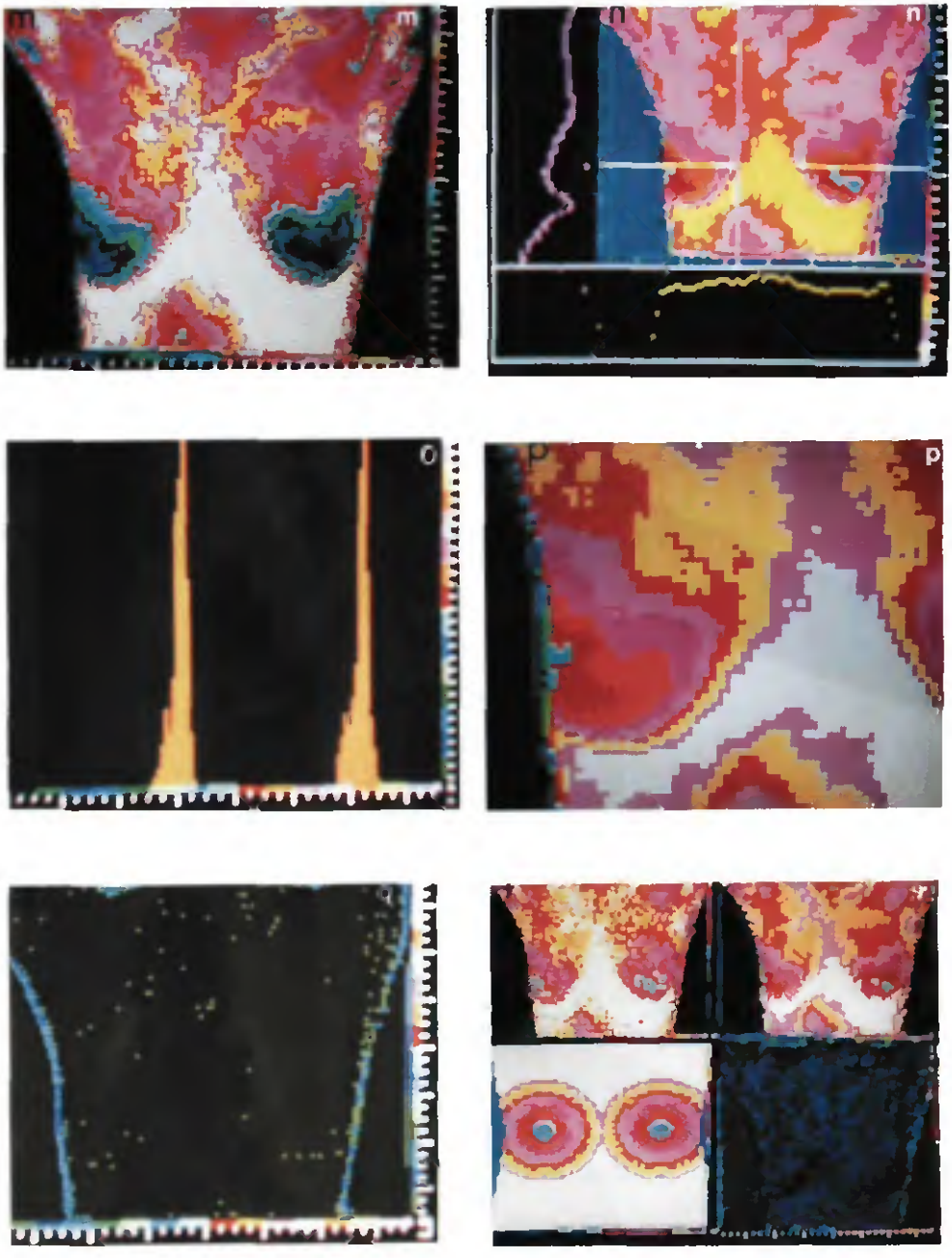

Fig. 6.7m-r Examples of the image analysis features included in the "MENU" of our CAT system software.

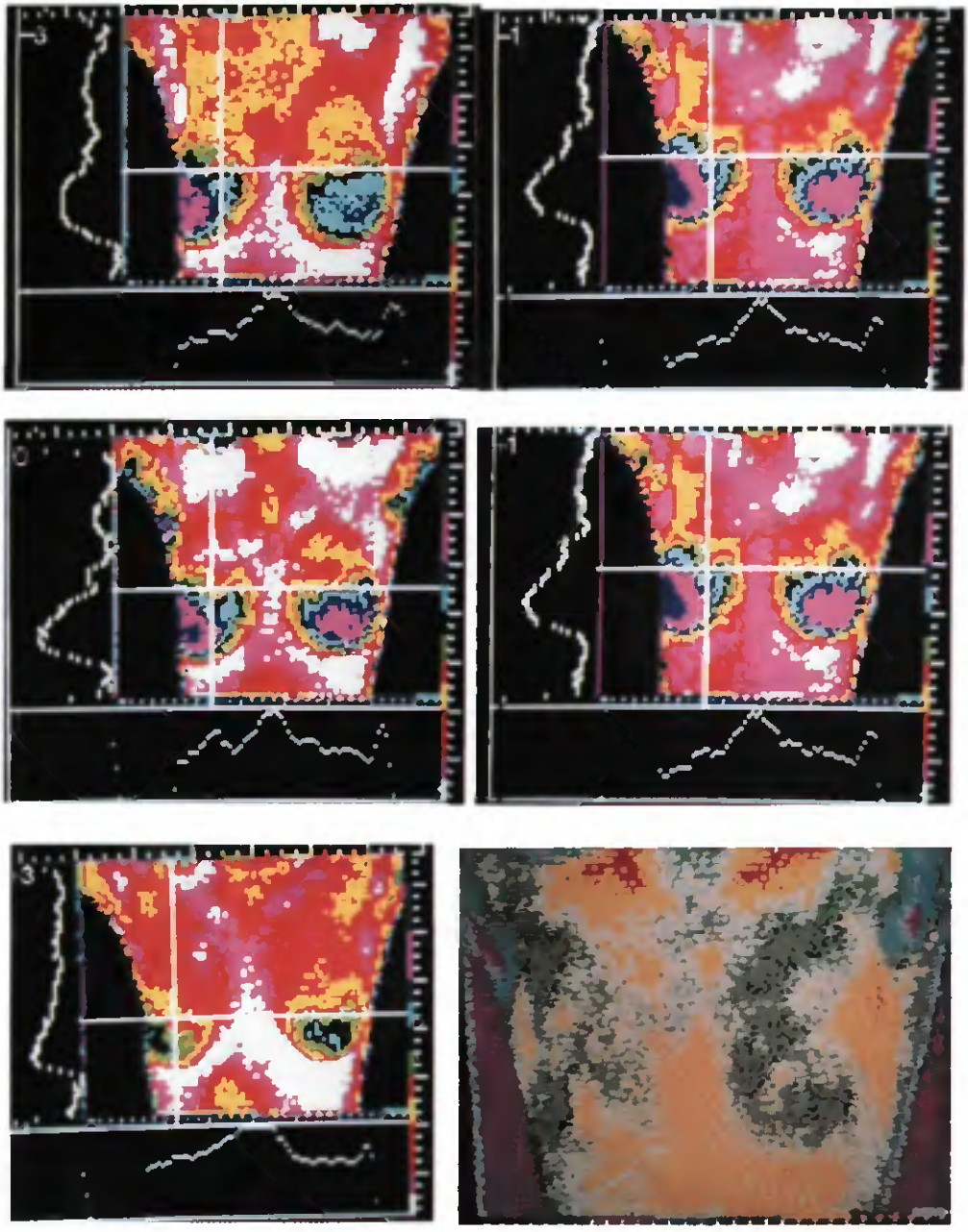

Fig. 6.17 Typical sequence of IRT images over the menstrual cycle, with corresponding X-Y *temperature line profiles. The numbers indicated on the image represent the day of the menstrual* cycle counted with respect to the day of LH surge.
The IRT image at the bottom right side shows a typical isotherm distribution useful in monitoring static and dynamic temperature areas.

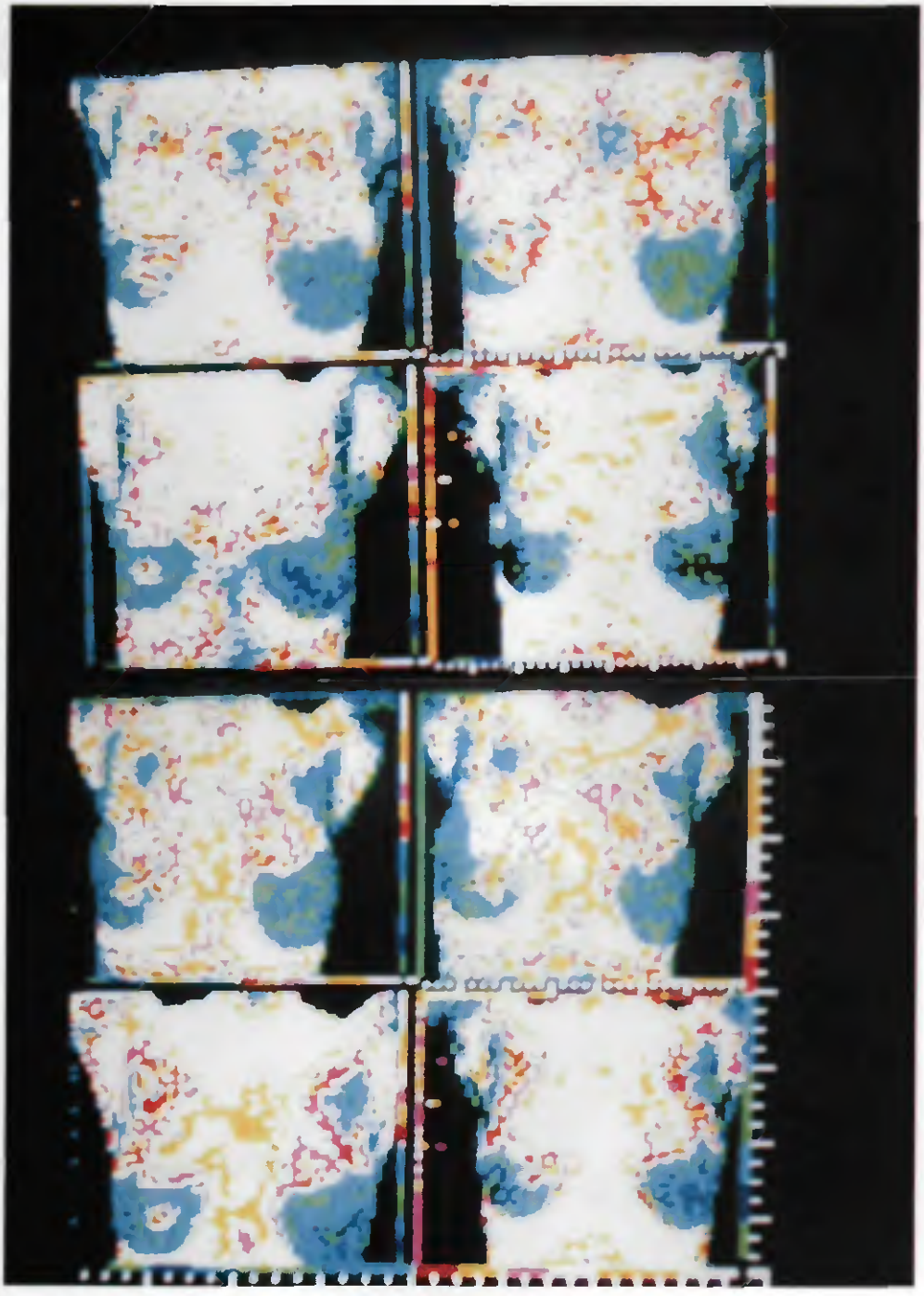

Fig. 6.22 A set of breast thermograms of an oral contraceptive user volunteer, in the middle part of the menstrual cycle.